공학박사학위논문

Design and Optimization of Industrial-scale Compression system for Its Efficient and Robust Operation

효율적이고 강건한 운전을 위한 산업 규모의 압축기 시스템의 설계 및 최적화

2018 년 8 월

서울대학교 대학원

화학생물공학부

이 원 제

Design and Optimization of Industrial-scale Compression System for Its Efficient and Robust Operation

지도교수 이 종 민

이 논문을 공학박사 학위논문으로 제출함

2018년 7월

서울대학교 대학원

화학생물공학부

이원제

이 원 제의 공학박사 학위논문을 인준함

2018년 7월

위원장	이원보	(인)
부위원장	이종민	(인)
위원	임영섭	(인)
위원	이철진	(인)
위원	윤인섭	(인)

Abstract

Design and Optimization of Industrial-scale Compression system for Its Efficient and Robust Operation

Wonje Lee
School of Chemical & Biological Engineering
The Graduate School
Seoul National University

Compression systems are one of the essential units in chemical processes. A compression system plays an essential role but consumes a significant amount of power. Also, this system is primarily employed to maintain a constant discharge pressure and needs to stay protected against surge phenomena. The surge phenomena causes back flow and vibration, which are damaging to the bearings, seals, and other parts of the compressor. Therefore, operating an efficient and robust compression system is the most important issue in plant design and management. A compressor needs to be operated within an operable range, which should be considered both at the design stage and at the operation stage.

First, the authors propose a new process design method that improves the operability of the compression system, away from the design approach that considers only the economics. The suggested approach differs from a traditional one in that it performs design and optimization with several steady-state operation regimes depending on the load variation. The proposed design approach makes a loss in the compressor equipment cost, but it reduces the operation cost over a wide range of operations, leading to the overall improvement of economics and operability of compressor.

Secondly, the author suggests the Nonlinear Autoregressive eXogenous Neural Net model (NARX NN)(Park, 2015) based real- time optimization for more efficient operation of industrial-scale multi-stage compression system in a commercial terephthalic acid manufacturing plant. NARX model is constructed to consider time-dependent system characteristics using actual plant operation data. The prediction performance is improved by extracting the thermodynamic characteristics of the chemical process as a feature of this model. And a systematic RTO method is suggested for calculating an optimal operating condition of compression system by recursively updating the NARX model.

Finally, the author proposes an advanced control system for robust operation of a parallel compression system. Control of a parallel compressor system has proven to be challenging because the control targets usually exhibit control interactions between the different control loops. To decouple this control

interference, Mitsubishi Heavy Industries has developed an advanced feed-forward control structure for parallel fixed-speed compressor systems. However, operation in the presence of an unpredictable disturbance presents a few technical challenges for this structure. Most of these problems result in poor load sharing and then operation in the recycle mode in order to protect the system from surge conditions. Moreover, an anti-surge control delay occurs when operating under a low load. To overcome these problems, an improved control structure that incorporates an additional discharge flow controller signal and a nonlinear signal calculator for anti-surge valve control is proposed.

Keywords: Compression system; Process design; Process modeling; Load variation; Neural Network; Real-time optimization; Techno-economic optimization; Anti-surge Control; Load-sharing; Control interference;

Student Number: 2014-21586

Contents

List of Figures

List of Tables

CHAPTER 1. Introduction

1.1. Research motivation

Compression systems are one of the most important parts of petrochemical, natural gas, and chemical plants. Compressors constituting the compression system are not only expensive but also have a critical impact on the overall chemical process. Therefore, operating an efficient and robust compression system is the most important issue in plant management. A compressor system is primarily employed to maintain a constant discharge pressure and needs to stay protected against surge phenomena. A surge phenomenon, i.e., unstable back-and-forth flow in the centrifugal compressor, occurs when the suction volumetric flowrate of the compressor is lower than the limit line, i.e., the surge flowrate line. When the suction volumetric flowrate is lower than surge line, the resistance of the discharge side is higher than the head increase across the compressor. In the condition, it is not possible to keep this pressure gradient any more. It causes a periodic local back and forward flow, which is the surge phenomena. The surge phenomena causes back flow and vibration, which are damaging to the bearings, seals, and other parts of the compressor. Therefore, in a real industry, a compressor needs to be operated within an operable range, which should be considered both at the design stage and at the operation stage. In the industry, however, a number of uncertainties in chemical processes,

including compression systems, make robust operation within this operable range difficult. Although there are many existing studies on the uncertainty of this process, there is a lack of studies considering the fluctuation of the process due to future load changes in the process design stage. A system designed to maximize the operability of the compression system according to possible variation of the load in the future can prevent the compressor from malfunctioning and increase the overall economical efficiency by increasing the operation time of the whole process.

Compression systems can be broadly categorized into two types according to their structure: Series Compression System (multi-stage compression system) and Parallel Compression System. First, an industrial scale multi-stage compression system has a complex nonlinearity. This is due to the complex correlation of the unknown state parameters of the compression stage and the expansion stage (for power generation) (Azlan Hussain, 1999; Haykin, 1994) that make up the compression system. Thus, the linear modeling method using only the input-output of the system is difficult to simulate this complex nonlinearity. Furthermore, the state of each stage is also affected by a number of stochastic trending factors. Stochastic factors such as aging of equipment or external environment affecting the efficiency of the compression system tend to be time-dependent in nature. Therefore, in order to design a model that accurately predicts the energy consumption of a multi-stage compression system, it is necessary to use a

nonlinear technique to simulate the complex nonlinearity of the system, as well as a modeling method that can reflect time-varying factors. In addition, the system cannot be precisely sensed because it is the system of the state because it is difficult to accurately monitor the multi-stage system. Therefore, these modeling issues must be solved for efficient operation of the series compression system.

In parallel compression systems, there are issues that need to be addressed in relation to control. Surge phenomena are generally caused by poor matching of the compressor, inappropriate compressor design, and an inadequate anti-surge control system. Because a surge phenomenon shuts down the entire process and causes mechanical damage to the centrifugal compressor, the control system should quickly prevent a surge. For these reasons, various parametric studies have been conducted, and various scenarios have been analyzed to achieve instant and stable anti-surge control. However, discharge-pressure control and anti-surge control usually occur in opposite directions because of control interference. This inner-compressor control interference can cause a control instability or significant oscillations. A load-sharing control system should also be incorporated in a parallel centrifugal compressor system. Load sharing is an important consideration for energy efficiency and control in a parallel compressor system. This inter-compressor control interference can cause inefficient or overloaded operation; hence, it should be decoupled for stable and efficient operation.

Therefore, a parallel compressor system requires an advanced control structure rather than a simple feedback control structure.

1.2. Research objectives

The objective of this thesis is to propose an integrated solution for the energy efficient and robust operation of industrial-scale compression systems from the new design approach of compression systems to modeling, optimal operation strategy and control system development.

First, a new design approach for robust and efficient operation of the compression system under load changing conditions is proposed. The proposed approach is applied to the PRICO® Single Mixed Refrigerant (SMR) process to evaluate the economics of actual gas field well depletion scenarios. Compared with existing design approach, it shows that flexible operation of compressor is possible. Next, the author designs a multi-stage compression system model that has better prediction performance than existing models by using actual operation data and artificial neural network structure, and provides a platform capable of efficient and sustainable operation through real-time optimization technique and model re-update. Finally, the author develop a control system to solve the control issues that may occur while operating the actual compression system, and evaluate the

robustness of the proposed control system by applying it to various operation scenarios.

1.3. Outline of the thesis

Chapter 1 provides the research motivation and the objective of the thesis. In Chapter 2, A new design approach is proposed to deal effectively with the load variation caused by depletion of gas filed. In addition to showing the techno-economic assessment of the proposed approach for the actual gas filed well depletion scenario, it also shows that the compressors in the liquefaction process operate more robustly. Chapter 3 includes NARX modeling of industrial-scale multi-stage compression systems and real-time optimization results using them. In Chapter 4, the development of an advanced control system for an industrial-scale parallel compression system. It also shows that efficient and robust operation is possible by applying to various operating scenarios. Chapter 5 presents the conclusion and the suggestion for the future works.

CHAPTER 2. Process Design Approach Considering Compressor Operability- Application to LNG liquefaction process

2.1. Introduction

Environmental concerns and limited availability of fuel resources have increased interests in natural gas and made natural gas the fastest growing fuel (1.6% per annum, p.a.) among other dominant fossil fuel resources. In particular, liquefied natural gas (LNG) grows seven times faster than the pipeline gas trade owing to its flexible means of transport in response to regional supply and demand fluctuations and long-distance trades (BP, 2017). Despite the geological mismatch between natural gas fields and consumers, the traditional natural gas upstream processing is mainly carried out onshore (Lee et al., 2012). However, recent developments in the technology of LNG floating production, storage, and offloading (LNG-FPSO) have facilitated installing conventional onshore LNG processing facilities into the sea, which allows scattered small- and mid-sized offshore gas reserves to be economically recovered with lower infrastructure requirements than that of the traditional onshore fixed facilities (Yang et al., 2018).

Liquefying natural gas requires significant energy use to satisfy cryogenic temperature around -160°C. This energy intensive yet necessary process has

drawn the attention of many researchers to improving energy efficiencies, especially via process simulation and optimization in the process systems engineering (PSE) society. Numerous liquefaction processes have been introduced with different refrigerant types and process configurations over the last decades, mainly for large-scale liquefaction processes (WorleyParsons, 2013). Since raw feed gas is mainly hydrocarbon mixture, the enthalpy varies nonlinearly along temperature change during cooling and liquefaction. Mixed refrigerant (MR) cycles effectively reduce the temperature difference between the refrigerant cycle and natural gas, while pure refrigerant cycles are relatively simple but require more number of refrigeration stages. Representative processes using pure refrigerant are ConocoPhillips optimized cascade® process and turbo expander using nitrogen. Dual mixed refrigerant (DMR), propane pre-cooled mixed refrigerant (C3MR) with or without a nitrogen refrigeration cycle, parallel mixed refrigerant (PMR), and mixed fluid cascade process (MFCP) are the example processes using MR for large-capacity LNG production. Among the major companies having MR technologies are Air Product and Chemicals Inc. (APCI), Shell, Statoil/Linde, and Axens (WorleyParsons, 2013). These processes with MR have been hot topics for research in design and optimization, producing numerous research articles regarding new configurations, exergy analysis, and design optimization with different objective functions and algorithms. For further information regarding aforementioned liquefaction cycles and the overall review in LNG plants,

please see the review articles (Lee et al., 2017; Lim et al., 2013). Also, Qyyum et al., (2017) and Khan et al., (2017) give a thorough review and extensive literature analysis specifically on the optimization of natural gas liquefaction process in PSE community and future direction in LNG industry.

The small-scale NG liquefaction process, typically less than 1 million tons per annum (MTPA), is often used as a peak shaving plant to compensate unmet demand for natural gas (Mingot and Cristiani, 1997). Single mixed refrigerant (SMR) liquefaction process is promising when it comes to the offshore application due to its compactness, lightweight, and simplicity. Recent studies on SMR liquefaction process includes energy (Xu et al., 2014) and exergy analysis (Mehrpooya and Ansarinasab, 2015; Mokarizadeh Haghighi Shirazi and Mowla, 2010; Qyyum et al., 2018a), process alternative configurations (Xiong et al., 2016), use of modified/combined optimization algorithms (Aspelund et al., 2010; Khan and Lee, 2013; Lee et al., 2002; Morin et al., 2011; Na et al., 2017; Park, 2015; Pham et al., 2017, 2016; Qyyum et al., 2018b), consideration of external factors such as ambient temperature (Moein et al., 2015; Park et al., 2016; Xu et al., 2013), various objective functions (besides energy/power consumption), problem formulations (Cao et al., 2016; Lee et al., 2017; Lee and Moon, 2016; Mehrpooya and Ansarinasab, 2015; Nguyen and de Oliveira Júnior, 2018), new modeling approaches (Vikse et al., 2018), and efficient operation systems (Won and Kim, 2017; Won and Lee, 2017).

The majority of these studies focus on the design or optimization with a minimum amount of the energy or unit power consumption as an objective function, e.g. compression work; only a few economic analyses are presented. Lee and Moon, (2016) perform energy and cost analysis of SMR process with two different objective functions of compression energy and the total annualized cost (TAC) using genetic algorithm (Psichogios & Ungar). Castillo and Dorao, (2012) conduct cost minimization of SMR process using an integrated model for decision-making framework where multi-level and multi-objectives are solved simultaneously. Nguyen et al., (2017) carry out simple comparative economic evaluation study of floating LNG (FLNG) facilities with various number of trains for liquefaction process. However, the abovementioned economic studies are carried out based on a single steady-state operating regime, either with a simple economical evaluation model (no optimization) or without considering the economic efficiency according to the number of trains. This design approach might lead to a miscalculation of costs, given the fluctuation in feed gas conditions and an overall natural gas production rate considering well depletion. As small gas fields can be exhausted in a few years and peak shaving offshore floating facilities can be relocated to new gas fields, the optimal design values and operating conditions derived by a single steady-state regime and feedstock information without considering uncertainties may be not optimal. Moreover, since the capital investment for small-scale application accounts for a large portion in the total cost, economic

evaluation according to the number of trains should not be ignored. Also, robust system design is required for process operation under such load uncertainty. Especially, it is essential to secure the operability of the compressor within the refrigeration cycle.

In this study, PRICO® SMR process considering the reduction in feed gas load according to well depletion is designed. And a techno-economic evaluation framework formulated as a nonlinear program (NLP) coupled with a process flowsheet simulator is introduced. . Finally, an optimal PRICO® SMR process is suggested and concluding remarks about compressor operability are provided.

2.2. Process Modeling

2.2.1. Problem Description

The traditional design approach focuses on finding optimal configuration and operating conditions to meet a design specification, i.e., production of 1 MTPA liquefied natural gas, assuming feed gas conditions are fixed. What this approach overlooks is feed gas load reduction and composition change according to well depletion and consequentially movement of development field. The principle of depletion is commonly described by the Hubbert peak theory (Maggio and Cacciola, 2012); the production curve of non-renewing resources approximates a bell curve, which means that once the production reaches a peak, it will start to decline exponentially. Production rate starts to increase at first by going through a dewatering phase, reaches a stable gas production phase, and then enters a decline stage. This indicates that natural gas production inevitably comes with a feed gas load reduction, not just "fluctuation", along the well depletion. Due to the circumstances, a comprehensive design approach to decide a proper equipment size and operating conditions under changing steady-state operation regimes is required so that long-term economics and near optimal operations are ensured even if the feed gas load is reduced.

Herein, we propose a comprehensive optimal design of PRICO® SMR process for small-scale offshore application by considering the feed natural gas

load reduction and the number of trains. The gas production curves of Maui and Kapuni gas fields in New Zealand (Ministry of Business Innovation and Employment, 2014) are sampled and normalized with a peak production rate of 1 MTPA. Figure 2-1 shows the normalized production profile of each gas field well. Several steady-state operating regimes in terms of the production rate are then chosen. To evaluate the influence of train capacity on economics and energy objectives, one and two-train cases are considered. Each train case is then optimized with the conventional approach of using one steady-state regime (Cases 1 and 3) and with the proposed approach of considering several steady-state regimes (Cases 2 and 4).

Case 1: One-train with a fixed load

Case 2: One-train with load reduction

Case 3: Two-train with a fixed load

Case 4: Two-train with load

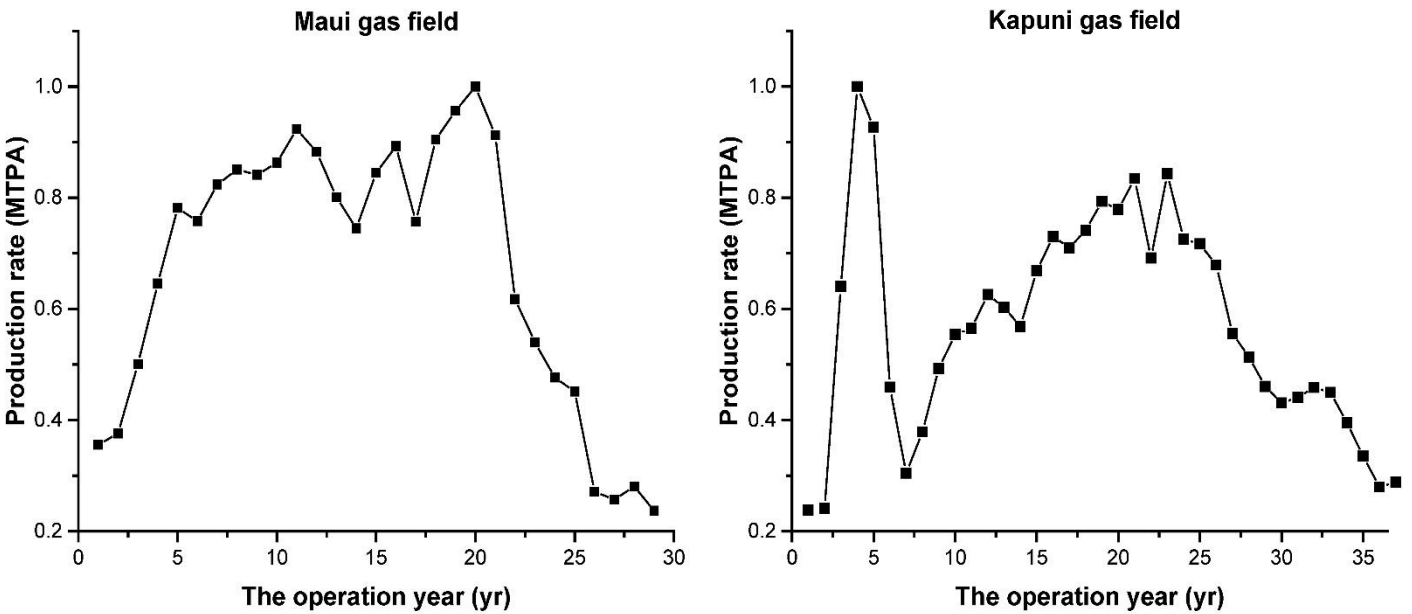

Figure 2-1. The normalized production profiles of natural gas wells with the maximum production rate of 1 MTPA (Left: Maui gas field and right: Kapuni gas field)

2.2.2. PRICO® SMR liquefaction process

The PRICO® SMR process is the simplest configuration of the single mixed refrigerant process and extensively studied over the last decades. It was first used in the Skikda LNG plant in Algeria in 1981 and operated for 23 years. Because it is simple and lightweight compared to other LNG liquefaction processes, it is known to be suitable for offshore plants and can be operated with flexibility (Remeljej and Hoadley, 2006). To liquefy pretreated natural gas at high pressure, single MR stage is used to facilitate transport and storage of LNG at the atmospheric pressure. The mixed refrigerant is pressurized through the compression stages and enters a multi-stream heat exchanger where it is cooled and liquefied by cold MR stream. The liquefied MR expands and its temperature decreases as it passes through the Joule-Thomson valve, enters the main heat exchanger in the reverse direction to hot MR stream and natural gas, and then has a cycle shape to return to the compression stages. The main heat exchanger is a plate-and-fin apparatus with a brazed aluminum core. A natural gas stream enters the main heat exchanger and comes out in the form of liquefied natural gas with the temperature of -160°C. Compression stage consists of compressors and sea water intercoolers, with limited compression ratios up to 4 and after-chilled temperature of 40 °C for realistic operation.

The process flow diagram and the names of each unit and stream are given in Figure 2-2. The feed specifications and design assumptions are listed in Table

2-1 (Khan and Lee, 2013). The feed natural gas is mainly composed of 91.3 mol% methane, 5.36 mol% ethane, and 2.14 mol% propane, and it is assumed that no natural gas liquid (NGL) recovery process is required to satisfy the heating value of LNG product. MR consists of methane, ethane, propane, n-butane, and nitrogen. Peng-Robinson equation of state is used to predict thermophysical properties in the PRICO® SMR process as it is widely accepted to simulate LNG system. Flowsheet modeling is performed using the Aspen HYSYS®, which is a qualified commercial process flowsheet simulator in the LNG industry. The purpose of this study is to propose a new design approach considering the life time of the gas field well and compare it with the results of the traditional approach. Therefore, design variables are determined by the two different design approaches while the given feed conditions and simulation basis remain the same. The design variables include the composition of the MR, the heat exchange area of the main heat exchanger, the flowrate of MR, temperature and pressure of MR_cold_in stream, and pressure ratio of the compression stage.

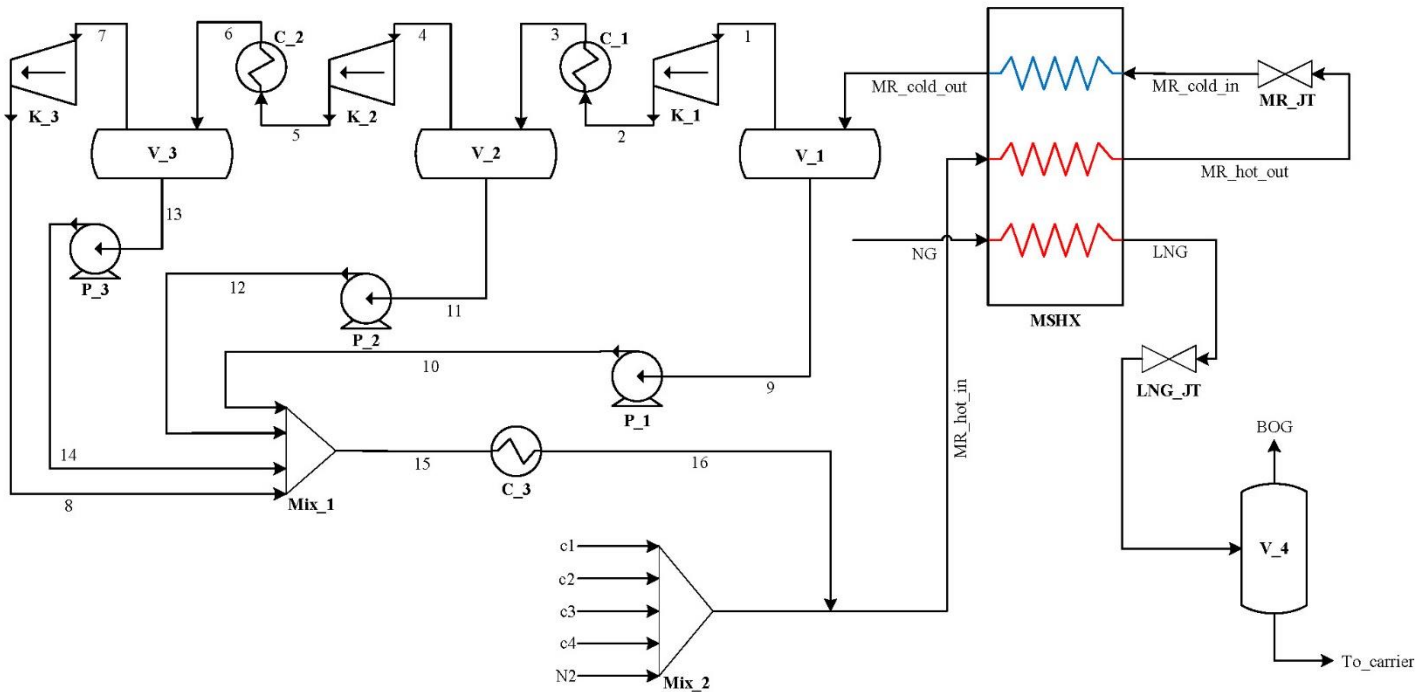

Figure 2-2. Process flow diagram of PRICO® SMR liquefaction process

Table 2-1. Feed natural gas specifications and design assumptions

Property	Value
NG Pressure	50 bar
NG Temperature	32 °C
NG composition [mole fraction]	
Methane	0.9135
Ethane	0.0536
Propane	0.0214
i-butane	0.0046
n-butane	0.0047
i-pentane	0.0001
n-pentane	0.0001
nitrogen	0.002
Compressor polytropic efficiency	0.8
Main heat exchanger pressure drop	
Hot stream (Δp)	1 bar
Cold stream (Δp)	1 bar

2.3. Process Optimization

2.3.1. Optimization Framework

Figure 2-3 shows the difference between the suggested approach considering load reduction scenarios and the conventional design approach with 100% load standard for PRICO® SMR process. The traditional approach assumes that the process will be operated in a single steady-state regime, which means the production rate does not change along the well development. The process design and optimization were carried out with one set of design specification, such as 1 MTPA of LNG production. On the other hand, the proposed approach considers several sets of design specification; the production rate changes along the well development, and thus the production rate is not fixed as 1 MTPA but varies along with the change in operation regimes. In order to compare the design approaches, two optimization steps are performed. The first step is to determine the optimum MR composition and unit size that are fixed given the load changes. The second step is to determine the operating variables that give the minimum operating cost according to the scenario including the load changes. The difference from the traditional approach is to consider the load capacity at the stage of determining the unit size and optimal MR composition. The load reduction scenarios, which are based on the production profile of the natural gas field well, calculate the load capacity according to the number of trains. The new approach determines the MR composition and the unit sizing

data that can yield the maximum profit at three different production rates, 100% of the maximum production rate (1 MTPA), minimum production rate, and medium production rate.

Since the optimization framework proposed in this study externally calculates the simulation model using a sequential process simulator (Aspen Hysys), it is difficult to obtain the gradient of the objective with respect to the design variables. Hence, derivative-free optimization such as genetic algorithm (Psichogios & Ungar), which is known to yield reasonable solutions for NLP, is adopted. Simultaneously determining MR stream and the area of the main heat exchanger may generate many infeasible solutions due to hidden constraints in this nonlinear system. This problem makes it difficult to compare the different design approaches using only the local optimization solver with the base case design. Therefore, we designed a structure to input possible variable sets within proper variable bounds into the simulation model through the communication module between Aspen HYSYS® and MATLAB optimization algorithm. The simulation results are again evaluated for economics through Matlab with a penalty for infeasible solutions. Even though this modeling and optimization structure requires a lot of computation time to find a global solution, it is suitable to show the difference between the two approaches and compare the results. In this SMR process, there are four types of physically infeasible regions, which are 1) a case without solution (divergent

system), 2) a case with a temperature cross at main heat-exchanger, 3) a case with gas inflow to compressor, and 4) a case with a very low temperature value after the inter-cooler.

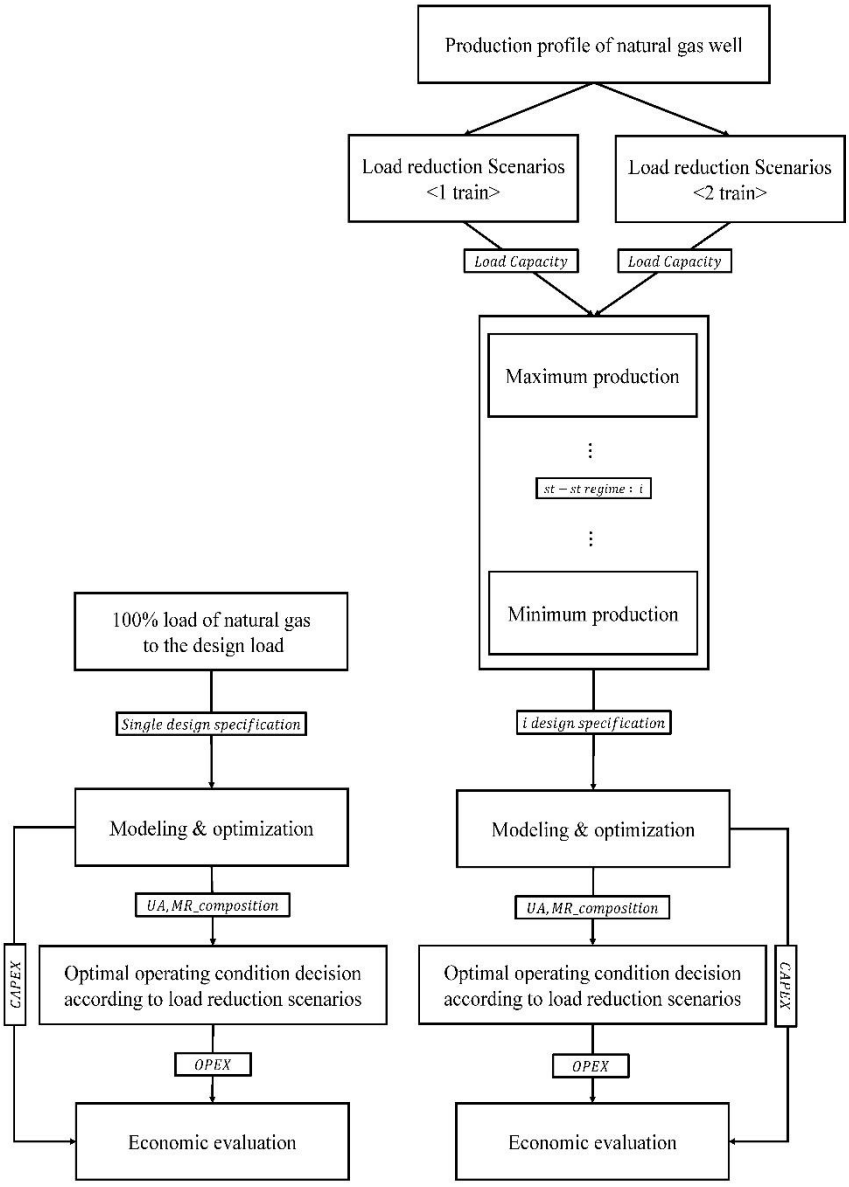

Figure 2-3. Optimization framework for the traditional (left) and proposed (right) design approaches

2.3.2. Optimization Formulation

2.3.2.1. Optimization for unit sizing and MR composition

The goal of optimization is to determine the unit size and MR composition to maximize the net present value (NPV) of the process.

$$\min_{x\in\mathbb{R}^{1\times n}} -\mathrm{NPV} - \gamma \mathrm{p} = \mathrm{f}(x) \qquad \text{(P1)}$$

subject to

$$\mathrm{A}\mathbf{x} = b$$

$$x_{LB} \le x \le x_{UB}$$

$$\mathrm{h}_p(x) = 0 \quad p = 1,2,3,\dots,m$$

$$h_j(x) = 0 \quad j = 1$$

$$g_i(x) \le 0 \quad i = 1,2,3,\dots,7$$

$$\mathrm{p}(x) = \begin{cases} 0 & if \quad h_p(x) = 0 \; and \; g_i \le 0 \; and \; s_k(x) = 0 \\ 1 & if \quad h_p(x) \ne 0 \; and \; g_i > 0 \; and \; s_k(x) \ne 0 \end{cases}$$

h_p, h_j, and g_i represent convergence of the process simulator, an equality constraint, and inequality constraints. x is an optimization variable vector to be determined. This includes the heat exchange area (Xenos et al.) for determining the size of the heat exchanger, the pressure ratio to determine the size of the

compressor, the MR composition, and the operating parameters to be determined again in the next step. In the case of using a maximum production rate, only 8 are the optimization variables because optimization is performed based on a single steady-state regime in the process flowsheet. The objective function is the calculated NPV value at the maximum production rate, as in many other existing studies. On the other hand, in the case of considering the load reduction, there are 14 optimization variables corresponding to all three models of different production rates. NPV is determined by weighted average of the NPV values of the three models, and only the unit sizing data of 100% load is used for the unit cost included in the NPV calculation. The ratio of the NPV of the three models is determined by the shape of the production profile of the gas field well and can vary depending on which profile is used. However, in general, it is difficult to know the production profile of the well in the process design stage, and the equal weights, i.e., 1: 1: 1, were used in this study. Since the purpose of this step is to determine the optimal unit cost and composition of MR for each case, rather than quantitative comparison of each case, we do not need an exact ratio of the three objectives. A and b represents the mass balance of MR compositions. Table 2-2 shows the lower and upper bounds of the optimization variable and design constraints of one- and two-train cases. Design constraints include the gas inflow into the compressors, the temperature cross of the heat exchanger, and the temperature constraints of the MR_hot stream entering the heat exchanger. In order to increase the model convergence

in the optimization process and to avoid getting stuck in a local minimum, a penalty term γp is added to the objective function if the process simulator determines that at least one stream or units isn't converged, the design constraint is violated, or the set of variables is infeasible, it sets p(x) as 1 to activate the penalty value γ. For the GA, 50 populations, 0.8 of the crossover fraction, and 20 of the maximum generation were used (Na et al., 2017). The GA algorithm is terminated if the average relative change in the best fitness function value over stall generation value is less than or equal to TolFun (default value 1e-6) or the number of generations has reached the maximum generation value. The optimization was carried out using Aspen Hysys v8.8 and MATLAB R2016a on a PC with Intel® Core™ i5-4590 CPU at 3.30 GHz and 6 GB RAM running Window 10.

Table 2-2. Design variables, their bounds, and constraints

Design variables	Standard load	Unit	Lower bound	Upper bound
MR flowrate (one-train)	Common	10^2 kgmol/hr	150	400
MR flowrate (two-train)	Common	10^2 kgmol/hr	50	200
MR Composition	Common	mol%		
Methane			24	27
Ethane			35	38
Propane			3	6
n-butane			20	25
Nitrogen			18	4
UA (one-train case)	Common	10^7 kJ/°C-hr	4	5
UA (two-train case)	Common	10^7 kJ/°C-hr	2	3
Condenser pressure	Max	bar	30	45
P(MR_cold_in)	Max	bar	3	5
Condenser pressure	Mid	bar	25	40
P(MR_cold_in)	Mid	bar	3.5	4.5
Condenser pressure	Min	bar	20	40
P(MR_cold_in)	Min	bar	3.5	4.5
Design constraints				
$\Delta T_{min} \geq 3℃, minimum\ intermal\ temperature\ approach\ (temperature\ cross)$				
$\mathrm{LMTD} \geq 3℃, \log mean\ temperature\ difference\ \ (temperature\ cross)$				
$T_{MR_{cold_{out}}} \geq T^{dew}_{MR_{cold_{in}}} + 3℃\ (vapor\ fraction\ at\ 1st\ compressor)$				
$T_{MR_{hot\_in}} \geq 40℃$				
$P_{MR_{cold\_in}} \leq P_1 \leq P_2 \leq P_{MR_{hot\_in}}$				
$\sum m_j = 1,\ \ j \in chemicals\ in\ MR$				

2.3.2.2. Determine operating variables according to load reduction scenario

The objective of the optimization in this step is to determine the operating variables with minimum operating costs per year according to the load reduction scenario after fixing the device size and MR composition determined in the previous step.

$$\min_{x \in = \mathbb{R}^{1\times 4}} \mathrm{W}_c + \gamma \mathrm{p} = \mathrm{f}(x)$$

subject to

$$x_{LB} \leq x \leq x_{UB}$$

$$h_p(x) = 0 \quad p = 1,2,3,\dots,m$$

$$g_i(x) \leq 0 \quad i = 1,2,3,\dots,7$$

$$\mathrm{p}(\mathbf{x}) = \begin{cases} 0 & if \quad h_p(x) = 0 \; and \; g_i \leq 0 \; and \; s_k(x) = 0 \\ 1 & if \quad h_p(x) \neq 0 \; and \; g_i > 0 \; and \; s_k(x) \neq 0 \end{cases}$$

x is the optimization variable vector to be determined, including the pressure ratio, the pressure of the MR_cold entering the heat exchanger, and the flowrate of the MR. W_C means the amount of power to pressurize the MR after heat exchange. The power of the compressor is set as the objective function because it accounts for the largest portion of the operating cost of the LNG liquefaction process. Lower and upper bounds and design constraints of the optimization

variables are the same as those described in Chapter 2.3.2.1, and the penalty function and optimization solver are also the same. In this study, there are four cases to compare, including one-train and two-train cases applying a conventional approach and one-train case and two-train cases applying design method considering load reduction, as mentioned in Chapter 2.2.1. Table 2-3 shows load variation trends in two wells with only the different production profile in nearly same range of production rate. For the same gas field well, one-train case and two-train case have different load reduction scenarios for the same production profile. One-train case requires capacity up to 23.7% load based on 1 MTPA. In the case of a two-train case, it is possible to design with less capacity because it has a range of up to 47.4% load based on 0.5 MTPA. For each of the four cases, the optimum operational expenditure (OPEX) for each year is calculated through iterative optimization according to this load change scenarios.

Table 2-3. Feed natural gas specifications and design assumptions

Year	Maui gas field			Kapuni gas field		
	one-train [MPTA]	two-train [MPTA]		one-train [MPTA]	two-train [MPTA]	
		Train 1	Train 2		Train 1	Train 2
0 (excluded)	0.094	0.237	0.000	0.067	0.067	0.000
1 (excluded)	0.126	0.237	0.000	0.128	0.128	0.000
2 (excluded)	0.176	0.237	0.000	0.176	0.176	0.000
3	0.355	0.355	0.000	0.239	0.239	0.000
4	0.376	0.376	0.000	0.241	0.241	0.000
5	0.501	0.264	0.237	0.640	0.500	0.140
6	0.646	0.409	0.237	1.000	0.500	0.500
7	0.781	0.500	0.281	0.927	0.500	0.427
8	0.758	0.500	0.258	0.459	0.459	0.000
9	0.824	0.500	0.324	0.304	0.304	0.000
10	0.851	0.500	0.351	0.379	0.379	0.000
11	0.841	0.500	0.341	0.493	0.493	0.000
12	0.863	0.500	0.363	0.554	0.487	0.067
13	0.923	0.500	0.423	0.565	0.498	0.067
14	0.883	0.500	0.383	0.625	0.500	0.125
15	0.801	0.500	0.301	0.602	0.500	0.102
16	0.745	0.500	0.245	0.568	0.500	0.068
17	0.845	0.500	0.345	0.668	0.500	0.168
18	0.893	0.500	0.393	0.730	0.500	0.230
19	0.757	0.500	0.257	0.710	0.500	0.210
20	0.905	0.500	0.405	0.742	0.500	0.242
21	0.956	0.500	0.456	0.793	0.500	0.293
22	1.000	0.500	0.500	0.778	0.500	0.278
23	0.912	0.500	0.412	0.835	0.500	0.335
24	0.617	0.380	0.237	0.692	0.500	0.192
25	0.540	0.303	0.237	0.843	0.500	0.343
26	0.476	0.476	0.000	0.726	0.500	0.226
27	0.451	0.451	0.000	0.717	0.500	0.217
28	0.271	0.271	0.000	0.679	0.500	0.179
29	0.257	0.257	0.000	0.219	0.219	0.000
30	0.281	0.281	0.000	0.241	0.241	0.000
31	0.237	0.237	0.000	0.640	0.500	0.140

2.3.3. Economic Evaluation Model

The basic economic objective function is to maximize net present value (NPV) of the liquefaction process. The majority of previous studies have focused on minimizing the power consumption, which omits the consideration of capital investment in the design stage and consequently worsens optima (Park, 2015). Since NPV is the sum of the future value of the selected process at the time of design and the investment cost, it is appropriate to compare the approach used in this study.

$$\text{NPV} = \sum_{I=1}^{N} TACF_i \times \beta_i + \sum_{j=-2}^{-1} TACF_j \times \beta_j + TACF_0 \times \beta_0 \qquad \text{(Eq. 2-1)}$$

NPV is calculated as the product of the total annual cash flow and the present value factor ($\beta_{i,j,0}$). The value of the total annual cash flow (TACF) from -2 to 0 is determined by the value of the fixed capital investment and is determined in Chapter 2.3.2.1. On the other hand, the value of TACF from 1 to N (operating life time) is determined as

$$TACF_i = AOCF_i = AGP_I \times (1-\theta) + AD_i \qquad \text{(Eq. 2-2)}$$

$$AGP_1 = AS_1 + ATPC_1 - AD_1 - SC \qquad \text{(Eq. 2-3)}$$

$$AGP_k = AS_k + ATPC_k - AD_k \ (\text{k} = 2, \dots, 6) \qquad \text{(Eq. 2-4)}$$

$$AGP_k = AS_k + ATPC_k \ (\text{k} = 7, \dots, \text{N}) \qquad \text{(Eq. 2-5)}$$

Θ denotes the tax rate, SC denotes the start-up cost, and AD_i denotes the annual depreciation. The value of the annual depreciation factor is referred to as the Modified Accelerated Cost Recovery System (MACRS) (IRS, 2015). According to the MACRS, depreciation from 1 to 6 years is deducted. The main determinants of TACF are annual sales (AS) and annual total production cost (ATPC). AS is calculated by the amount of LNG produced annually, and ATPC is calculated by the amount of utility cost, the amount of natural gas, and the equipment cost. In the conventional NPV calculations, the fixed value is used without reflecting the change of the production rate of the gas field well and only the economic conversion of the future value and the past value is considered. In this study, for the accurate comparison of the two different design approaches, the optimum operating cost for each year determined according to the changing load is reflected in the NPV calculation. First, in Chapter 2.3.2.1, determine the optimum equipment cost and MR composition for each case. Next, by assigning AS and ATPC, which are calculated according to the optimum operating conditions determined in Chapter 2.3.2.2, to Eq. 2-1 to 2-5, the economics model can consider load reduction scenarios. As the currency unit, millions of U.S. dollars is used for all values of economic evaluation. The equipment cost estimation approach is adapted from Couper, (2005) and Peters et al., (2003)

2.4. Result and Discussion

2.4.1. Optimization Results

2.4.1.1. Capital cost analysis

Figure 2-4 shows the objective function value versus function evaluation of each case as GA runs in the first optimization step. The objective function of case 1 and case 3 using the traditional design approach based on fixed single design loads, 1 MTPA and 0.5 MTPA respectively, is minimization of (-) NPV_max (net present value at fixed single design load). Each time function evaluation is repeated, the MR composition and the equipment size are determined to yield the maximum profit at 100% design load. Conversely, the objective function of case 2 and case 4 using the new design approach considering load variation is a linear combination of (-) NPV_max, (-) NPV_medium and (-) NPV_min. We determine the optimum equipment size and MR composition considering load variation by setting the objective function to maximize the profit at three different design loads. The purpose of this step is to compare the capital cost between the result of the new design approach and that of the traditional approach. Therefore, the specific value of NPV for each case in Figure 2-4 is not subject to comparison but to determine if the objective function value is nearly unchanged as the solver runs. All four cases have undergone the same number of iterations (1550), but the resulting number of iterations is different because evaluation results that do not converge or violate the design constraints were excluded.

Figures 2-5 and 2-6 show the differences in key economic variables and MR composition optimization results for the one-train scenario (cases 1 and 2) and the two-train scenario (cases 3 and 4), respectively. The different design approaches described above determine the installation cost of the main heat exchanger and other pieces of equipment and the composition of the MR, which are fixed even as the load variation scenario is changed. The optimal design considering load variation uses smaller heat exchange area, which leads to a decrease in the equipment cost of main heat exchanger. However, it also leads to an increase in the MR flowrate under 100% load operation and leads to an increase in the compressor equipment cost. In the case of a one-train, the price increase of the compressor is larger than the price reduction of the heat exchanger, which makes the total capital investment become larger. However, in the case of two-train, the decrease in the price of heat exchanger is similar, but the increase of the compressor price is smaller than that of the one-train case. This difference can be found in the optimal MR flowrate change shown in Table 3-4. In the two-train case, the MR flowrate increase was smaller than that of the one-train case when the new approach was applied (one-train case: 22% increase, two-train case: 9% increase). The increase in MR flowrate resulting from the application of the new approach reduces operating costs at 100% load operation and equipment costs of the other units except the heat exchanger to account for load variation. Therefore, the two-train cases have less load variation than the one-train case, which causes a relatively small loss in

the equipment cost of the compressor. This is offset by a reduction in the equipment cost of the heat exchanger provided by the small heat exchanger area, and thus has less total capital investment.

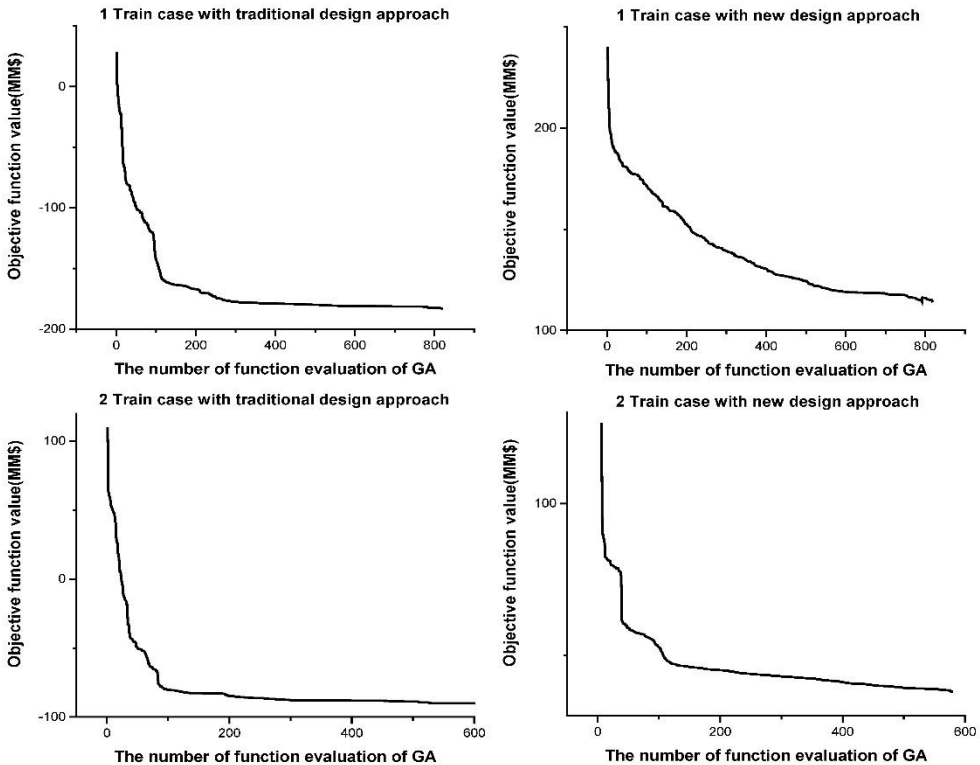

Figure 2-4. Best-found solution trajectories of objective function values of NLP problem through function evaluation on 4 cases

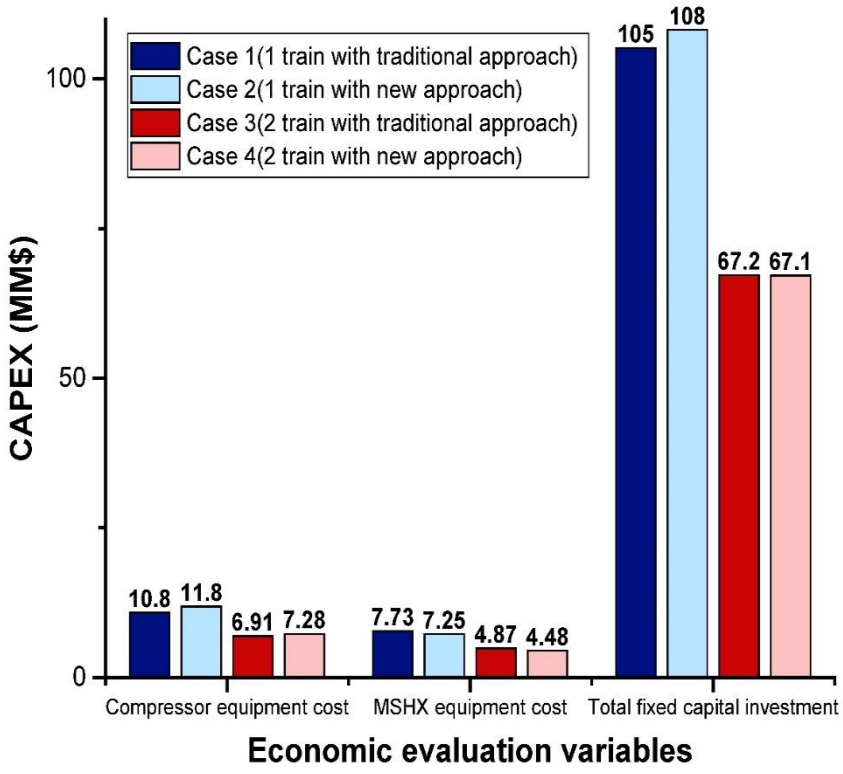

Figure 2-5. Key economic variables related to CAPEX

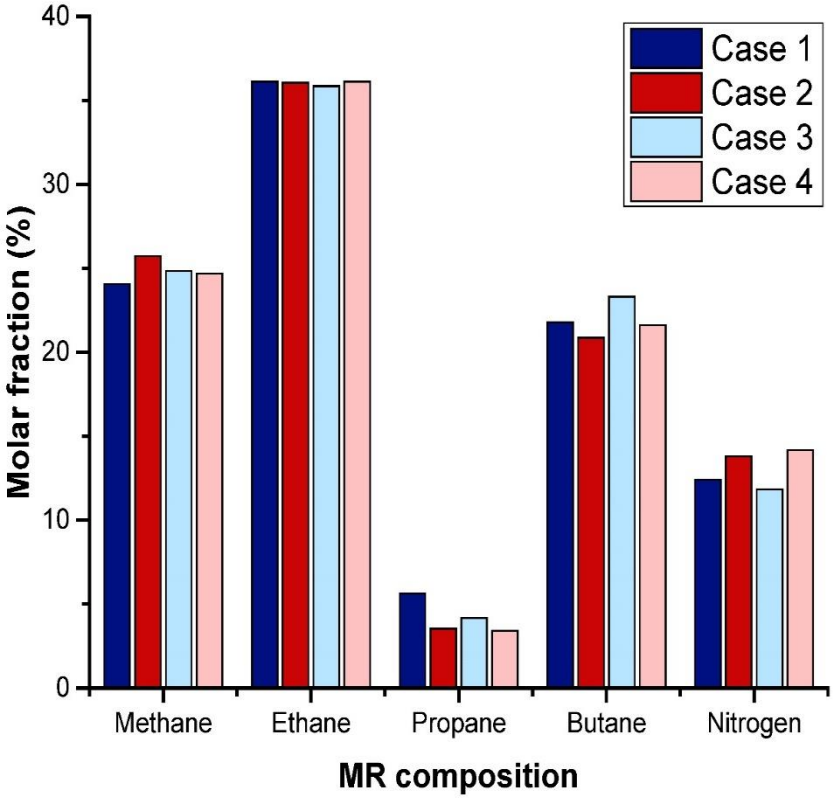

Figure 2-6. Comparison of MR composition

Table 2-4. Best-found solutions of decision variables at the production of 1 MTPA

Optimization variables	Unit	Case1	Case2	Case3	Case4
MR	mol%				
Composition					
Methane		24.1	25.7	24.8	24.7
Ethane		36.1	36.1	35.8	36.1
Propane		5.6	3.5	4.2	3.4
n-butane		21.8	20.9	23.3	21.6
Nitrogen		12.4	13.8	11.8	14.2
UA	10^3 kJ/°C·hr	45,886	42,043	24,770	22,213
Condenser pressure	bar	41.1	41.3	42.5	43.7
MR flowrate	10^2 kgmol/hr	201.0	246.4	110.3	121.8
P(MR_cold_in)	bar	3.4	3.8	3.8	4.0

2.4.1.2. Annual energy consumption analysis

Figure 2-7 shows the amount of power in the compression stage depending on the load at one- and two-trains. The power consumptions are decreased as the load decreases in all cases, but it is not in the linear relationship. This is because the heat exchanger size and design constraints require the minimum amount of heat exchange. Even if the load is reduced to 23%, the flowrate of the MR required should be 60-70% of maximum MR flowrate. Therefore, it is difficult to operate economically because a large amount of operating cost is required compared to the production amount of LNG under small load operation. The new design approach proposed in this study can secure economical operation at nearly minimum load while giving up some economic efficiency in operating cost at a load close to 100% and capital investment. As can be seen from the result of one-train, more amount of power is consumed in the operation of the process designed by the proposed approach at a large load over 80%. However, for the load between 23% (minimum) to 70%, the process operation of the suggested design approach is more economical. On the other hand, in the cases with two-train, it is more complicated to compare the two design approaches. This is because the increase in the number of trains leads to an increase in the number of operation scenarios. Therefore, in the case of two-train cases, it is necessary to analyze the results of the two design approaches by dividing the sections in load. The section 1 is set to operate at near maximum load (0.5 MTPA) where both trains are in operation. The intermediate load can

be divided into two cases, with or without two-trains, which are called section 2 and section 3, respectively. Finally, the area near the minimum load, which should only be operated by a single train, is section 4. In section 1, it is more economical to operate the process based on the traditional design approach, as in one-train case. However, section 2, which requires one-train to run at maximum load and the other train to handle the natural gas load reduction, is different from section 1. This is because the gap between the min-max load of the two-train cases is close to that of the one-train case. Hence, the train responsible for handling load variation is mainly operated near the minimum load. Therefore, the proposed approach for the low load handling train is more economical. Sections 3 and 4 show the same tendency with the one-train case because it is a single train operation. In section 3 where the load is relatively large, the traditional approach is more efficient, but the section 4 near the minimum load shows the opposite result. The reason why the result of the proposed approach is advantageous as the load decreases in a single train is due to the shift in the optimization result to a smaller heat exchange area, as mentioned above. The reduction of the heat exchange area leads to an increase in the MR flowrate under 100% load operation. This causes more power to be consumed in a flowrate of 80% or more. However, design with a small heat exchange area can satisfy the design constraints under small load operation even with less amount of MR flowrate due to the reduction in the amount of heat exchange per hour. This can be confirmed by the trend of the MR flowrate

according to the load changes in the one-train and two-train cases in Figure 2-8. In the case designed with the traditional approach, the flowrate of the MR tends to continuously increase as the load decreases. However, in the case designed with the proposed approach, the flowrate tends to slightly decrease to 60-70% of the MR flowrate at the maximum load, and then the flowrate tends to increase in the small load operation. This is also the result of the shift of the optimized solution to the small heat exchange area, and the optimized heat exchange area allows for more optimized operation in the intermediate level load operation. Therefore, the process design considering load reduction scenarios can prevent an excessive increase in operation cost caused by small load operation. The changes in MR flowrate for each load are closely related to the robust operation performance of the process. A dramatic change in the MR flowrate can interfere with safe operation in the compression stage consisting of multi-stage compressors. In both one-train and two-train cases, the variation of the MR flowrate according to the load is less in the new approach. Especially, in the two-train cases including less load variation, there is almost no difference in MR flowrate between min-max load. This also demonstrates the reduction in capital investment in the two-train case using the new approach discussed in Chapter 2.4.1.1. Even with the new approach applied, operation near minimum load cannot avoid an increase in MR flowrate. However, since the gap to the minimum load is smaller than that of the one-train case, the increase of the MR flowrate can be minimized.

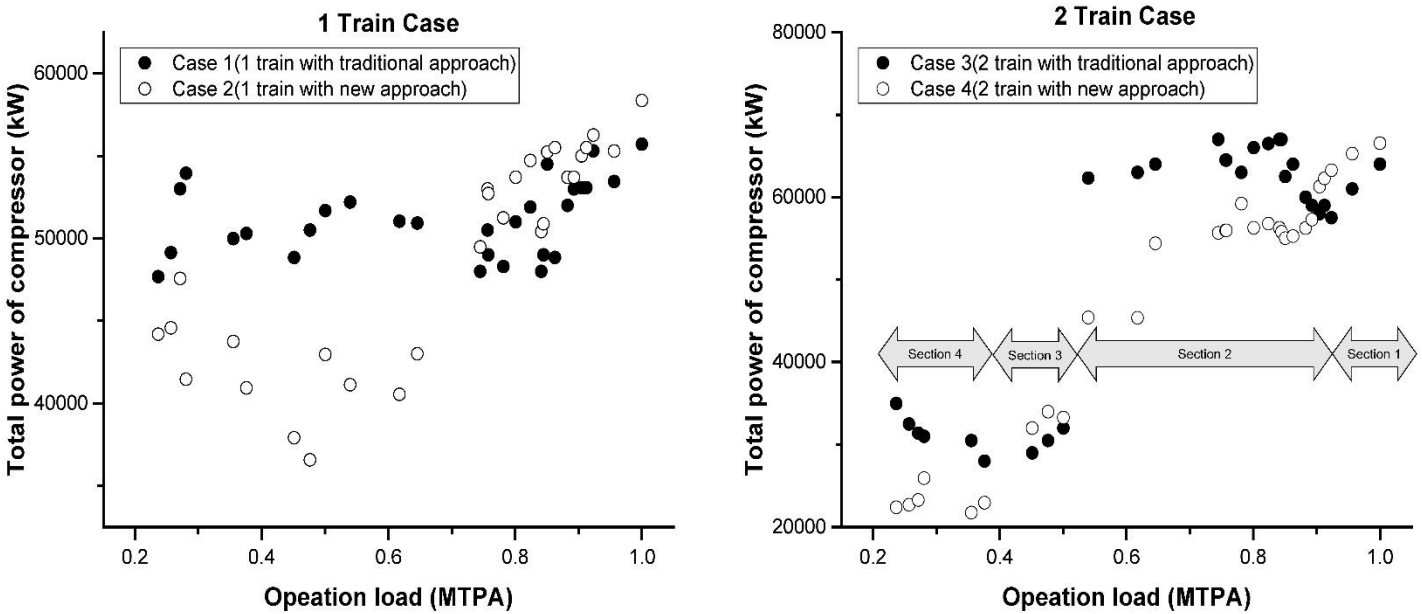

Figure 2-7. The power consumptions in compression stage depending on the load at 1 train and 2 train cases

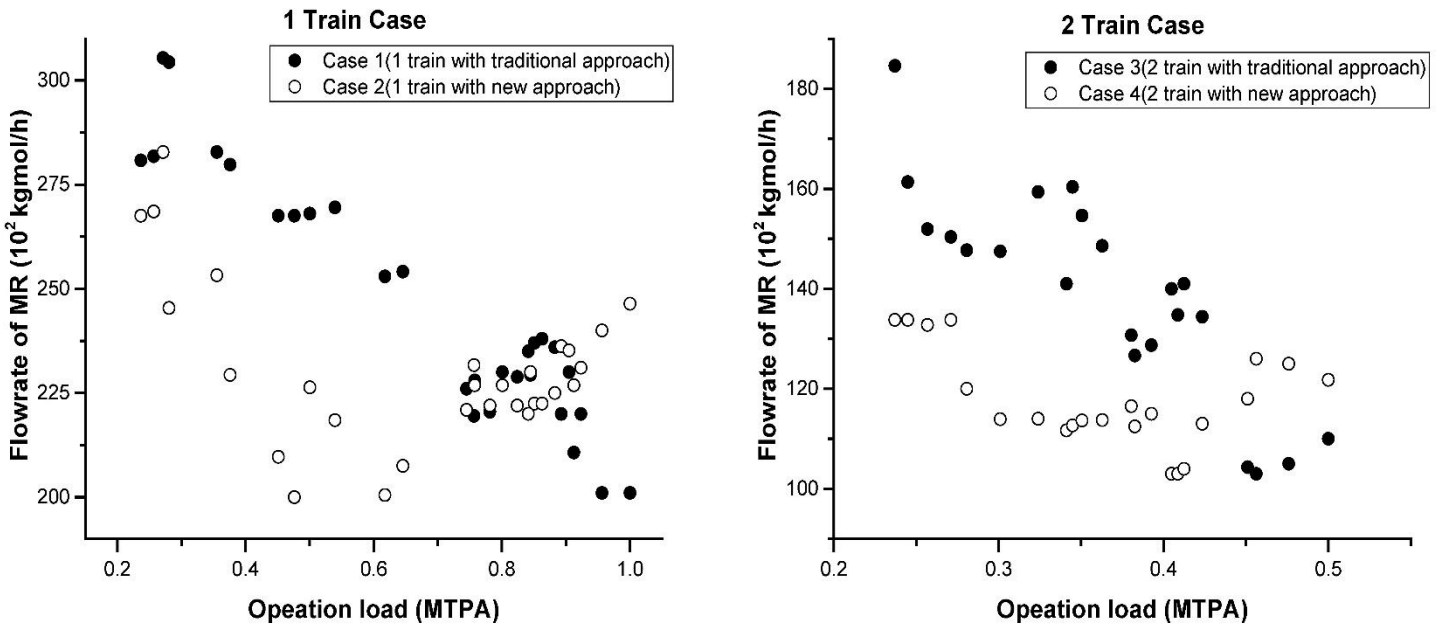

Figure 2-8. The MR flowrate depending on the load at one-train and two-train case

2.4.2. Case Study: Maui and Kapuni Gas Field

Figure 2-9 shows the cumulative discounted cash flow for operation years for the Maui gas field and the Kapuni gas field, and Table 2-5 is the net present values of the cases 1 to 4. The NPV was calculated based on the year when the profit was maximized for each case and well. So, it is the same as the cumulative discounted cash flow at the last profitable year. In the case of Maui gas field, the last profitable year of one-train cases (cases 1 and 2) is 21 years after operation and 20 years for two-train cases (cases 3 and 4). In the case of the Kapuni gas field, cases 1, 2, 3, and 4 have values of 28, 29, 26, and 28, respectively. The profitable operating year is long in one-train case where the equipment cost is low overall, and it can be confirmed that it is lengthened in the case of applying the design approach proposed in this study. In cases 3 and 4 of the Maui gas field where the total NPV is negative, the sum of the total revenues during the operation year does not exceed the investment in the unit cost. This means that the design of the process should take into account the decline in the price of LNG.

As mentioned earlier, process design based on the suggested design approach has higher equipment and installation costs than using the traditional design approach in one-train case. In the two-train cases, however, there is almost no increase in the investment cost due to the proposed design approach. As a result, the cumulative cash flows of both approaches are similar. As we have analyzed

in Chapter 2.4.1.2, the design considering the load variation gives more profit than the traditional design in the operation of less than 80% load in both one-train and two-train cases. Conversely, traditional design is more economical when operating over 80% load. This means that process design considering load variation can be more economical in a wider operating region. In the case of one-train, it can be seen that the economic trend of the new approach and the traditional approach can be changed depending on the type of natural gas well. In the case of Maui gas field, the natural gas production in most operation hours is between 0.8 and 1 MTPA. Therefore, a process designed by the traditional design approach is more economical. In the case of Kapuni gas field, it supplements the production of depleted wells by installing additional wells starting from 10 years after operation (Ministry of Business Innovation and Employment, 2014). In this way, the economic efficiency of the process design considering the load variation is better than that of the process using the traditional approach in the case of the wells where most of the production years are less than 80% of the maximum load. This means that the economic benefits of the proposed approach can exceed the economic loss from the installation cost according to the shape of production curve. It should be noted that in most cases, the production cycle of the gas field cannot be accurately predicted prior to the process design stage. Therefore, the design approach that takes account of load variation is economical in a wider operating window, and it is possible to respond effectively to a wider variety of well production shapes.

On the other hand, the proposed approach clearly shows the economical efficiency of the two-train. There are two main reasons for the different results depending on the number of trains. The first is due to the less capital investment of the design with the new approach, and the second is due to the difference in the operation scenarios of the one-train case and the two-train cases. For example, when operating at 0.85 MTPA, the operating cost of a one-train case model with a traditional approach is lower. However, the overall operating cost is better in the new approach because the two-train case operates at 0.5 MTPA and 0.35 MTPA, respectively and the gain at 0.35 MTPA is greater than the loss of operating costs at 0.5 MTPA (100% load). Therefore, in the two natural gas wells applied in this study, the economical efficiency of the two-train case using the new approach could be improved. Also, as the number of trains increases, the probability of each train operating near the minimum load increases, so the economics of the proposed design approach is expected to be even better. But this can also be varied depending on the well production shape and the operation scenarios of each train.

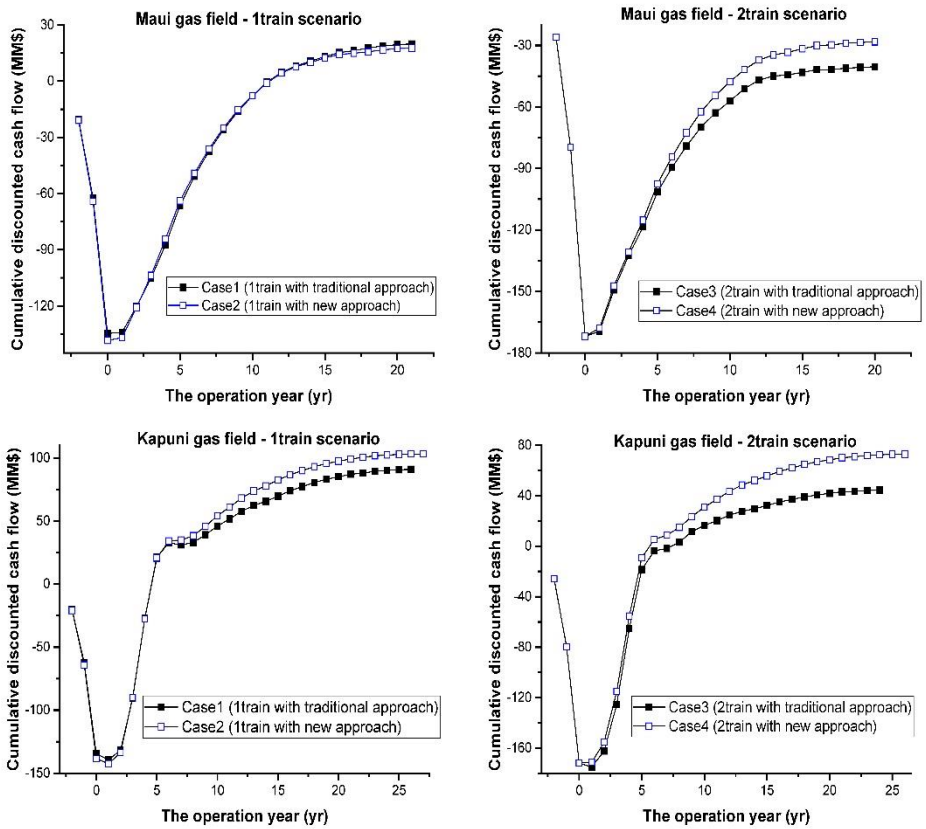

Figure 2-9. Cumulative discounted cash flow profile of Maui gas field and Kapuni gas field

Table 2-5. Net present values of Maui and Kapuni gas fields production

Name of gas field	Case 1	Case 2	Case 3	Case 4
Maui (opeartion year) (LNG 5$/TCF)	20MM$ (21yr)	18MM$ (21yr)	-40MM$ (20yr)	-28MM$ (20yr)
Kapuni (operation year) (LNG 7$/TCF)	90MM$ (28yr)	103MM$ (29yr)	44MM$ (26yr)	73MM$ (28yr)

2.4.3. Compressor Operability

Figures 2-10 and 2-11 show the operating point profile with load variation at each compressor stage. The left figure is the trend of the system designed according to the traditional 100% load design approach and the right is the result of the system designed according to the approach proposed in this study. In order to compare the results of the above dynamic simulation, the shift of the characteristic map due to the change of the compressor size should be considered. However, it is difficult to obtain the data of the compressor characteristic map in the changed size. Also, because the purpose of this chapter is to see the movement of the operating point, we have modeled the compressor characteristic map through the numerical equation of the compressor.

$$P2 = f(U1, M, U2) \times P1 = (1 + (\eta\_C \times H(ideal))/(C\_p \times T1))\text{^}(\gamma/(1-\gamma)) \times P1 \quad \text{(Eq. 2-6)}$$

$$H(ideal) = f(U2) = \sigma \times (U2)\text{^}2 \quad \text{(Eq. 2-7)}$$

$$\eta\_C = f(M, U1) = A \times M\text{^}2 + f(U1) \times M + f(U1\text{^}2) \quad \text{(Eq. 2-8)}$$

Equation 2-6 shows the relationship between the discharge pressure and the suction pressure of the compressor. The energy supplied during the compression process is a function of the rotational speed proportional to the radius of the compressor and the compression efficiency determining the energy used for the actual pressurization is a function of the compression flow rate and

the rotational speed of the inlet. Therefore, the enthalpy supplied was calculated according to the increasing compressor size. Also, the parameters of equation 2-8 were estimated from the existing characteristic map. We have modeled a new compressor characteristic map on the assumption that the same parameters are used.

The change of the operating point is determined by the operating variables determined by the optimization step. In the first stage, the temperature and pressure of the stream entering the compressor are determined by the degree of heat exchange. Therefore, the variation of the change of the compression flow into the 1st stage becomes larger than the 2nd stage. This can be confirmed by the degree of change of the operation point. In addition, the operating efficiency of the compressor increases as the operating point approaches the surge line. As can be seen from the figure, the operating efficiency of the compressor itself decreases as the load decreases. Therefore, it would be an important point to improve the efficiency of the system by providing a compressor with a characteristic map that can operate more efficiently according to the change in the operating point.

However, the important part of this chapter is the operating of the driving point's own profile. Frequent changes of the operating point are one of the factors that interfere with the robust operation of the compressor itself. In particular, in the case of a compressor which must be operated within a suitable

operating range, such frequent and large changes of the operating point are very fatal since they increase the likelihood of malfunctioning such as surge. As can be seen from the figure below, the system with the design approach that considers the load variation has a smaller deviation than the existing design approach. This means that the proposed methodology designs a compressor system that can operate more robustly. Therefore, it is necessary to design the system considering these parts in the design stage, so that the operability of the system including the compressor can be improved.

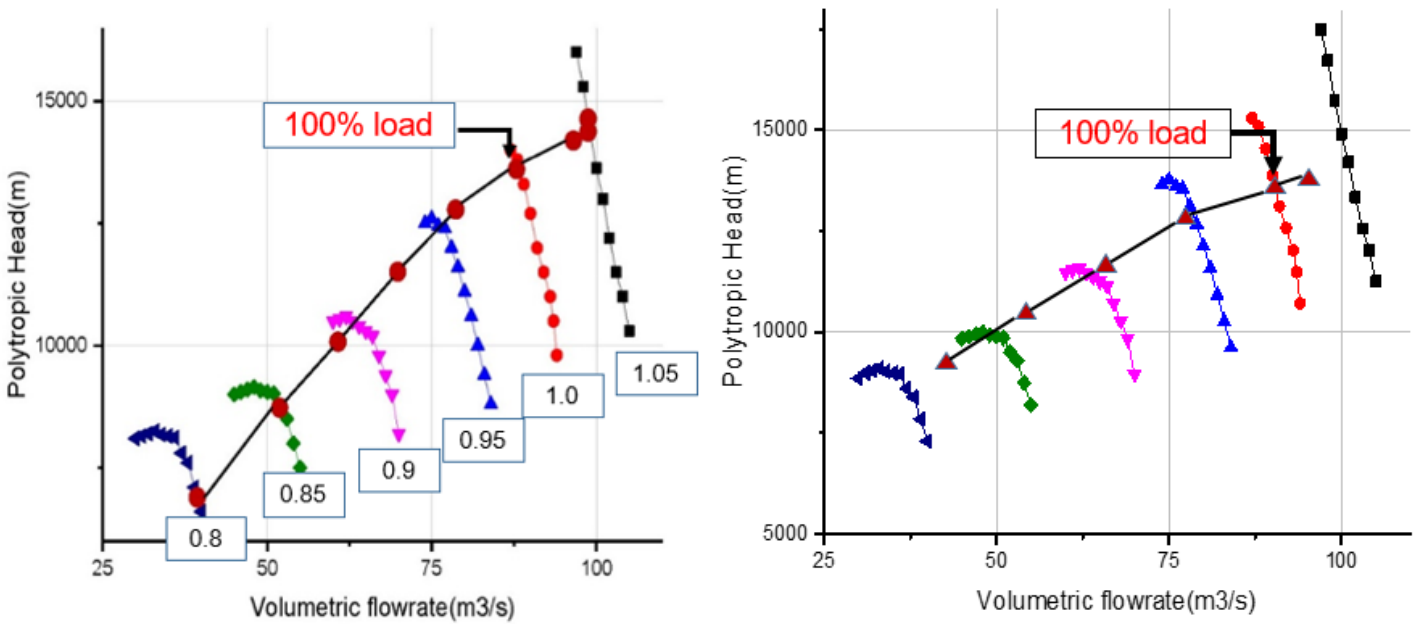

Figure 2-10. Operating point profile of 1st stage of compressor along load: left (traditional) & right (suggested)

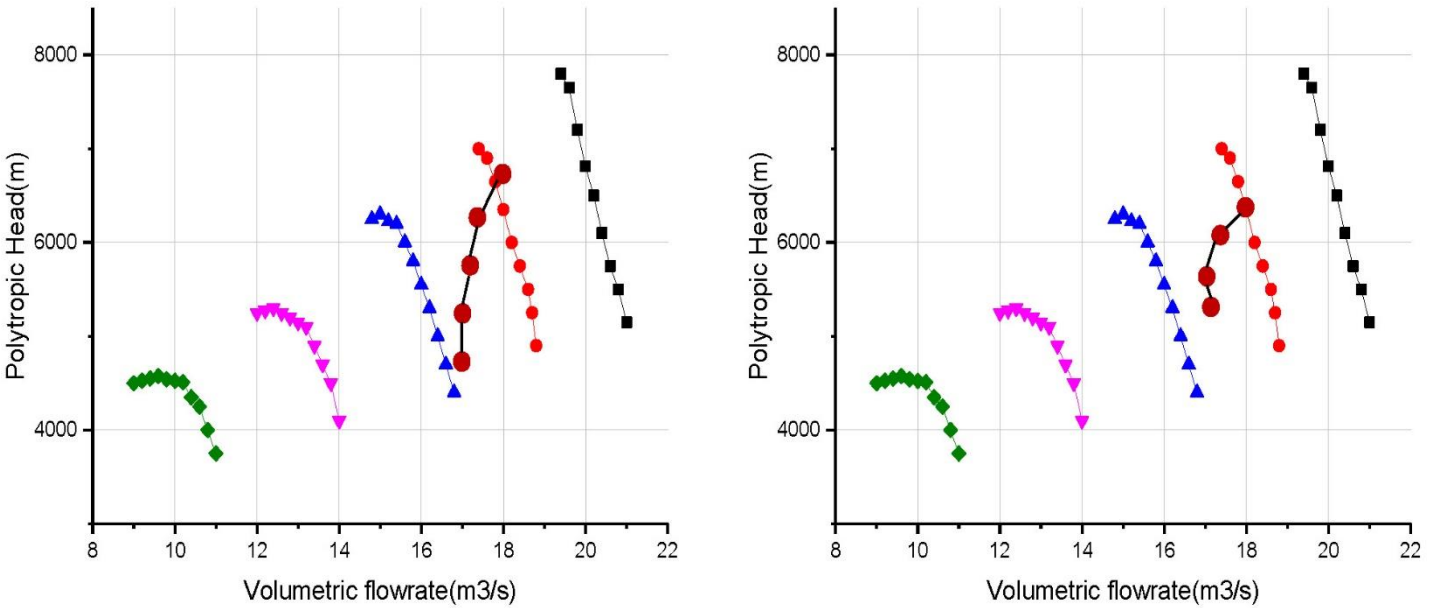

Figure 2-11. Operating point profile of 2nd stage of compressor along load: left (traditional) & right (suggested)

CHAPTER 3. Modeling of Industrial-scale Multi-stage Compression System using Neural Network*

3.1. Introduction

Compression systems are one of the essential units in chemical processes. In general, the primary purpose of a compressor in a compression system is to pressurize the target material to the desired pressure, and various types of compressor, e.g., centrifugal compressors, reciprocating compressors, rotary compressors, etc., are used according to the conditions of a given process (Gravdahl & Egeland, 2012). Among them, centrifugal compressors are most widely used to compress and supply a significant amount of air and gas at high pressures in various chemical processes. They are combined with drivers such as steam turbine, gas expander, and electric motor to form air and gas supply net- work (Han et al., 2004). In particular, 75–85% of the total electric power consumption of the TPA (Terephthalic Acid) process is consumed by the air and gas supply network, and the compression system plays an essential role but consumes a significant amount of power (Kroschwitz & Howe-Grant, 1991).

* This chapter cites the author's published journal article: Lee, W., Na, J., Kim, K., Lee, C., & Lee, J. (2018). NARX modeling for real-time optimization of air and gas compression systems in chemical processes. Computers and Chemical Engineering, 115, 262-274.

Therefore, optimal operation of a compression system is important, and many studies have been conducted. Leducq et al. (2006) proposed a predictive optimal control algorithm using a non-linear model of the vapor compression unit in the refrigeration system. He et al. (1998) constructed a simple low-order dynamics model of the vapor compression system and designed the optimal MIMO (Multi-input and Multi-output) against disturbances. Also, Romeo et al. (2009) conducted a study to minimize the amount of power consumed in carbon dioxide multi-stage compression systems in the carbon capture and storage (CCS) process. At the core of this optimal operation study is the modeling of a compression system, and in particular, a model that accurately predicts total energy consumption given the operating condition is required. However, in an industrial scale multi-stage compression system, it is impossible to predict the performance of a system only through a model based on first-principle equations. In the case of a multi-stage system, it is difficult to accurately monitor the state of the system because all the variables inside the system cannot be precisely sensed. This also poses a challenge for model validation. Meanwhile, such a complex first-principle model is also difficult to apply to real-time optimization because of its complexity and reliability when key parameters are changing in a stochastic manner due to aging, exogenous disturbances, etc. To solve these problems, several studies have been conducted that design a data-driven black box model of compression system (Ghorbanian & Gholamrezaei, 2009; Gresh, 1998; Han & Han, 2003; Xenos et al., 2015).

However, these models focus on nonlinear function fitting, especially using a feed-forward multi-layer perceptron neural networks structure. Because these regression tools are not designed with stochasticity, e.g., aging of equipment and time-varying disturbances, in mind, they can suffer from significant deviations from the real plant data.

Basically, an industrial scale multi-stage compression system has a complex nonlinearity. This is due to the complex correlation of the unknown state parameters of the compression stage and the expansion stage (for power generation) that make up the compression system. Thus, the linear modeling method using only the input-output of the system is difficult to simulate this complex nonlinearity. Furthermore, the state of each stage is also affected by a number of stochastic trending factors. Stochastic factors such as aging of equipment or external environment affecting the efficiency of the compression system tend to be time-dependent in nature. Therefore, in order to design a model that accurately predicts the energy consumption of a multi-stage compression system, it is necessary to use a nonlinear technique to simulate the complex nonlinearity of the system, as well as a modeling method that can reflect time-varying factors. In this respect, the purpose of this study is twofold. First, we perform regression and prediction of a multi-stage compression system in air and gas supply network using Nonlinear Autoregressive eXogenous Neural Net (NARX NN) model for time-series data-driven modeling. Furthermore, we do not use all the sensor data but perform feature

extraction by combining a first principle model with the sensor data. This solves the problem of extrapolation and model overfitting. The predictive performance of the model is verified by comparing it with the feed-forward multi-layer perceptron neural networks and the NARX NN model without feature extraction. The second goal is to calculate an optimal operating condition of the air and gas supply network consisting of five multi-stage compression systems using the NARX NN prediction model. We propose a Real-Time Optimization (Puig-Arnavat et al., 2010) strategy that continuously updates the model with the optimal operating conditions verified by the actual data and repeatedly finds the operating condition at the next time step. This proposed NARX-RTO methodology is validated by virtual plant based on actual plant data set.

3.2. Problem Description

3.2.1. Process description

Fig. 3-1 shows the schematic structure of the air-gas supply network in a commercial TPA manufacturing plant in Korea (Han et al., 2004). This air-gas network, which serves to supply a large amount of compressed air and gas, is utilized in various chemical processes. The network used in this study consists of a total of five multi-stage compression systems, and the configuration of each system is summarized in Table 3-1 (Han et al., 2004). The compressed air mainly enters the oxidizer to initiate the reaction. More than 90% of the off-gas

generated after the reaction is composed of inert high-pressure nitrogen, and the expander recovers the electric power from the high-pressure off-gas and supplies it to compress the air. The insufficient electric power is supplemented by the electric motor. Fig. 3-1 also shows the flow shift between each system in the network. This network is operated with a fundamental mass balance between the flows into the compressor and expander and the target flow rate required for the reaction.

Fig. 3-2 is a schematic diagram of an n-th multi-stage compression system consisting of m compressors and k expanders in the air and gas supply network. Humid air enters the first suction stage of the compressor and is pressurized to the desired pressure. The compression part consists of several successive compression stages and controls the temperature with the existing intercooler between each stage. The intercooler serves to minimize the power to the compressor by lowering the temperature of the discharged air. The expander consists of several expansion stages, and there exists a re-heater between the stages to maximize the energy recovery.

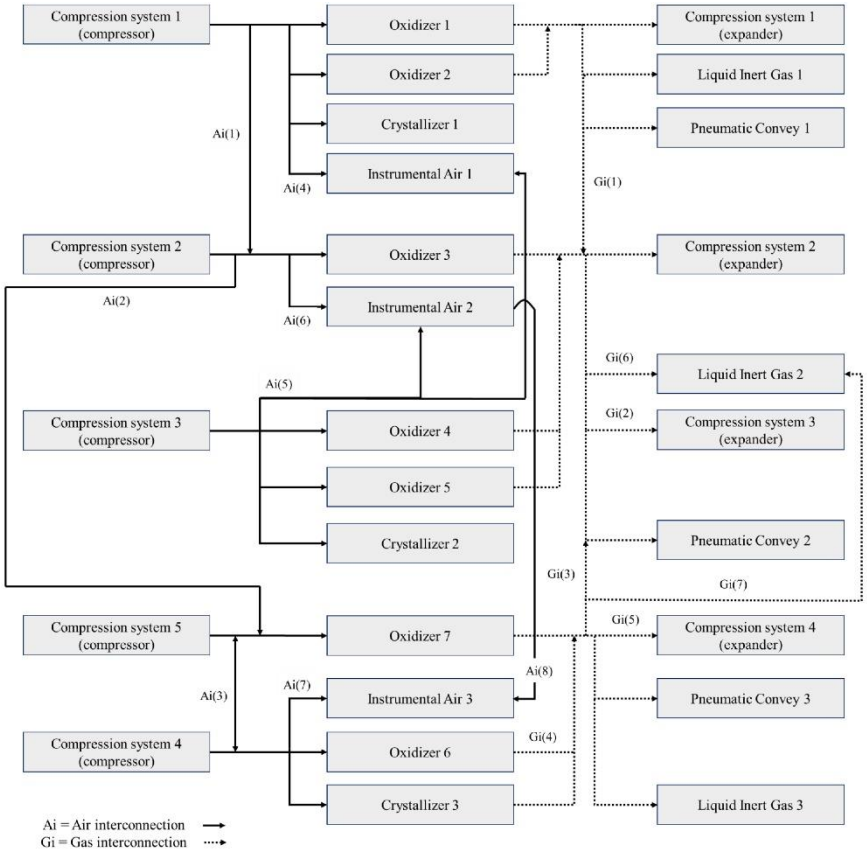

Figure 3-1. Structure of air & gas supply network

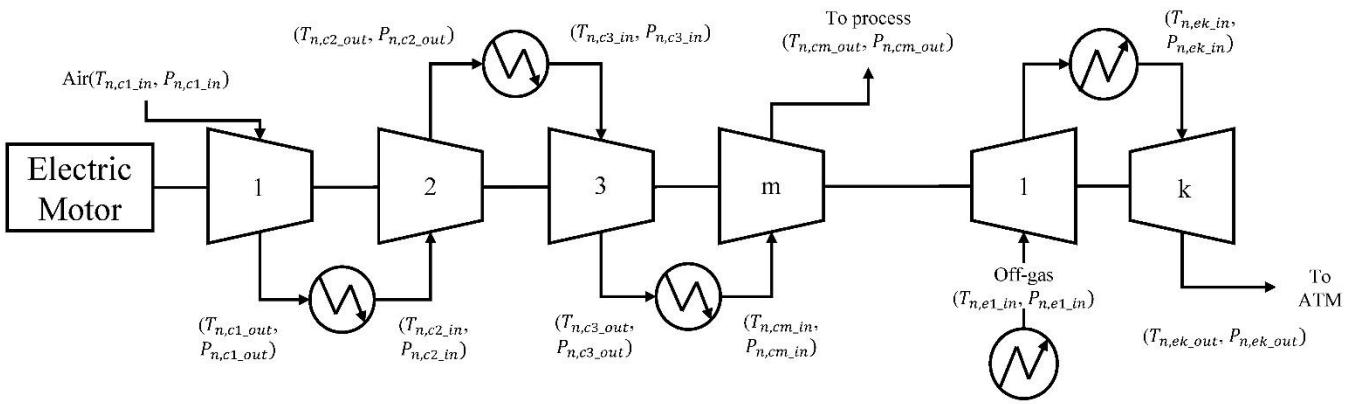

Figure 3-2. Scheme of the *n*-th multi-stage compression system

Table 3-1. Configuration of the multi-stage compression systems

Compression system #	Number of compression stages	Number of expansion stages	Number of electric motor
1	3	2	1
2	4	2	1
3	4	2	1
4	4	2	1
5	4	0	1

3.2.2. Limitations of first-principle models

In general, the efficiency of the compressor or expander determines the pressure and temperature of the stream being compressed or expanded (Gravdahl & Egeland, 2012). The above-mentioned efficiencies include the mechanical efficiency that occurs in a typical rotating machine and the thermodynamic efficiency (adiabatic efficiency, polytropic efficiency, isentropic efficiency, etc.) that is determined by the internal mechanism. This is an indication of how much of the actual consumption or produced power is used for the pressure change of the internal fluid. Therefore, it is essential to accurately measure the temperature and pressure of the stream before and after compressor (or turbine) to model the efficiency and power consumption of compressor (or turbine). However, accurate measurement of the temperature and pressure before and after the stage may not yield good predictions because existing mathematical models contain many thermodynamic approximations (Han & Han, 2003). Furthermore, it is difficult to measure temperature and pressure between the stages in multi-stage compression system due to the spatial constraints (Han & Han, 2003). Therefore, it is difficult to model the inherent characteristic curve of stages and power consumption of each stage with rigor for a multi-stage compression system only with the information on the inlet of the first stage and the outlet of the last stage.

To overcome these limitations, data-driven modeling methods based on field data have emerged from the existing shortcut model. Gresh (1998) estimated

the overall power of a multi-stage compression system using measurement data. Ghorbanian and Gholamrezaei (2009) predicted compressor performance map using artificial neural networks. Han et al. (2004) also conducted a study to predict the power of a multi-stage compression system using neural networks. However, the above methodologies do not reflect the dynamic characteristics of a system. Future forecasts of the system may depend not only on the measurements at the current time but also on those of the past time. Hence, model prediction can be improved by including the relevant data at past time points rather than simply mapping between the input and output at the current time instant.

3.2.2.1. Variation of system efficiency due to disturbance

Fig. 3-3 shows a simplified schematic of the design methodology of the virtual plant model using the commercial simulator, Aspen HYSYS®. The virtual plant model used in this study has two purposes. The first is to show the efficiency change of the system over time by estimating the temperature and pressure between stages, and the second is to verify and overcome the overfitting of the designed NARX model. In this section, we try to show the relation between the environmental factors and the efficiency change of the system by analyzing the difference between the output of the virtual plant model and the actual amount of power used. As mentioned above, the efficiency

of each stage determines the pressure and temperature of the stream coming out of the stage. This means that the compression efficiency and the expansion efficiency of each stage can be inversely estimated by estimating the pressure and temperature of discharge stream. The design method presented in Fig. 3-3 uses an algorithm that determines the temperature and pressure between the stages to minimize deviation from the actual output data. Since this virtual plant model is not intended to find the exact system efficiency but to see the system efficiency change over time, we apply two assumptions for the convergence of the algorithm. Typical compressors and expanders operate within a reasonable pressure ratio range, and the efficiency of the system mainly affects the temperature of the discharge stream. Therefore, by using the assumption that the pressure changes in each stage are the same, the degree of freedom in the design phase is reduced and the convergence of the algorithm is increased. Also, the deviation constraint was chosen to be within the appropriate range (30 kW) because it was aimed to see the approximate tendency. First, this virtual plant model was designed using the first measured data value after the plant operation. The temperature and pressure between the stages determined at this time mean the internal state of the system at the beginning of the operation and are fixed to see only the influence of the external environment. And then, the operation data of the process according to time is substituted into this initial model. Generally, the offset occurring between the virtual plant model and the actual plant arises from complex factors such as changes in internal parameters and

external environment. Therefore, the internal state of the system needs to be fixed according to time. This type of analysis requires a lot of assumptions, but the approximate trend of the system's impact on disturbance such as external temperature and humidity can be seen. By comparing the offset and external trends in time, we select external factors to be reflected in the design of NARX model.

Fig. 3-4 shows the time-dependent trends of power consumption of the virtual plant model and the actual power consumption trend. Fig. 3-4 also shows the trends of the offset between the virtual plant and the actual plant and the change in the external temperature on the same graph. It is not known precisely which function it is, but there seems to be some correlation between the two, assuming that the behavior between offset and external temperature over time is similar. Also, even if the system is operated under the same external conditions, it can be seen that the effect on the actual system varies with time. In other words, it can be seen that the multi-stage compression system is influenced by the external environmental conditions, and the degree of influence varies in time. In this study, it is assumed that the external environmental conditions affecting the compression system efficiency are the external temperature and the external humidity. External humidity, which does not have a clear trend over time because of a severe fluctuation, is difficult to analyze using the same methodology and was not addressed in this section. However, temperature and humidity basically have the same tendency depending on the season, and even

if the external temperature is the same, it can be confirmed that the same amount of electricity is not consumed. So, the external humidity is also selected as an external disturbance variable that changes the machine operation efficiency. Fig. 3-5 shows the difference between the amount of power used in the model of the 2nd, 3rd, 4th and 5th multi-stage compression system and the amount of power used in the actual plant. This confirms that the model-plant offset is affected by the change in external temperature in Fig. 3-4. It also shows that each system has different external disturbance influence functions. Therefore, modeling that accurately reflects different influence functions for each system is necessary for the operation of the network.

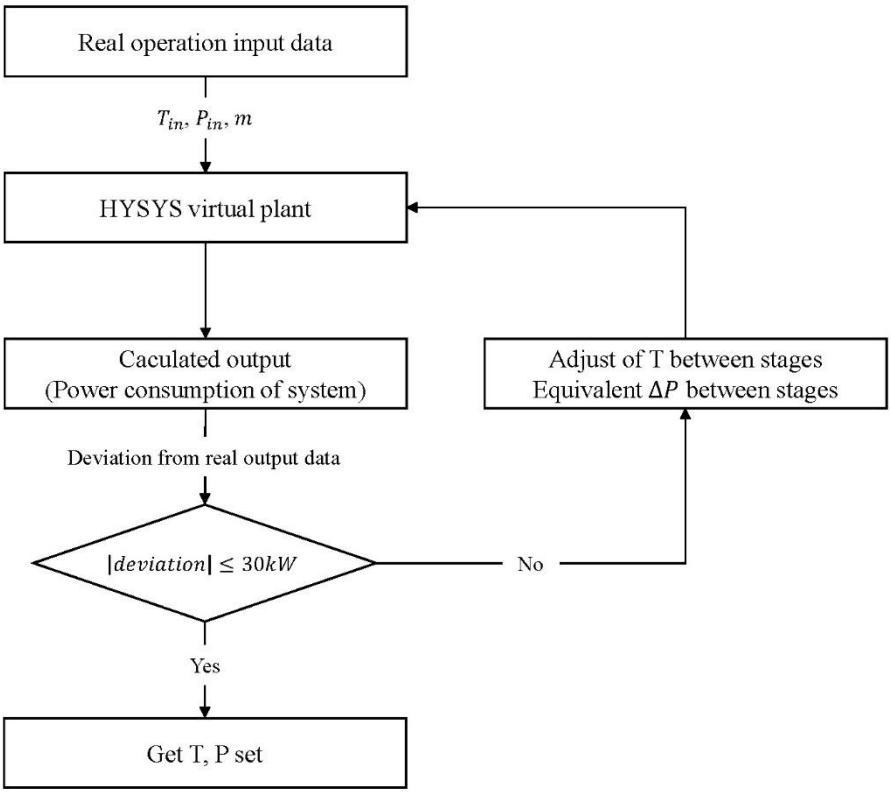

Figure 3-3. Temperature and pressure estimation algorithm for virtual plant design from real operation data

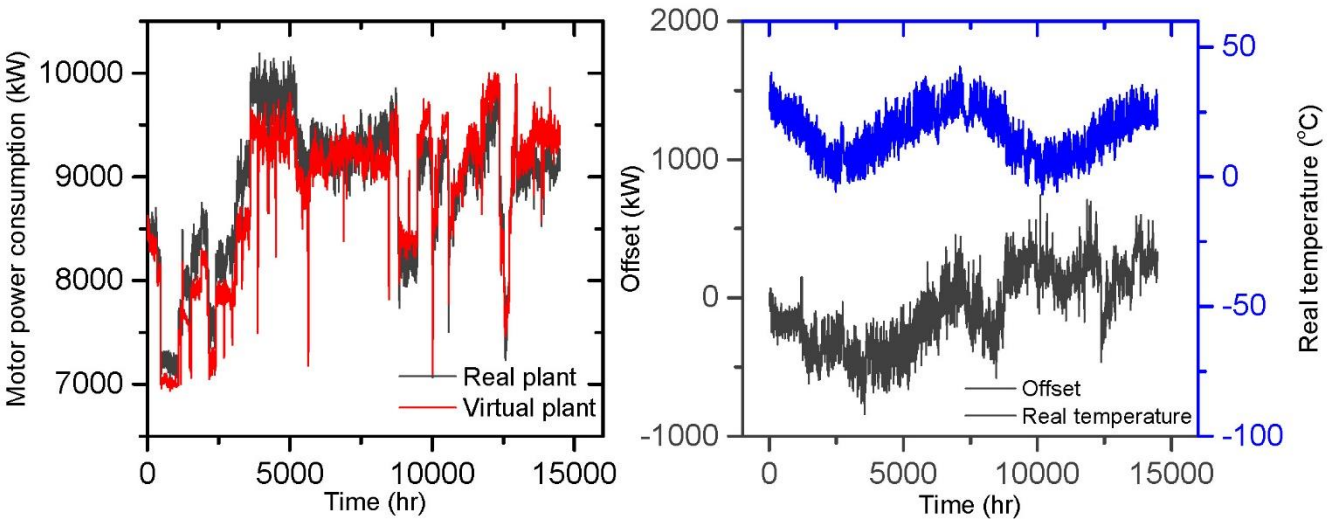

Figure 3-4. Motor power consumption trend of first compression system of actual plant and virtual plant & Comparison of offset and external temperature trends

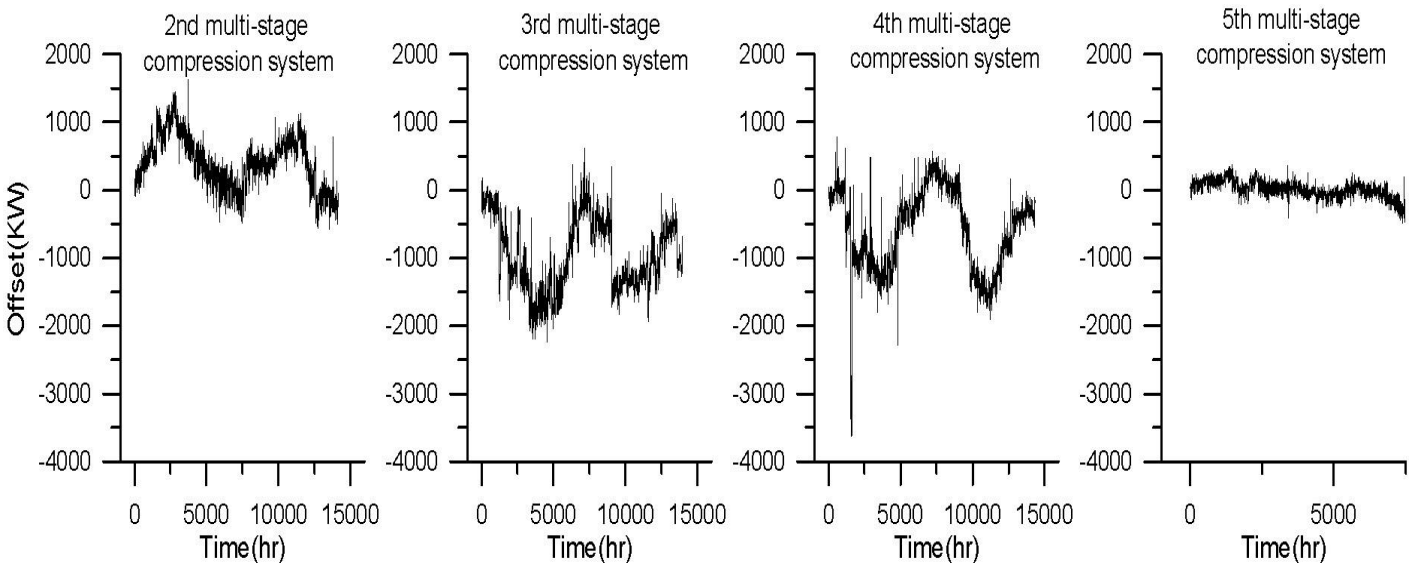

Figure 3-5. Model-plant offset in 2nd to 5th multi-stage compression system

3.2.2.2. Efficiency of a system that decreases with time

In general, the operating efficiency of a process unit is reduced from the initial design over time. In particular, if a compressor is kept operating without maintenance, the blade is damaged from corrosion and aging, and the compression efficiency is decreased (Kurz & Brun, 2012). Fig. 3-6 shows the total pressure ratio value for the volume flow into the compressor at the time of consumption of the same power during the total operating time of 16,000 hrs in the first multi-stage compression system. It can be seen that even if the same flow rate is introduced over time, it has a lower head value. In order to see only the effect of deterioration over time, a comparison between data with the same external conditions is required. Therefore, we use the operation data (1 ~ 2000hr) in the summer of the first year of operation and the operation data (around 16000hr) in the summer of the next year. Since these two sections correspond to both ends of the operating data handled, it is believed that the effect of decreasing efficiency over time is most clearly shown. In addition, Fig. 6 shows the operating points with the same operating conditions at a specific time, and it can be seen that as the time elapses, more power is consumed with the same operating condition.

Therefore, the amount of power used in a multi-stage compression system cannot be regarded as a function of a manipulated input only. The external disturbance and the aging of the system cause the difference between the model

and the actual plant operation, and it is necessary to construct the model including these parameters that change with time. The model structure for predicting the power consumption of a multi-stage compression system based on the analysis in 2.2.1 and 2.2.2 is shown in Fig. 3-7. x_1 is the manipulated variable of the multi-stage compression system. g_c and g_e mean thermodynamic equations to compute the ideal power of the compressor and expander according to the manipulated variable. Function h and f are virtual functions representing the external disturbance effect and the aging effect, respectively. The first principle model based on thermodynamic equations is basically limited in that it can not take into account the influence of unknown factors. Also, when applied to a target process that lacks information on the interstage, it can not design each stage model, and thus shows a large deviation from the actual plant. Furthermore, since it is impossible to quantitatively analyze unknown factors such as external disturbance and aging of equipment using only operation data, it is difficult to extract virtual functions h and f independently. Therefore, the empirical model combined with the NARX is used in this study because it can more accurately reflect the unmeasurable information and the unknown nature of the system. The neural-net type surrogate model including the NARX structure automatically extracts the nonlinear features of the unknown factors from the operation data to construct the latent space. In particular, the NARX model is known to have strengths in

complex nonlinearity modeling as well as time-series data prediction. However, this surrogate model is difficult to analyze the physical meaning of each latent space due to the existence of hidden layer, and therefore, the robustness of the model is questionable in designing the model for prediction. To solve this problem, we designed a structure that can more effectively reflect the characteristics of the system in which the first principle is embedded by extracting features of input through thermodynamic equations rather than using all manipulated variables. The NARX model using this feature extraction can effectively overcome the limitations of the existing first principle model by learning the effects of these stochastic factors on their own and show excellent prediction performance.

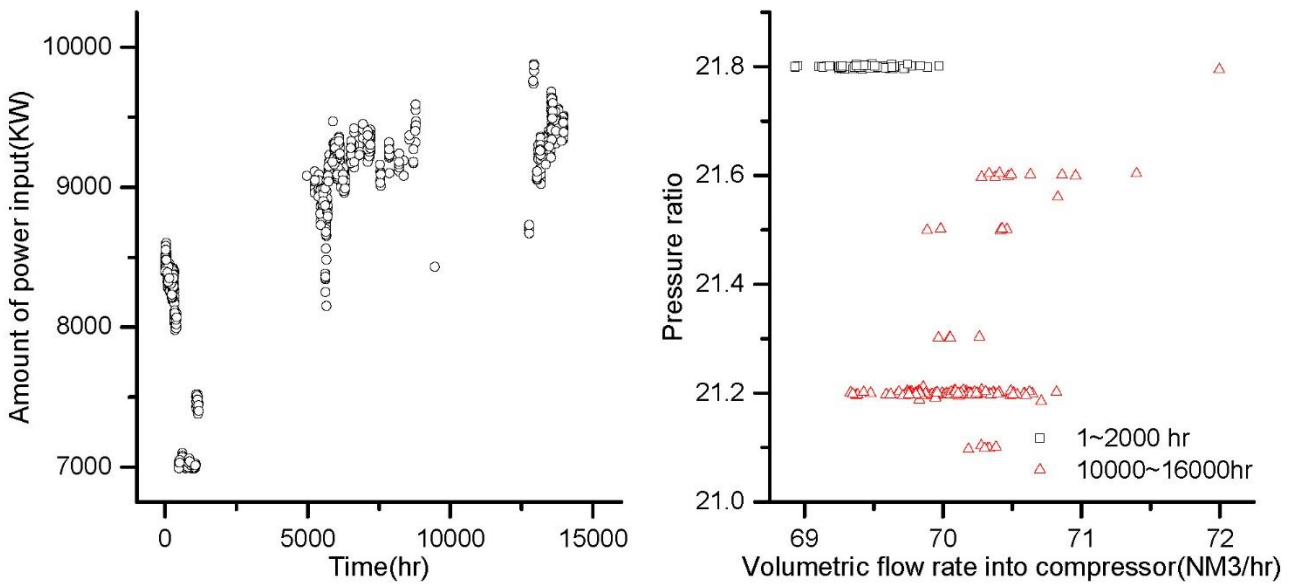

Figure 3-6. Amount of power input over time with the same operating condition & Compressor operating map with the same work input.

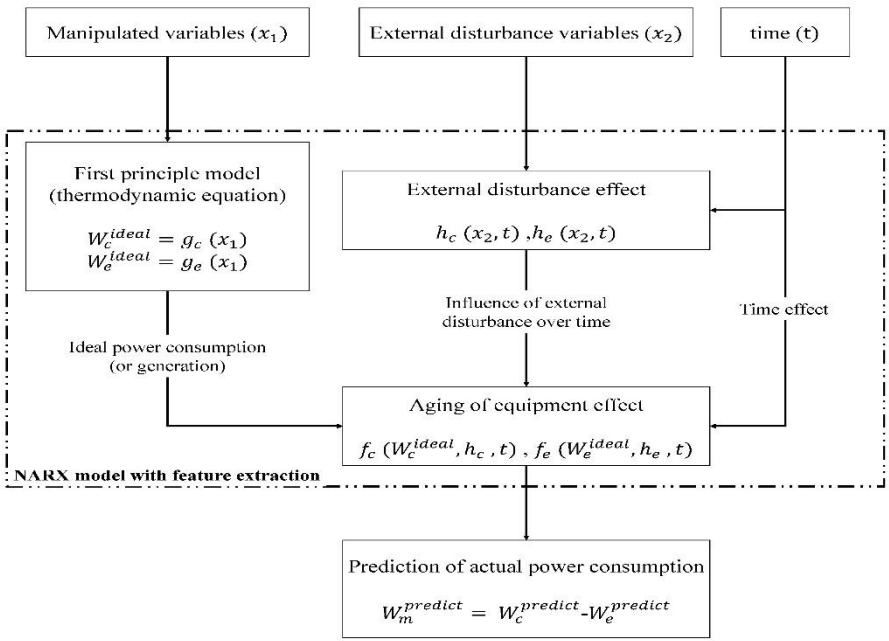

Figure 3-7. Model structure to reflect external disturbance effect and aging of equipment over time.

3.3. Long Term Prediction using NARX model

In this study, we estimated the power of five multi-stage compression systems using Nonlinear Autoregressive eXogenous Neural Net (NARX NN) model. In general, basic neural net has been widely applied as a data-driven modeling method for designing black box models of chemical processes (Azlan Hussain, 1999; Haykin, 1994). However, most chemical processes have dynamic characteristics, and the compression system of air & gas network also shows temporal changes in the overall efficiency. Therefore, in order to design a rigorous prediction model of multi-stage compression system, Recurrent Neural Net methodology applicable to modeling time series data should be considered. However, since the basic RNN methodology has a disadvantage that the gradient is lost through a large number of hidden layers, it has a limitation in applying it to long-term prediction. NARX NN has been known to have excellent performance in long-term prediction of time series data because it does not have the issue of gradient loss of existing basic RNN (Menezes & Barreto, 2008; Ruiz et al., 2016; Tsungna et al., 1996). This is due to the structural advantages of NARX, where the output data goes directly into the input without going through the layer.

The hidden layer inside the NARX model extracts the information from the output and input of the operation data to create an arbitrary feature. The existence of these arbitrary features can overcome the limitations of the existing

first principle model because it can reflect the stochastic nature of the process that the output and input data contain. However, even if this stochastic nature is reflected, the data-driven black box model including the NARX model basically has a disadvantage that it is vulnerable to extrapolation (Psichogios & Ungar, 1992). For a neural net based model, this problem is in the randomness of the model that results from the creation of arbitary feature. In this study, we designed the feature extraction method that reduces the input dimension using the first-principle equations to minimize the randomness of the NARX model and to improve the long-term prediction performance. This first principle equation based on thermodynamics extracts the thermodynamic relationship of the manipulated variables of the process and creates a new input set. By transferring the extracted input set including the thermodynamic information of this chemical process to the NARX model, the randomness of the model can be minimized. This is a complementary form of a first principle model and a NARX model, and is particularly suitable for chemical processes that can be used to find basic relationships. The NARX model combining these feature extraction methods not only improves long-term prediction performance but also overcomes the problem of model overfitting.

3.3.1. First principle based feature extraction

The neural network modeling method may suffer from undue extrapolation problems and lead to unacceptable performance compared to linear function

approximation methods due to the over-fitting. To overcome these drawbacks, a new training input was designed by extracting the features of the original input using first-principle thermodynamical equations. Table 2-2 shows the raw input set and the input set after feature extraction for each multi-stage compression system. $W_{n,c}^{ideal}$ is the minimum power consumed by the compressor of the nth compression system. It is assumed that the pressure ratio of each stage is kept constant, the temperature before and after the stage is constant at all stages, and the pressure drop does not occur in the compressor and other auxiliary components. $W_{n,e}^{ideal}$ is the ideal power produced by the expander of the nth compression system. The expansion ratio between stages is kept constant, the temperature and pressure are the same before and after the stage, and the discharge pressure at the last stage is assumed to be atmospheric pressure. The feature extraction of the input is calculated using equations (1) and (2) from (Gravdahl & Egeland, 2012; Han & Han, 2003), and the ASPEN thermodynamic data was used given the raw input data sampled every hour. As mentioned in Section 2, the difference between the simple thermodynamic model and the actual plant is due to the temperature difference between the unmeasurable stages, the effect of external disturbance, and the system aging. The feature extraction through thermodynamic models allows the neural net model to focus on the offset caused by these factors.

$$W_{n,c}^{ideal} = \frac{N_C \tilde{k}_{air} \tilde{F}_c R T_{amb}}{(\tilde{k}_{air} - 1)\tilde{M}_{air}} \left[\left(\frac{P_{n,Cm\_out}}{P_{amb}} \right)^{(\tilde{k}_{air}-1)/N_C \tilde{k}_{air}} - 1 \right] \quad \text{(Eq. 3-1)}$$

$$W_{n,e}^{ideal} = \frac{N_e \tilde{k}_{gas} \tilde{F}_g R T_{amb}}{(\tilde{k}_{gas} - 1)\tilde{M}_{gas}} \left[\left(\frac{P_{amb}}{P_{1,ek\_in}} \right)^{(\tilde{k}_g-1)/N_e \tilde{k}_g} - 1 \right] \quad \text{(Eq. 3-2)}$$

Table 3-2. Raw input training set and extracted input training set

Compression system #	Raw input set	Input set after feature extraction
1	$V_{1,c}, T_{1,amb}, P_{1,C3_{out}}, H_{1,amb}, V_{1,e}, T_{1,e1_{in}}$ $T_{1,e2_{in}}, P_{1,e1_{in}}, \gamma_{1,o2}, \gamma_{1,co2}, \gamma_{1,co}$	$W_{1,c}^{ideal}, W_{1,e}^{ideal}, T_{1,amb}, H_{1,amb}, T_{1,e2_{in}}$
2	$V_{2,c}, T_{2,amb}, P_{2,C4_{out}}, H_{2,amb}, V_{2,e}, T_{2,e1_{in}}$ $T_{2,e2_{in}}, P_{2,e1_{in}}, \gamma_{2,o2}, \gamma_{2,co2}, \gamma_{2,co}$	$W_{2,c}^{ideal}, W_{2,e}^{ideal}, T_{2,amb}, H_{2,amb}, T_{2,e2_{in}}$
3	$V_{3,c}, T_{3,amb}, P_{3,C4_{out}}, H_{3,amb}, V_{3,e}, T_{3,e1_{in}}$ $T_{3,e2_{in}}, P_{3,e1_{in}}, \gamma_{3,o2}, \gamma_{,co2}, \gamma_{3,co}$	$W_{3,c}^{ideal}, W_{3,e}^{ideal}, T_{3,amb}, H_{3,amb}, T_{3,e2_{in}}$
4	$V_{4,c}, T_{4,amb}, P_{4,C4_{out}}, H_{4,amb}, V_{4,e}, T_{4,e1_{in}}$ $T_{4,e2_{in}}, P_{4,e1_{in}}, \gamma_{4,o2}, \gamma_{4,co2}, \gamma_{4,co}$	$W_{4,c}^{ideal}, W_{4,e}^{ideal}, T_{4,amb}, H_{4,amb}, T_{4,e2_{in}}$
5	$V_{5,c}, T_{5,amb}, P_{5,C4_{out}}, H_{5,amb}$	$W_{5,c}^{ideal}, T_{5,amb}, H_{5,amb}$

3.3.2. NARX modeling

After eliminating the outlier of the actual operation data of the air & gas network for about 3 years, the data were divided into a training set, validation set, and prediction set. The first purpose of the compression system operation is to pressurize the gas to be compressed to a desired pressure. If the discharged pressure does not maintain a certain level or fluctuates, it is considered that there is an abnormal operation or a change between steady states. Therefore, the operation data of the shut-down section in which the discharged pressure greatly falls and the operation data of the section in which the pressure value oscillates due to the shift of the state of the system are set as outliers and removed from the training data set. This is the reason five multi-stage compression systems have different numbers of data even though they are at the same time point. Table 3-3 shows the number of data per set in each multi-stage compression system. The NARX model is trained by the Levenberg-Marquardt backpropagation algorithm and has a test set and a validation set for model self-validation. The default rates are 70:15:15 for training, validation, and test, respectively. The prediction set is a data set for verifying the predictive performance of the model and consists of the data of the latter part of the process operation data. Specifically, of the data sets with outliers removed, the first 10000 data points were used as the training set, validation set, and test set. The extrapolation performance of the model was verified by selecting 500 data points that were not used in the modeling. In the case of the fifth compression

system, the number of data used for modeling is smaller than that of the compression system due to frequent interruptions such as shutdown. However, since it is a relatively simple system without an expander compared to others, the number of data points are enough for modeling.

NARX (Çoruh et al., 2014; Menezes & Barreto, 2008; Tsungna et al., 1996) is a class of discrete-time nonlinear system in the general form of

$$y_t = f(u_t, u_{t-1} \cdots u_{t-d_u}, y_{t-1}, y_{t-2} \cdots y_{t-d_y}) \qquad \text{(Eq. 3-3)}$$

where $\boldsymbol{y_{t-d_y}}$, $\boldsymbol{u_{t-d_u}}$ are the electric motor power output and the inputs after feature extraction, respectively, at the delayed time points. As mentioned in Introduction, the objective of this study is to present the optimal operating condition of the next time step through nonlinear multivariate time series prediction with NARX model. Therefore, during the training phase, the compressed input at time t is included, but at the optimization stage, the input at time t is the optimization variable. Fig. 3-8 shows NARX network mapping performance by Multilayer Perceptron (MLP) with $\boldsymbol{d_u}, \boldsymbol{d_y}$ and one-hidden layer. MLP is a class of feedforward artificial neural network. NARX model has a single input and a single output, with a delay line on the inputs, and the outputs fed back to the input by another delay line. Thus, the structure of the NARX model can be expressed in the form of a multilayer perceptron with a feed-back connection.

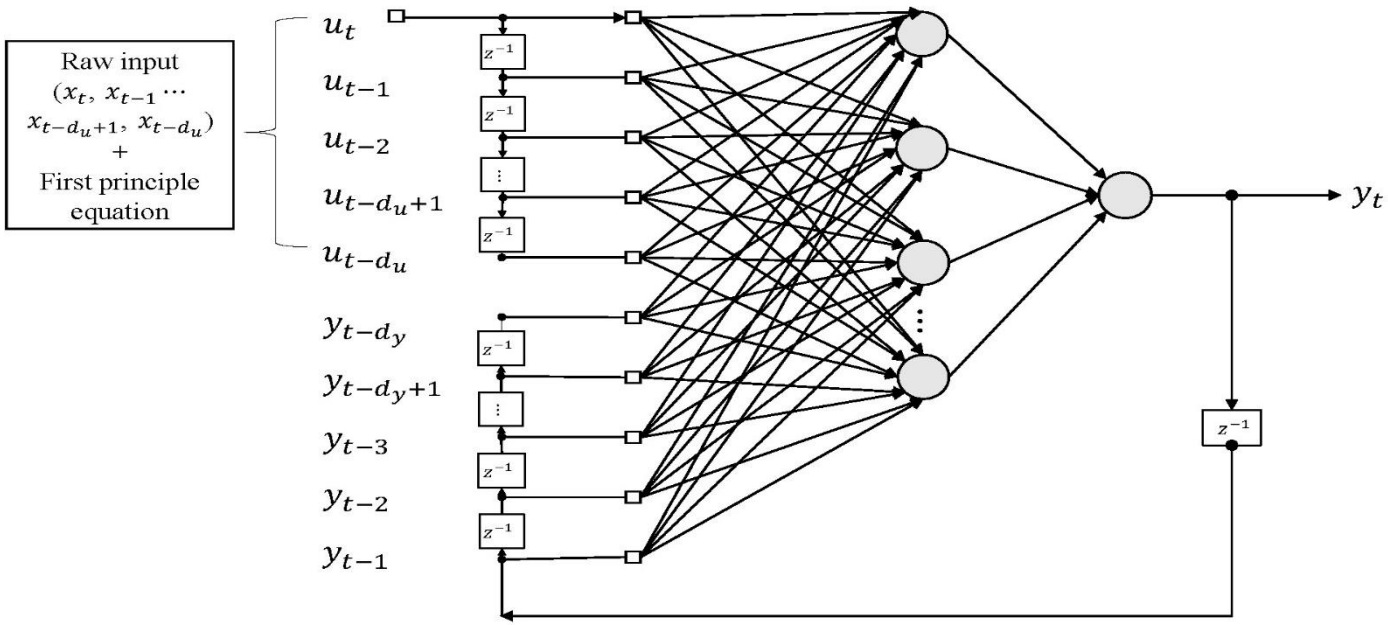

Figure 3-8. NARX network with delayed inputs, delayed outputs and current input with one hidden layer (z^{-1} = backward time shift operator)

Table 3-3. The number of data in the training and prediction sets for each compression system

Compression system #	Number of data in training set , validation set, and test set)	Number of data in prediction set
1	7000, 1500, 1500	500
2	7000, 1500, 1500	500
3	7000, 1500, 1500	500
4	7000, 1500, 1500	500
5	3500,750,750	500

3.4. Real-time Optimization

Fig. 3-9 shows the structure of NARX-RTO for multi-stage compression system. The NARX model of a total of five multi-stage compression systems in the air & gas network predicts the amount of power according to the input set after feature extraction and the external disturbance information at the next time step. The optimization step determines the raw input set that minimizes the amount of power expected at the next time step if the external disturbance value is measured. Once the raw input sets of the future time steps and their outputs are determined, the data is validated through the virtual plant and then the model is retrained using the output from the virtual plant to update the model at each specified time step. When a new data set is available, the existing initial data is removed and the number of data to be trained is maintained. This avoids excessive modeling time with a steady increase in the number of training data. It also allows the model to reflect the characteristics of the system better that the new incoming data contains. Virtual plant design used the same method as mentioned in Section 3.2.2.1. The compression stage and the expansion stage in the multi-stage compression system have different states for each stage. Accurate dynamic simulation for each stage requires reliable information on the degraded mechanical efficiency, the effect of external disturbance, the rotational speed of the compressor and the expander, etc. However, most of such information is difficult to obtain, which limits the rigorous design of a

detailed virtual model of the multi-stage compression system. To overcome these limitations, we design a concise virtual plant model with iterative updates. First, the temperature and pressure before and after each stage at the optimization step are determined using the actual operation data which may not be optimal. After determining the temperature and pressure values before and after the stage at the optimization stage, the optimized raw input set is input to the virtual plant again, and the total power of each system is calculated and compared with the result of the NARX-RTO model. The validation and correction of the optimization result through the virtual plant prevents overfitting that may occur in the modeling stage. For the more accurate design of RTO system, the iterative update must be performed through the actual plant. However, this study was performed through the virtual plant using the commercial simulator because actual plants were not available for validation of the optimization results.

In this study, the prediction window is set to 1(hour) and real-time optimization is performed. Generally, the larger the prediction window, the more optimal result can be obtained because the operating conditions at the next time can be determined based on the accurate trend of the system. However, the proposed model does not consist solely of manipulated variables (flow, temperature, pressure, etc.) of the system but includes unknown external disturbance variables (external temperature and humidity). This means that to expand the prediction window requires another model that can predict future

external disturbance changes. The presence of another prediction model can cause the uncertainty of the model, which can reduce the robustness of the model. Also, in the case of external temperature and humidity, a large trend can be expected qualitatively, but it is difficult to get accurate values on a time scale. Therefore, in this study, we set the prediction window to 1hr assuming that the value of the external disturbance variables at the next time step to be predicted is the same as the value measured at the current time without designing a separate external disturbance prediction model. The changes in the external temperature and humidity over an hour are negligible, and the compressors and expanders of the compression system covered in this study have their own power ranges, so there is no significant trend change in the output of the system.

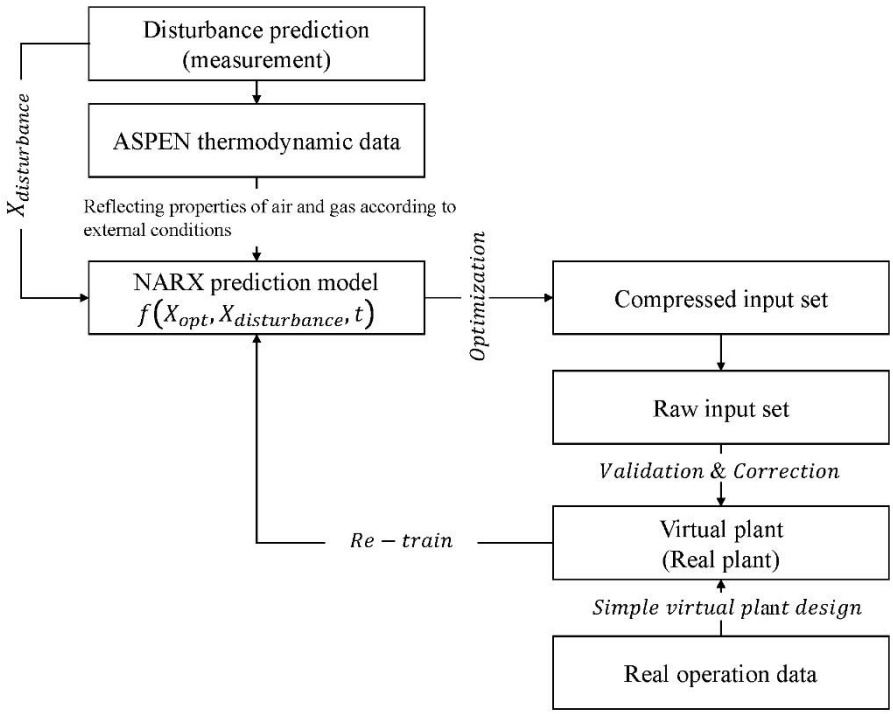

Figure 3-9. NARX-RTO structure

3.4.1. Optimization formulation

The goal of optimization is to minimize the total power consumption of the five multi-stage compression systems.

$$\min_{X_{opt}=[x_1,x_2,\cdots,x_{32}]} W_{n,motor\_predicted} = \mathrm{f}(X_{opt}) \quad \text{(Eq.3-4)}$$

such that

$$\mathrm{A}X_{opt} = b \quad \text{(Eq.3-5)}$$

$$X_{opt,L} \leq X_{opt} \leq X_{opt,U} \quad \text{(Eq.3-6)}$$

$$W_{n,M,L} \leq W_{n,M} \leq W_{n,M,U}, \quad \mathrm{n} = 1,2,3,4,5 \quad \text{(Eq.3-7)}$$

$$P_{n,cm_{out}} \leq V_{n,c} \times \alpha_{n,c_{surge}} + \beta_{n,c_{surge}} \quad \mathrm{n} = 1,2,3,4,5 \quad \text{(Eq.3-8)}$$

$$P_{n,cm_{out}} \geq V_{n,c} \times \alpha_{n,c_{stonewall}} + \beta_{n,c_{stonewall}} \; \mathrm{n} = 1,2,3,4,5 \quad \text{(Eq.3-9)}$$

$$P_{n,e1_{in}} \leq V_{n,e} \times \alpha_{n,e_{surge}} + \beta_{n,e_{surge}} \quad \mathrm{n} = 1,2,3,4,5 \quad \text{(Eq.3-10)}$$

$$P_{n,e1_{in}} \geq V_{n,e} \times \alpha_{n,e_{stonewall}} + \beta_{n,e_{stonewall}} \; \mathrm{n} = 1,2,3,4,5 \quad \text{(Eq.3-11)}$$

X_opt is an optimization variable vector to be determined. It contains most of the variables except the discharge pressure of the compression system and the suction pressure of the expansion system, which must be determined by the user among manipulated variables present in the air & gas supply network. Equation (3-5), including A and b, represents the mass balance of the air & gas

supply network consisting of five compressors and four expanders. The total amount of air and gas supplied is kept constant even if the flow rate changes due to optimization. Equation (3-6) shows the lower and upper bounds of all the optimization variables. Table 3-4 shows the lower and upper bounds of each variable. Equation (3-7) represents the appropriate operating range of the existing motor in the compression system. Equations (3-8) - (3-11) constrain the operation range of compressors and expanders. This is to prevent the surge phenomena that damage blades due to the backflow if the flow rate drops below a certain level and the stonewall phenomena that occur when operating above a certain level (Botros et al., 2000; Jung et al., 2017). The parameters of each equation were estimated from the characteristics map of the compressor and expander supplied by the vendors. The GA algorithm is the most common meta-heuristic algorithm and has been successfully applied to various chemical process optimization problems (An et al., 2018; Lee et al., 2016; Na et al., 2017). Therefore, the GA algorithm is used to solve the global optimization problem including the linear and non-linear constraints. For the GA, 50 populations, 0.8 of the crossover fraction, and 20 of the maximum generation were used. The GA algorithm stops if the average relative change in the best fitness function value over stall generation value is less than or equal to TolFun (default value 1e-6) or the number of generations has reached the maximum generation value. The parameters of this GA algorithm were selected considering the convergence and reproducibility based on the results of previous studies. The

optimization was carried out using Aspen Plus v8.8 and MATLAB R2016a on a desktop computer with Intel® Core™ i5-4590 CPU at 3.30 GHz and 6 GB RAM running Window 10.

Table 3-4. Lower & upper bounds of the optimization variable

# of variable	Optimization variable	Lower bound	Upper bound	# of variable	Optimization variable	Lower bound	Upper bound
1	$V_{1,C}$	50	71.1	**17**	$V_{4,e}$	40	88.8
2	$V_{2,C}$	61.5	64.6	**18**	Gi(1).	0	8
3	$V_{3,C}$	50	82.9	**19**	Gi(2)	-50	60
4	$V_{4,C}$	50	82.7	**20**	Gi(3)	0	60
5	$V_{5,C}$	25	36.5	**21**	Gi(4)	0	60
6	Ai(1)	0	5	**22**	Gi(5)	0	120
7	Ai(2)	0	30	**23**	Gi(6)	0	10
8	Ai(3)	-30	30	**24**	Gi(7)	0	10
9	Ai(4)	0	7	**25**	$T_{1,e1_{in}}$	409	415
10	Ai(5)	0	5	**26**	$T_{2,e1_{in}}$	400	425
11	Ai(6)	0	5	**27**	$T_{3,e1_{in}}$	405	425
12	Ai(7)	0	5	**28**	$T_{4,e1_{in}}$	408	417
13	Ai(8)	0	5	**29**	$T_{1,e2_{in}}$	412	417
14	$V_{1,e}$	39.9	40.1	**30**	$T_{2,e2_{in}}$	412	416
15	$V_{2,e}$	23.6	50	**31**	$T_{3,e2_{in}}$	395	412
16	$V_{3,e}$	40	85	**32**	$T_{4,e2_{in}}$	418	428

3.5. Result and Discussion

3.5.1. Long-term prediction performance

Fig. 3-10 shows the prediction performance of the five compression systems in the air & gas network. The prediction window is 500 hr each, which is outside the range of data used for modeling. We compare three modeling methods: Simple feed-forward multi-layer perceptron using raw input set without the input feature extraction, NARX NN using raw input set, and NARX NN using the input set through feature extraction. Fig. 3-10 shows that the prediction performance of the NARX with the feature extraction model is superior in all compression systems. However, performance differences with the basic neural net model for the 1st, 2nd, 3rd, and 4th multi-stage compression systems are remarkable, whereas the 5th multi-stage compression system has relatively small differences (NARX + feature selection methodology compared to simple feed-forward multilayer perceptron modeling = 1st – 67%, 2nd-56%, 3rd-65%, 4th-44%, 5th-28%). This is attributable to the simple structure of the fifth multi-compression system without an expander. In the case of the first to fourth multi-compression systems, characteristics change with time in both the compressor and the expander inside the system. On the other hand, the characteristic change of the fifth system occurs only in the compressor. This difference of structure causes a difference in prediction performance improvement. In this regard, it is necessary to use the proposed method using NARX NN with the feature extraction for modeling complex compressor networks. Also, five multi-stage

compression systems exhibit different prediction performance improvements. This means that even with similar systems the efficiency change in time can be different. The efficiency reduction rate due to the aging process of each stage in the compressor and expander cannot be constant, and the external disturbance does not always have the same effect on all stages due to the mechanical factors that change instantaneously depending on the operating conditions of the stage.

In the case of simple feed-forward multilayer perceptron modeling, the mean square prediction error is 300% compared to the case using the NARX NN modeling method. Also, the results of the simple feed-forward multilayer perceptron methodology in all multi-stage compression models of the target process show a tendency to predict the amount of power lower than the actual operating results. This is because the model does not correctly learn the difference between the efficiency of the system at the training time and that of the system at the prediction time. The efficiency at the time of forecast is expected to be lower than that of the past due to the aging of the system, ambient temperature, and humidity. The simple feed-forward multilayer perceptron model does not learn such a decreasing trend properly, leading to the poor prediction of the required amount of electricity. Modeling with neural networks can be disadvantageous in that the user cannot accurately understand the physical meaning of the weighting parameters of hidden layers. Therefore, we cannot accurately analyze the cause of the difference in prediction performance.

This makes it difficult to analyze the cause of the difference in prediction performance. However, a model should reflect stochastic factors affecting the system efficiency in time, NARX model structure is appropriate for modeling the system in this regard.

Taking advantage of the existing first-principle relations in constructing the NARX model for selecting input feature could prevent the overfitting and show better prediction performance. In general, the performance of a neural net based model with training and validation sets, which are often chosen randomly. This is because many modeling parameter sets give satisfactory fitting performances with more number of input variables than that of the output variables. The model parameters are determined by arbitrarily selected training and validation sets, which may lead to overfitting and incorrect model parameters if the data sets were poorly divided. Using the input set through feature extraction can reduce the effect of overfitting owing to the reduced dimension. Moreover, since the feature extraction is based on the thermodynamic model of the compressor and expander, NARX model is responsible for only the offset that is occurring due to the effects of disturbance and the aging of the system over time. As a result, the NARX model with feature extraction could reduce Mean Squared Error (MSE) by 20% on average compared to the NARX model without feature extraction and by 43.5% on average compared to the simple feed-forward multilayer perceptron model without feature extraction. The MSE of each modeling method for five multi-stage compression systems is

summarized in Table 3-5. In conclusion, time series modeling, which combines the proposed NARX model with feature extraction based on the first principle model, can achieve dramatic improvements in model performance compared to simple nonlinear fitting when applied to various dynamic systems operating in the field.

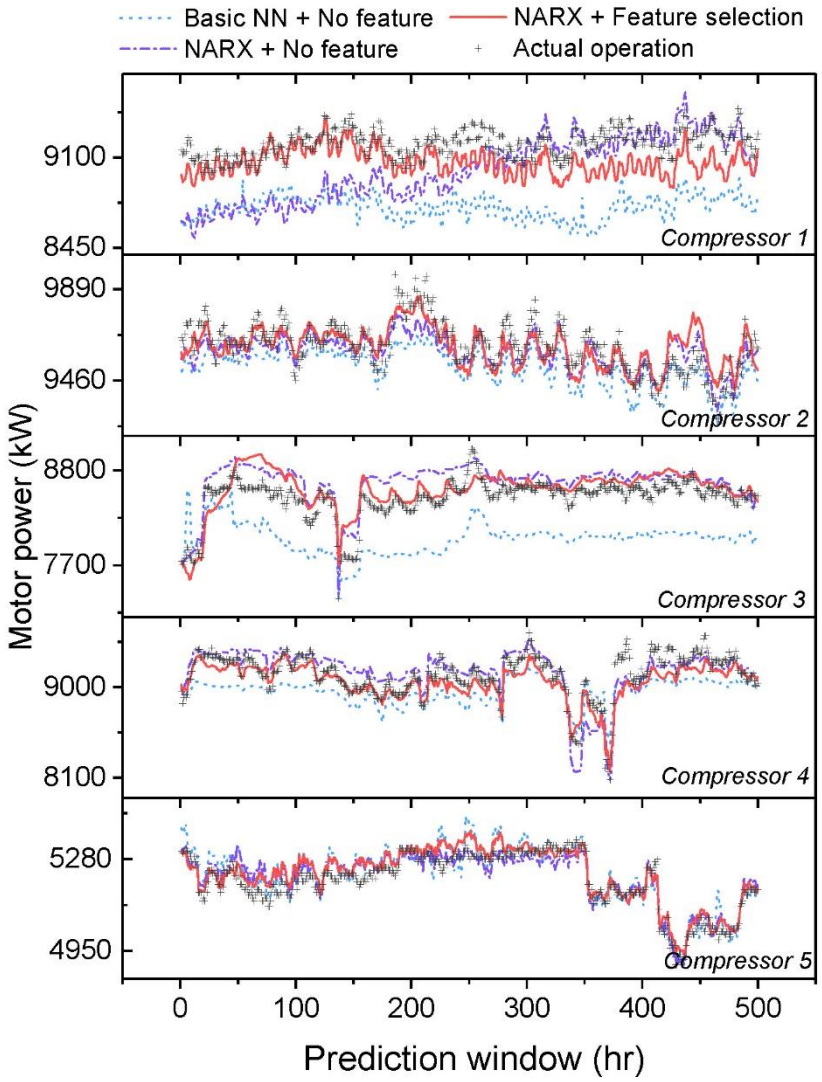

Figure 3-10. Prediction performance comparison of 1st~5th multi-stage compression system

Table 3-5. Mean squared error between modeling methodology and actual operating value

Model	1st compression system	2nd compression system	3rd compression system	4th compression system	5th compression system
Simple NN+ no feature selection	10338.958	2653.705	11378.31	4725.647	1179.428
NARX+ no feature selection	6065.407	1597.852	4565.14	3046.706	899.2753
NARX+ feature selection	3404.824	1150.069	3953.58	2635.378	842.8104

3.5.2. NARX-RTO result using virtual plant model

Fig. 3-11 shows trend lines in the prediction window of total power consumption during actual operation and the results of the NARX-RTO model. It also shows the accuracy of the virtual plant design and the verification of the optimization results through the output of the virtual plant according to the actual input conditions and the optimal input conditions derived by the NARX-RTO. As a result, an average of 4% (about 1400 kW) of power can be saved based on virtual plant results over 52 hours. The integrated NARX model updates every 5 hours and requires about 5 minutes of calculation time. Hence, the real-time update is not an issue when applied to an actual plant. The NARX model developed in this study estimates the output of the next time step by using the 5 hour-delayed input set and the output set. Accordingly, we updated the model every 5 hours. The virtual plant designed with actual data shows an average accuracy of 99.6%, and the virtual plant and NARX-RTO model with the optimized raw input set has an average accuracy of 98.3%. In addition, we use the result of the virtual plant designed by actual plant data instead of using the result of the model itself in the optimization and model update stage at the next time step. In this way, it was possible to remedy the inaccuracies of the NARX-RTO that occurred at the beginning of the model update.

Table 3-6 also shows the variation of the optimization variables in the prediction window of 1 hr (ambient temperature = 298 K, ambient humidity = 74.2%) and prediction window of 52 hrs (ambient temperature = 305 K,

ambient humidity = 68.8%). The flow rates for the first and second compressors were reduced, and the flow rates through the third and fourth compressors were increased. This results in lowering the flow rate of the system with relatively low compression efficiency and increase the flow rate of the system with relatively high efficiency within a level satisfying the basic mass balance of the system according to a given external disturbance condition. The model of each system designed by the NARX NN modeling method predicts the output and parameters given the past input and output data. The predicted parameters are difficult to measure such as the temperature between the compression stages, the rotational speed of each stage, the friction loss, etc. The change in the flow distribution between the compressors comprehensively calculates the effect of the predicted parameters, external disturbance and the aging effect over time. This makes it possible to generate a minimum amount of power under given conditions. Basically, in the prediction window 1 and 52 hrs, the increase in the flow rate of the multi-stage compressor of the third compression system is the largest. This means that the compression efficiency of the third system is the highest. If the mass balance was no longer able to increase the flow rate of the third system, it could be seen that the flow rate of the fourth system was increased. On the contrary, the system with the lowest internal efficiency of the compressor is the first compression system, which shows that the flow rate is the most reduced. The nature of the data-driven model based on the neural net does not reveal the exact proportion of internal parameter influences, external

disturbance effects, and system aging effects on the overall change of efficiency. However, it can be deduced that the influence of the internal parameter is the greatest in that the amount of flow movement due to the change of the prediction window is smaller than the flow amount of movement due to the optimization. As the prediction window changes from 1 hour to 52 hours, the external disturbance value changes and the efficiency decreases due to aging. It can be seen that more amount of flow at 52 hours enters the fourth system and the flow at the second system decreases. This is the result of the NARX-RTO learning the characteristics of the system according to changes in external conditions and time, and arranging the flow rate into a system with better efficiency.

Similarly, in the case of the expander, the flow rate to the expander of the second and fourth systems increases and the flow rates of the first and third systems decreases. These changes show that the NARX model predicts that the expanders in the second and fourth systems have higher efficiency than the expanders in the first and third systems, and this is also the result of training the factors such as the internal state of the system, the influence of external disturbance, etc. Unlike the compressor, the expander has raw measurement data for each stage so that it can be used for model training and the optimal temperature for each stage can be determined. Therefore, the efficiency difference between stages can be analyzed through the optimal temperature of the off-gas entering each stage of the multi-stage expander calculated by

NARX-RTO. The most notable result is the multi-stage expander of the third system, in which the inlet temperature of stage 1 is increased, and the inlet temperature of stage 2 is reduced compared to the results before optimization. This means that the efficiency of the first stage is relatively higher than that of the second stage, and thus produces power through a relatively large temperature difference in the first stage with high efficiency and produces the minimum power in the second stage with low efficiency.

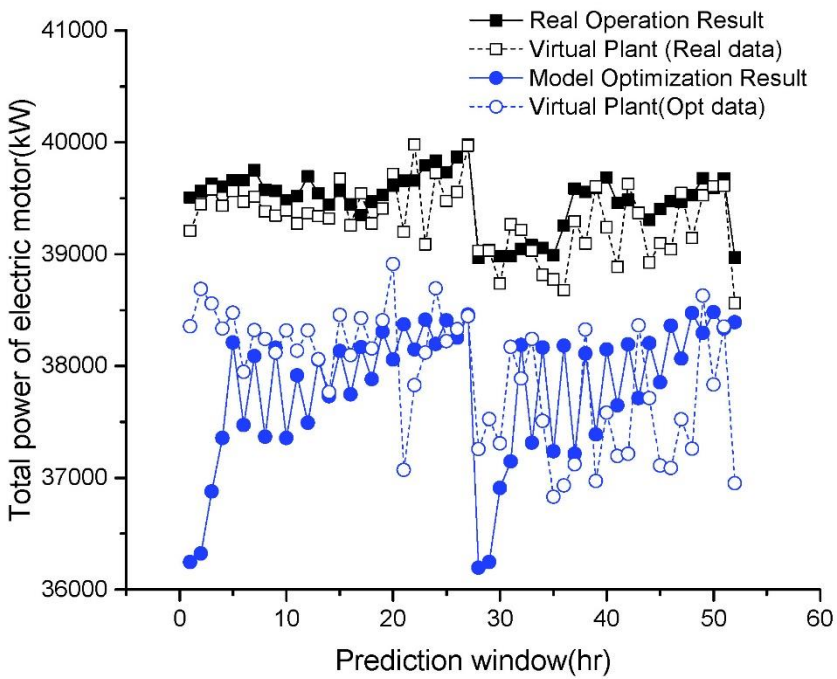

Figure 3-11. Result of NARX-RTO & validation.

Table 3-6. Comparison of optimization variables before and after NARX-RTO

Opt variable	Before optimization	After optimization (t=1hr,temp=298K,humidity=74.2%)	After optimization (t=52hr,temp=305K,humidity=68.8%)
1	71.10	66.20	66.20
2	65.70	64.60	64.25
3	75.90	82.90	82.90
4	80.90	82.30	82.65
5	36.30	36.50	36.50
6	0.30	0.00	0.00
7	15.50	13.60	13.60
8	0.20	2.10	2.10
9	3.60	1.80	1.80
10	0.00	0.00	0.00
11	3.20	5.00	5.00
12	2.10	2.10	2.10
13	0.00	0.00	0.00
14	40.00	39.90	39.90
15	22.40	25.53	25.10
16	76.20	74.97	75.40
17	87.50	88.50	88.50
18	5.10	5.10	5.10
19	28.20	29.93	29.50
20	2.50	2.30	2.30
21	41.70	41.90	41.90
22	108.00	108.20	108.20
23	9.60	10.00	10.00
24	7.10	6.70	6.70
25	411.00	409.00	409.00
26	425.00	425.00	425.00
27	419.00	425.00	425.00
28	416.00	417.00	417.00
29	416.00	416.72	416.32
30	415.00	412.00	412.00
31	415.00	395.00	395.00
32	418.00	418.00	418.00

CHAPTER 4. Design of Control System for Parallel Compression System[†]

4.1. Introduction

Centrifugal compressors are one of the most important equipment in petrochemical, natural gas, and chemical plants. A centrifugal compressor is expensive and has a critical effect on the entire chemical process. Therefore, the control and maintenance of a stable compressor system is critical to robust plant management. A compressor system is primarily employed to maintain a constant discharge pressure and needs to stay protected against surge phenomena. A surge phenomenon, i.e., unstable back-and-forth flow in the centrifugal compressor, occurs when the suction volumetric flowrate of the com pressor is lower than the limit line, i.e., the surge flowrate as indicated in Fig. 4-1. When the suction volumetric flowrate is lower than surge line, the resistance of the discharge side is higher than the head increase across the compressor. In the condition, it is not possible to keep this pressure gradient any more. It causes a periodic local back and forward flow, which is the surge phenomena. The surge phenomena causes back flow and vibration, which are damaging to the bearings, seals, and other parts of the

[†] This chapter cites the author's published journal article: Jung, J., Lee, W., Park, S., Kim, Y., Lee, C., & Han, J. (2017). Improved control strategy for fixed-speed compressors in parallel system. Journal of Process Control, 53, 57-69.

compressor. Therefore, a surge and particularly a surge at a high energy must be prevented during centrifugal compressor operation (McKee and Garcia-Hernandez, 2007). Surge phenomena are generally caused by poor matching of the compressor, inappropriate compressor design, and an inadequate anti-surge control system (Boyce, 2003). Because a surge phenomenon shuts down the entire process and causes mechanical damage to the centrifugal compressor, the control system should quickly prevent a surge (Stanley and Bohannan, 1997). For these reasons, various parametric studies have been conducted, and various scenarios have been analyzed to achieve instant and stable anti-surge control (Botros and Ganesan, 2008; Li et al., 2013; Shehata et al., 2009; Gravdahl et al., 2013; Helvoirt, 2007; Kvangardsnes, 2009).

However, discharge-pressure control and anti-surge control usually occur in opposite directions because of control interference (Rammler, 1994). This inner-compressor control interference can cause a control instability or significant oscillations. A load-sharing control system should also be incorporated in a parallel centrifugal compressor system (Rammler, 1994; Hansen, 2008; Manske et al., 2000; Xenos et al., 2015). Load sharing is an important consideration for energy efficiency and control in a parallel compressor system (Overvag, 2013). This inter-compressor control interference can cause inefficient or overloaded operation; hence, it should be decoupled for stable and efficient operation (Hansen, 2008; Grong, 2009).

Therefore, a parallel compressor system requires an advanced control structure rather than a simple feedback control structure (Stanley and Bohannan, 1997). Previous studies on multiple-compressor load sharing have traditionally focused on minimizing the energy consumption or maximizing efficiency in various operation scenarios (Manske et al., 2000; Han et al., 2004; Song et al., 2012; Widell and Eikevik, 2010; Cortinovis et al., 2016; Wright et al., 1998). These previous studies considered the energy efficiency under steady-state conditions or normal operating condition but not the controllability under the unpredictable disturbance. An advanced feed-forward control structure for a fixed-speed compressor was introduced by Mitsubishi Heavy Industries to decouple the control interference in the parallel compressor system (Kazuhiro and Kengo, 2006). This control system concentrates on controllability rather than the efficiency of the compressor using a feed-forward control structure. Moreover, this control system breaks down the compressor system into one master compressor and one or more slave compressors. The master compressor controls the discharge pressure using combined feedback and the feed-forward signal. The slave compressors are only controlled by the feed-forward signal.

This feed-forward signal successfully decouples both inner- and inter-compressor control interference. This type of feed-forward control structure is widely applied in industry. The conventional feed-forward control

structure solves several but not all of the major control problems associated with the parallel compressor system. For instance, it cannot provide load-sharing capabilities when the compressor is operating in the surge control region. Further, it has a dead time for anti-surge control when the compressor is operating under a low load. This paper outlines the inadequacy of the conventional control structure and suggests an improved control structure for parallel centrifugal compressor systems. The improved control structure involves the integration of discharge-pressure control, load-sharing control, and anti-surge control. Using a scenario, it is shown that the proposed control structure exhibits improved load sharing and instant anti-surge control capabilities over the conventional control structure.

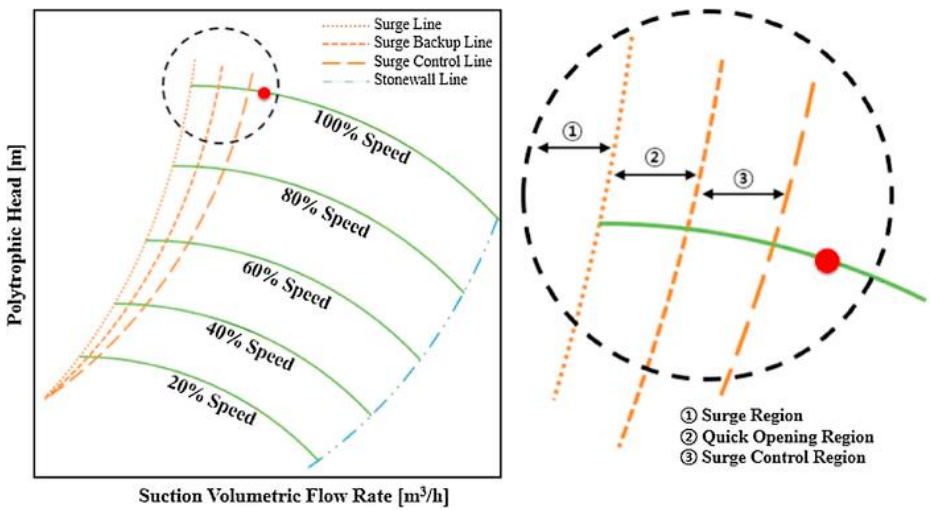

Figure 4-1. Compressor performance curve and anti-surge control lines

4.2. Problem Definition

Fig. 4-2 shows the conventional control structure for the parallel fixed-speed centrifugal compressor system introduced by Mitsubishi Heavy Industries (Kazuhiro and Kengo, 2006). A suction throttling valve (STV) controls the discharge pressure. When the discharge pressure is less than the set point, the STV opening increases. An anti-surge valve (ASV) prevents a surge phenomenon. When the suction volumetric flowrate is less than the surge control line, the ASV opens and recycles the discharge side stream to the suction side. The emergency shut down valve (ESDV) isolates the compressor system from the entire process. When the compressor shuts down, the ESDV immediately closes to protect the entire system. The master compressor solely controls the discharge pressure using the combined signal (CBS). The CBS is determined by the feedback signal (FBS) and feed-forward signal (FFS) according to Eq. (4-1). The weight factor, W1, is used to determine the pressure error sensitivity for the master compressor. The FBS is a valve-opening signal from the discharge-pressure controller, and the FFS is a signal for indicating the process target load, as given by Eqs. (4-2) and (4-3), respectively. The slave compressors use the FFS rather than the FBS to adjust the valve opening. This FFS successfully decouples the inner- and inter-compressor control interference under normal operating conditions. This feed-forward control structure determines the desired STV and ASV opening combination in

response to the change in the process target load, as indicated in Eqs. (4-4)–(4-15). The relationship between the desired valve opening and the target load (G(x), H(x)) is simply obtained from the steady-state conditions of the single compressor system. As the process load decreases, the desired STV opening decreases. When the process load is less than the threshold load, thereby causing a surge, the ASV begins to open to prevent a surge. Above the threshold load, only the STV opening is adjusted while the ASV remains closed. Below the threshold load, only the ASV opening is adjusted while the STV opening is fixed at its minimum value. This combination of the valve opening and process load is required to build the feed-forward control structure. This feed-forward control structure successfully decouples the inner- and inter-compressor control interference under normal operating conditions. The desired feed-forward control system can prevent a predictable surge phenomenon before the anti-surge controller becomes active. Although the feed-forward control system can prevent predictable surge phenomena, it cannot handle any unpredictable surge phenomena caused by a process disturbance, e.g., a change in the operating mode and process fluctuations. Therefore, an anti-surge controller is essential although the feed-forward control structure exists. Because there are two types of inlet signals for every single ASV, the valve opening signals OPASV_1 and OPASV_2 should be combined into a single signal. OPASV_1 is the signal from the feed-forward controller, and OPASV_2 is the signal from the anti-surge

controller. By using a high signal selector, the signal with the maximum value is selected as the final ASV opening, as indicated in Eq. (4-12).

. **Feed forward control structure for a parallel compressor system**

$$CBS = FFS + W_1 \times (FBS - P_0)$$

(Eq 4-1)

$$FBS = P_0 + K_P \times \left[e_P(t) + \frac{1}{\tau_I}\int_0^t e_P(t)\,dt\right], \quad e_P = P_{SP} - P_{PV}$$

(Eq 4-2)

$$FFS = F(Target\ Load) \times 100$$

(Eq 4-3)

For the master compressor

$$OP_{STV} = G(CBS), \qquad for\ CBS \geq Threshold\ point$$

(Eq 4-4)

$$OP_{STV} = OP_{STV\_Min}, \qquad for\ CBS < Threshold\ point$$

(Eq 4-5)

$$OP_{ASV} = MAX[OP_{ASV\_1},\ OP_{ASV\_2}]$$

(Eq 4-6)

$$OP_{ASV\_1} = 0, \qquad for\ CBS \geq Threshold\ point$$

(Eq 4-7)

$$OP_{ASV\_1} = H(CBS) \qquad for\ CBS < Threshold\ point$$

(Eq 4-8)

$$OP_{ASV\_2} = P_0 + K_P \times \left[e_{SF}(t) + \frac{1}{\tau_I}\int_0^t e_{SF}(t)\,dt\right], \quad e_{\mathrm{SF}} = SF_{SP} - SF_{PV}$$

(Eq 4-9)

For the slave compressor

$$OP_{STV} = G(FFS), \qquad for\ FFS \geq Threshold\ point$$

(Eq 4-10)

$$OP_{STV} = OP_{STV\_Min}, \qquad for\ FFS < Threshold\ point$$

(Eq 4-11)

$$OP_{ASV} = MAX[OP_{ASV_1},\ OP_{ASV_2}]$$

(Eq 4-12)

$$OP_{ASV\_1} = 0, \qquad for\ FFS \geq Threshold\ point$$

(Eq 4-13)

$$OP_{ASV\_1} = H(FFS), \qquad for\ FFS < Threshold\ point$$

(Eq 4-14)

$$OP_{ASV\_2} = P_0 + K_P \times \left[e_{SF}(t) + \frac{1}{\tau_I}\int_0^t e_{SF}(t)\,dt\right], \quad e_{SF} = SF_{SP} - SF_{PV}$$

(Eq 4-15)

The conventional control structure introduced by Mitsubishi Heavy Industry operate as an equal distance (or equal load distribution) control logic under desired operating conditions. Additionally, this feed-forward control structure is a specialized control structure for rapid response to a disturbance from the gas turbine in a parallel compressor system. This feed-forward control system delivers robust control performance for simultaneous discharge-pressure control and anti-surge control. However, this feed-forward structure has two disadvantages, the first of which is poor load sharing.

Poor load sharing occurs when the system operates in the unpredictable surge control region. When the anti-surge controller is active in the slave

compressor, the anti-surge controller increases the ASV opening to recycle the discharge stream to the suction side. Although it is not a problem for a single compressor system, it is a significant problem for a parallel compressor system, as indicated in Fig. 4-3. Because recycling the discharge flow in the slave compressor reduces the total discharge pressure, the master compressor begins to control the discharge pressure by opening the STV. As a result, the master compressor handles a much greater process load than the slave compressor. Because it reduces the suction volumetric flowrate of the slave compressor, the ASV opening of the slave compressor increases again. Although the suction volumetric flowrate is identical among the compressors, this is not the desired load sharing. Fig. 4-3 shows a simple example for different net flowrates in each compressor. Although all of the compressor suction volumetric flowrates are 75 m3/h (equal distance), the net process flowrates are 75, 50, 25, and 0 m3/h in the master compressor, slave compressor 1, slave compressor 2, and standby compressor, respectively. The standby compressor is installed for handling the failure of other compressors that can cause significant loss in revenue (Rasmussen and Kurz, 2009). In the worst case, the ASV of the slave compressor fully opens. This means that the slave compressor changes to the full recycle mode, as in the standby

compressor. On the other hand, the master compressor is forced to handle twice the normal process load, causing an overload.

The other problem associated with the conventional feed-forward control structure is the dead time of the anti-surge controller. This scenario occurs under certain operating conditions. For instance, for low-load operation, the ASV is already opened by the FFS to prevent a predictable surge. In this condition, the ASV opening does not change quickly, although an unpredictable process fluctuation causes the anti-surge controller to become active. Because the conventional control structure uses a high signal selector to combine OPASV_1 and OPASV_2 as a single signal, the ASV opening is maintained at a constant value until OPASV_2 becomes higher than OPASV_1. This implies that the conventional control system has structural limitations for rapid anti-surge control for low-load operation. Table 4-1 presents a simplified example of the anti-surge control delay. From 150 ms to 250 ms, OPASV does not change, although the anti-surge controller remains active. During this period, the suction volumetric flowrate of the compressor becomes closer to the surge flow line. Although the absolute delay time

is not significantly long, critical problems arise if the surge control does not become active immediately.

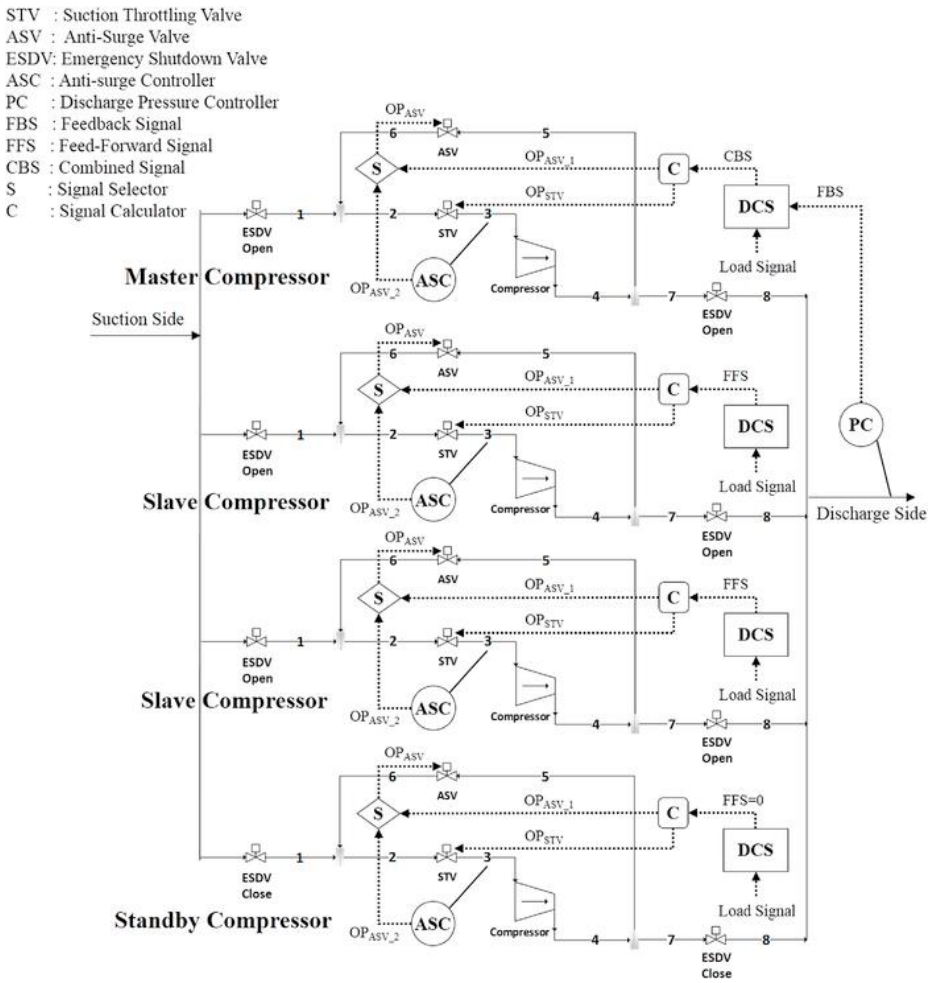

Figure 4-2. Conventional feed-forward control structure for the parallel compressor system.

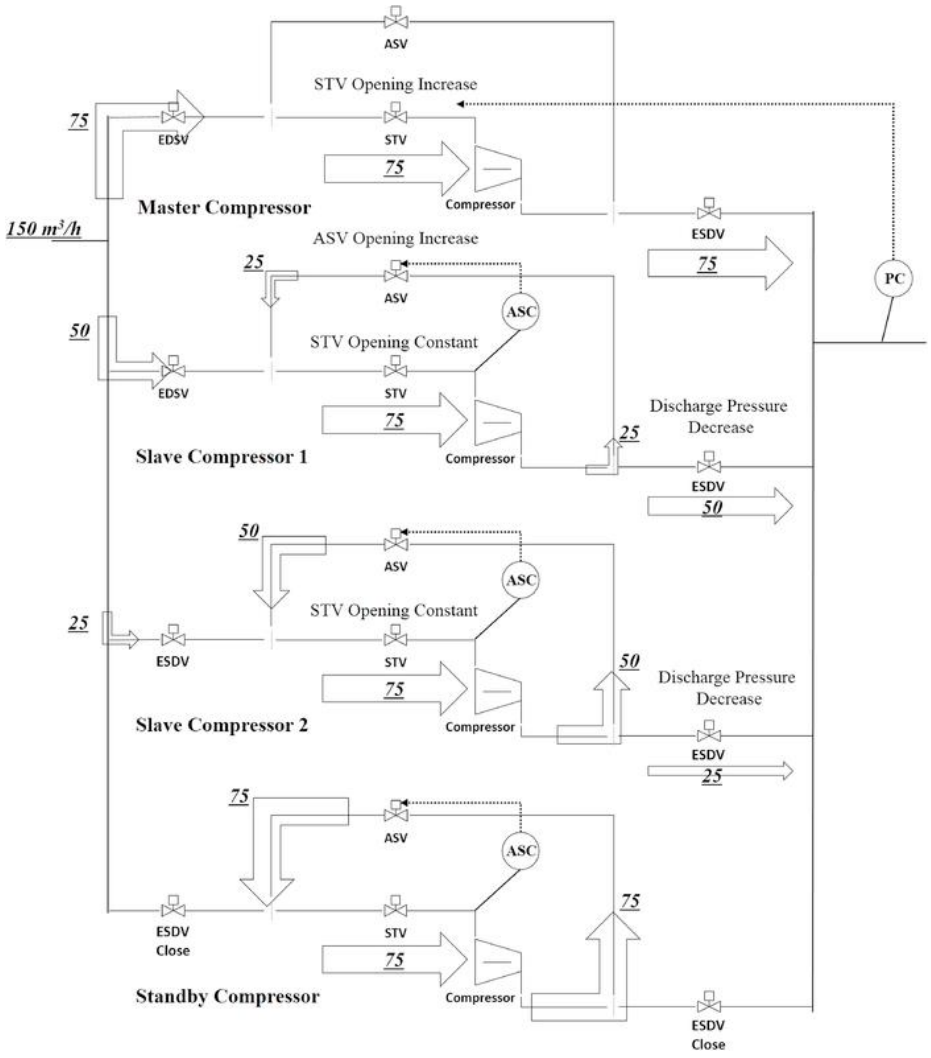

Figure 4-3. Example scenario of poor load sharing.

Table 4-1. Example scenario of anti-surge control delay

Process Time [sec]	1	2	3*	4*	5*	6	7
Suction Volumetric Flowrate [m^3/hr]	11100	11000	10900	10700	10400	11500	11400
Surge Control Line [m^3/hr]	11000	11000	11000	11000	11000	11000	11000
Anti-surge Controller	-	-	Active	Active	Active	Active	Active
Feed forward Signal (OP_{ASV_1})	50 %	50 %	50 %	50 %	50 %	50 %	50 %
ASC Signal (OP_{ASV_2})	0 %	0 %	10 %	20 %	40 %	70 %	60 %
ASV Opening (OP_{ASV})	50 %	50 %	50 %	50 %	50 %	70 %	60 %
Operation Region	Normal Region		Surge Control Region			Normal Region	

*Anti-surge control delay region

4.3. Improved Control Structure

The conventional feed-forward control structure is very practical and has robust control logic in a gas turbine system. The compressor system requires a quick response to a change in the turbine load, start up, emergency shut down. To handle a disturbance in the turbine section quickly, this feed-forward control logic is applied to real scenarios in industry. For this reason, we suggested the simplest method based on the conventional control structure for solving the problems with the poor load distribution and to obtain a quick surge response.

As indicated in Fig. 4-4, the discharge mass flowrate controller (FC) is added to the slave compressor for the desired load sharing. In addition, the high signal selector is replaced with a signal calculator for quick anti-surge control. First, for improving load-sharing control, the STV opening in the slave compressor is adjusted by the feed-forward signal (OPSTV_1) and discharge flowrate controller signal (OPSTV_2). To combine two signals into a single signal, the load-sharing weight factor (W2) is introduced, as indicated in Eqs. (4-16)–(4-19). When the anti-surge controller in the slave compressor is active, the ASV opens to recycle the discharge flow. As the discharge flowrate decreases, the discharge flowrate controller increases OPSTV_2. Although OPSTV_1 is constant because of the feed-forward signal, OPSTV_2 increases the final STV opening (OPSTV) according to Eq. (4-4). As the STV opening increases, the volumetric flowrate of the slave compressor increases. Finally, the slave

compressor easily escapes from operation in the surge control region. This improved load-sharing control structure prevents the slave compressor from switching to the full recycle mode. Furthermore, it helps to exit the surge region quickly by increasing the STV opening. Even a small value of W2 successfully ensures the desired load sharing. In the conventional control structure, the STV opening is not changed in the surge region. This can cause poor load sharing or operation in the full recycle mode for the slave compressor.

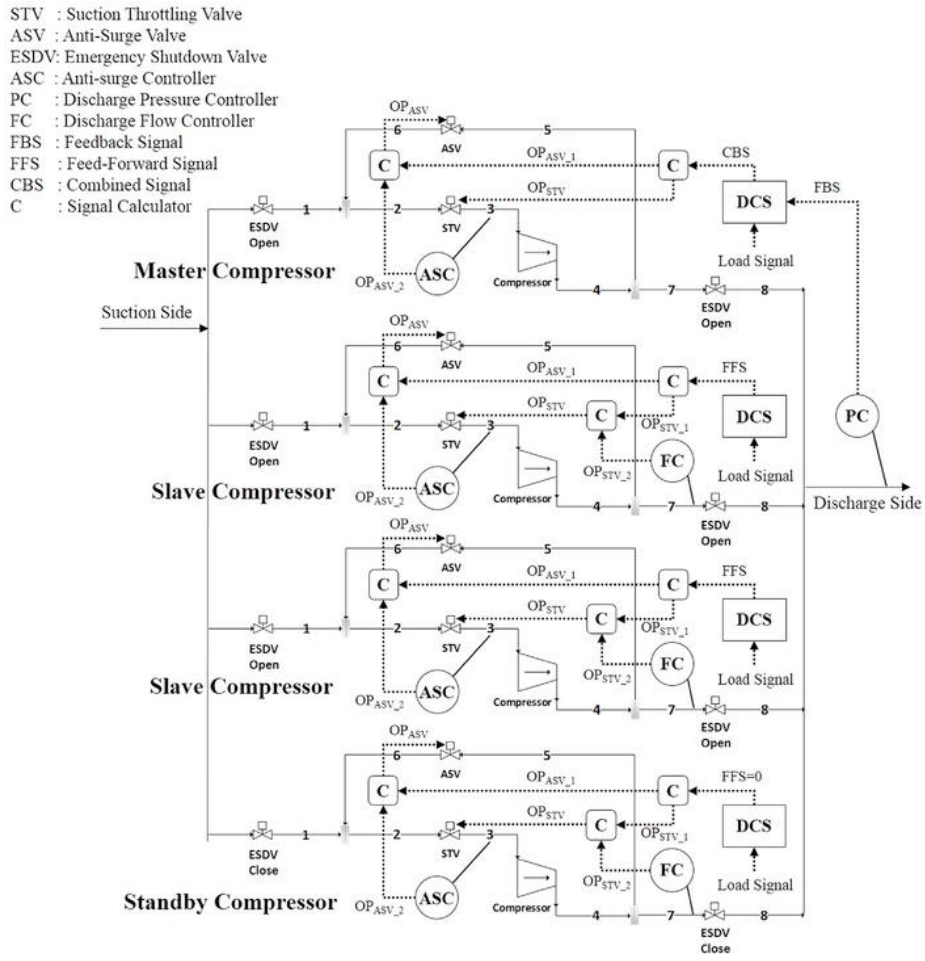

Figure 4-4. Improved feed-forward control structure for the parallel compressor system.

4.3.1. Improved load-sharing control structure for the slave compressor

$$OP_{STV\_1} = G(FFS), \qquad for\ FFS \geq Threshold\ point$$

(Eq 4-16)

$$OP_{STV\_1} = OP_{STV\_Min}, \qquad for\ FFS < Threshold\ point$$

(Eq 4-17)

$$OP_{STV\_2} = P_0 + K_P \times \left[e_{DF}(t) + \frac{1}{\tau_I}\int_0^t e_{DF}(t)\,dt\right], \quad e_{DF} = DF_{SP} - DF_{PV}$$

(Eq 4-18)

$$OP_{STV} = OP_{STV\_1} + W_2 \times (OP_{STV_2} - P_0)$$

(Eq 4-19)

To improve anti-surge controller dead time, the ASV opening is determined not by the high signal selector but by the nonlinear combination of OP_{ASV_1} and OP_{ASV_2}. As indicated in Eqs. (4-20) to (4-23), the nonlinear combination makes it possible to open the ASV immediately when the anti-surge controller becomes active. Although OP_{ASV_1} exists already, OP_{ASV_2} from the anti-surge controller increases the ASV opening without delay. Table 4-2 indicates the main difference

between the conventional control structure and the improved control structure.

the improved anti-surge control structure for the slave compressor:

$$OP_{ASV} = OP_{ASV\_1} + OP_{ASV\_2} - (OP_{ASV\_1} \times OP_{ASV\_2})/100$$

(Eq 4-20)

$$OP_{ASV\_1} = 0, \quad for\ x \geq Threshold\ point, \quad x = CBS\ or\ FFS$$

(Eq 4-21)

$$OP_{ASV\_1} = G(x) \quad for\ x < Threshold\ point, \quad x = CBS\ or\ FFS$$

(Eq 4-22)

$$OP_{ASV\_2} = P_0 + K_P \times \left[e_{SF}(t) + \frac{1}{\tau_I}\int_0^t e_{SF}(t)\,dt\right], \quad e_{SF} = SF_{SP} - SF_{PV}$$

(Eq 4-23)

Table 4-2. Comparison of the control structures of the conventional and improved control systems

	Conventional Control Structure	Improved Control Structure
Overall	$CBS = FFS + W_1 * FBS$ $FFS = F(Load\ signal)$ $FBS = E(e_P)$	
Master_STV	$OP_{STV} = G(CBS)$	$OP_{STV} = G(CBS)$
Slave_STV	$OP_{STV} = G(FFS)$	$OP_{STV} = OP_{STV\_1} + W_2 * (OP_{STV\_2}\text{-}50)$ $OP_{STV\_1} = G(FFS)$ $OP_{STV\_2} = E(e_{DF})$
Master_ASV	$OP_{ASV} = Max(OP_{ASV\_1}, OP_{ASV\_2})$ $OP_{ASV\_1} = H(CBS)$ $OP_{ASV\_2} = E(e_F)$	$OP_{ASV} = OP_{ASV\_1} + OP_{ASV\_2} - (OP_{ASV\_1} * OP_{ASV\_2})/100$ $OP_{ASV\_1} = H(CBS)$ $OP_{ASV\_2} = E(e_{SF})$
Slave_ASV	$OP_{ASV} = Max(OP_{ASV\_1}, OP_{ASV\_2})$ $OP_{ASV\_1} = H(FFS)$ $OP_{ASV\_2} = E(e_{SF})$	$OP_{ASV} = OP_{ASV\_1} + OP_{ASV\_2} - (OP_{ASV\_1} * OP_{ASV\_2})/100$ $OP_{ASV\_1} = H(FFS)$ $OP_{ASV\_2} = E(e_{SF})$

4.4. Modeling Basis

4.4.1. System Description

In this study, a dynamic model of a fuel gas supply plant was built using the commercial process simulator package ASPEN HYSYS ver. 7.3. The fuel gas supply plant model is based on an actual plant and consists of four compressor trains: one master compressor, two slave compressors, and one standby compressor. As indicated in Fig.4-5, fuel gas is compressed at a compressor train and supplied to the gas turbine. The main control target is to maintain a constant discharge pressure. As mentioned above, the conventional control structure separates the master compressor from the slave compressors. The master compressor solely controls the discharge pressure, whereas the slave compressor is controlled by the feed-forward signal. The standby compressor operates in the full recycle mode by the closing ESDV valves, as indicated in Table 4-3. The full recycle mode helps to maintain compressor operation during the transition mode (Kurz and White, 2009). Tables 4-4~4-6 list the stream and equipment information. For the anti-surge control system, the actual sampling rate is 40 ms, and the full valve opening time is 1 s (100%/s) because a rapid response is most important characteristic for an anti-surge controller. On the other hand, the process controller for the pressure, flowrate, temperature, etc. use 140 ms as a sampling rate and 16 s for the full valve opening (6.25%/s) because of the price issue and sample noise. The specified values have a ±20% deviation from the actual plant data for confidentiality reasons. To clarify the

superiority of our control structure over the conventional structure, the control performance is compared for two operating scenarios. The first scenario represents a decrease in the load set point to demonstrate load-sharing capabilities. The second scenario is a suction-side fluctuation to illustrate anti-surge control capabilities.

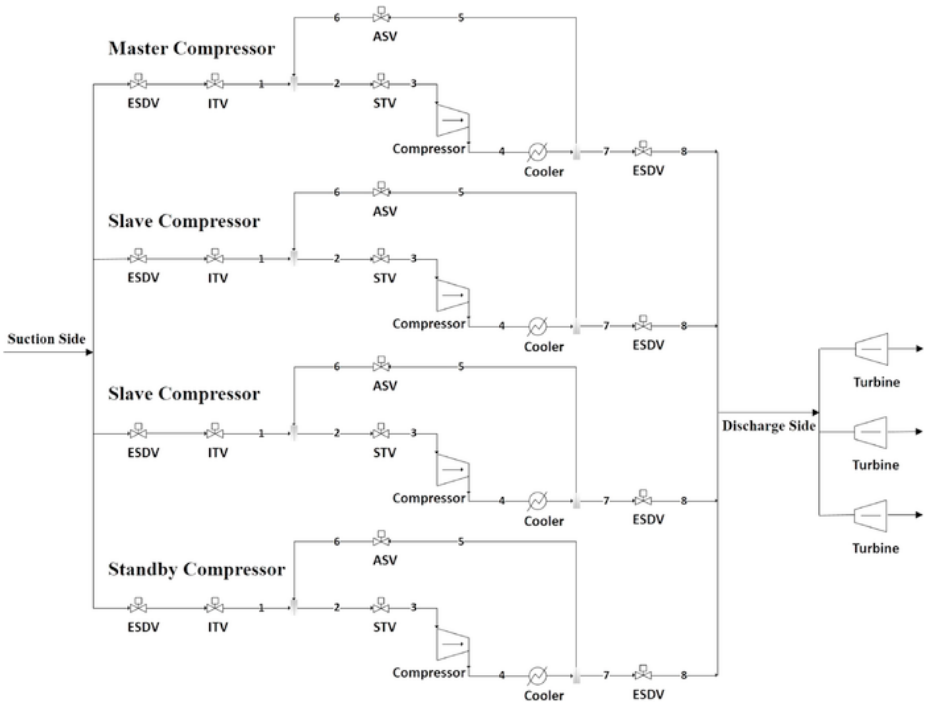

Figure 4-5. Configuration of the parallel compressor system for a fuel gas supply.

Table 4-3. Valves and motor for each compressor mode

	No. of Compressor	Target Load	ASV	STV	EDSV Valve
Master Compressor	1	1/3	Controlled by CBS	Controlled by CBS	Fully open
Slave Compressor	2	1/3	Controlled by FFS	Controlled by FFS	Fully open
Standby Compressor	1	0	Full Open	Full Open	Closed

Table 4-4. Stream information.

	Suction Side	Discharge Side	Unit
Temperature	60	60	ºC
Pressure	16.00 ± 0.05	34	barg
Mass Flow	30 ± 0.03	30	[ton/hr]
Molar Flow	1777 ± 18	1777	[kmol/hr]
Composition	Methane: 0.97 / CO2: 0.03		mol/mol
Molecular Weight	16.88		g/mol

Table 4-5. Equipment size information.

	Value	Unit
Synchronous Speed	1800	RPM
Full Load Speed	1793	RPM
Full Load Torque	29300	Nm
Full Load Power	5250	kW
Motor Inertia	800	kgm^2
Torque Speed Curve	NEMA Code B	-

Table 4-6. Compressor performance map.

Speed = 1800 RPM			
Volume Flow (Act m^3/h)	Head (m)	Polytrophic Efficiency (%)	Operation Region
8000	18500	78.3	Surge Region
8500	18730	81.0	Surge Region
9000*	18750	83.0	Surge Region
9500	18600	84.5	Surge Control Region
10000	18250	85.8	Normal Operation Region
10500	17780	86.8	Normal Operation Region
11000	17180	87.4	Normal Operation Region
11500	16530	87.5	Normal Operation Region
12000	15750	87.1	Normal Operation Region
12500	14800	86.1	Normal Operation Region
13000	13600	84.5	Normal Operation Region

***Surge Line**

4.4.2. Control Structure

Table 4-7 indicates the control system specifications that are typically used in a fuel gas supply plant. As mentioned in Section 4.3, the improved control structure consists of one additional flow controller and one nonlinear ASV calculator. Fig. 4-6 shows a simplified block diagram of the improved control structure. The feedback signal weight factor, W1, is set to 2, and the load sharing weight factor, W2, is set to 0.05. The FFS is defined as a percentage of the present target load divided by the maximum load. The STV opening function G(x) and ASV opening function H(x) represent the desired opening combination in a single compressor system. The entire control signal has a range from 0 to 100. The set point of the anti-surge controller is calculated through a linear regression of the surge flowrate at the maximum compressor speed. The synchronized speed of the motor is 1800 rpm, but the actual full-load speed of the compressor is 1793 rpm because of slip. As indicated in Table 4-8, the surge flow at a compressor speed of 1793 rpm is calculated on the basis of the surge flow at a compressor speed of 1800 rpm. The margin of the surge control line is set to 10% of the surge flowrate, and the margin of the surge backup line is set to 5% (Grong, 2009; Nored et al., 2008; Bentaleb et al., 2015). When the suction flowrate of the compressor reaches the surge control line, the anti-surge controller becomes active. When the suction flowrate of the compressor reaches the backup line, the interlock system immediately forces the ASV to fully open, as indicated in Fig. 4-1. Table 4-9 lists the control

parameters for the anti-surge controller. The anti-surge controller uses aggressive control parameters in the surge control region for a rapid response. Moreover, signal time delay of the anti-surge controller is much shorter than that of the process controller. The indicated control parameters are adjusted on the basis of the model stability because of confidentiality issues.

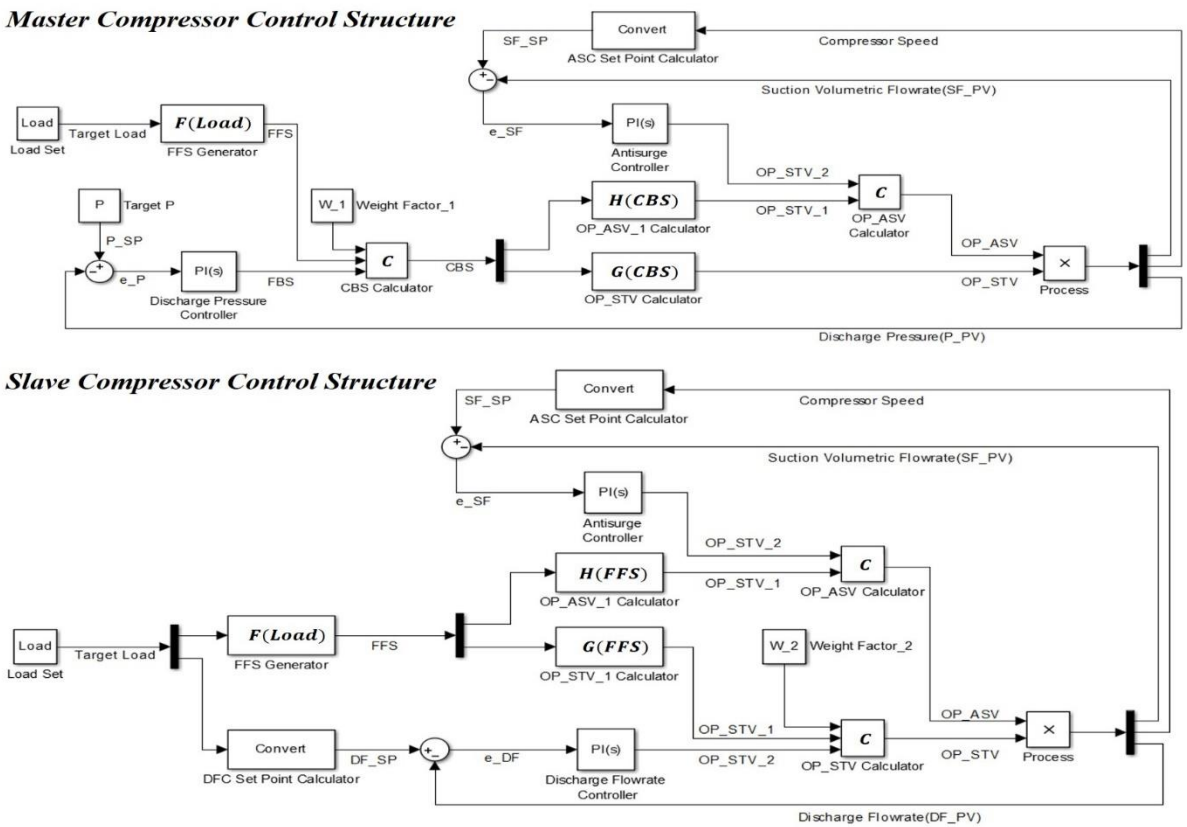

Figure 4-6. Control diagram for the master and slave compressors of the improved control system..

Table 4-7. Detailed information of the control structures.

	Conventional Control Structure	Improved Control Structure
FFS generator	*F(Target Load) = Target Load / Maximum Load * 100*	
FBS generator (Pressure Controller)	*Equation (1-2)* P_{SP} *= 34 barg,* P_0 *= 50*	
CBS Calculator	*Equation (1-3)* W_1 *= 2*	
OP_{STV_1} Calculator	*G(x) = 12/20 * (x-80) + 68, for x > 80, x = CBS or FFS* *G(x) = 68, for x < 80, x = CBS or FFS*	
OP_{STV_2} Calculator (Discharge Flow Controller)	-	*Equation (3-3)* DF_{SP} *= Target Load / 3,* P_0 *= 50*
OP_{STV} Calculator	-	*Equation (3-4)* W_2 *= 0.05*
OP_{ASV_1} Calculator	*H(x) = 0, for x > 80, x = CBS or FFS* *H(x) = 1.25*(80-x), for x < 80, x = CBS or FFS*	
OP_{ASV_2} Calculator (Anti-surge Controller)	*Equation (2-9)* SF_{SP} *= 9591* m^3*/hr,* P_0 *= 0*	
OP_ASV Calculator	*Equation (2-10)*	*Equation (3-5)*

Table 4-8. Surge controller set points.

	Speed 1800 RPM	**Surge Line Margin**	**1st order regression**	**Speed 1793 RPM**
Surge Line	9000 [m^3/hr]	0%	Speed * 5.00	8965 [m^3/hr]
Surge Backup Line (Quick Opening Interlock)	9450 [m^3/hr]	5%	Speed * 5.25	9412 [m^3/hr]
Surge Control Line (Surge Control SP)	9900 [m^3/hr]	10%	Speed * 5.50	9860 [m^3/hr]

Table 4-9. Controller parameter specifications.

		Kc	Ti	Td	Time delay
Turbine Flowrate Controller		0.500	0.100 s	-	1.0 s
Discharge-Temp. Controller		0.500	0.100 s	-	1.0 s
Discharge-Pressure Controller		0.500	0.100 s		1.0 s
Anti-surge Controller	Normal Opening Region	0.250	0.100 s	-	0.2 s
	Surge Control Region	2.500	0.100 s	-	
	Quick Opening Region	Interlock, Immediately Fully Open			

4.5. Simulation Results

4.5.1. Load-sharing performance in the turn-down scenario

Fig. 4-7 shows the results for the control performance when the total process load changes from 90% to 70%. As the total process load decreases, the suction volumetric flowrate decreases at first (regions A1 and B1). When the suction volumetric flowrate reaches the anti-surge control line, the anti-surge controller of the slave compressor becomes active (regions A2 and B2). Therefore, the ASV of the slave compressor is opened by OPASV_2 instead of OPASV_1. To maintain a constant discharge pressure, the STV opening of the master compressor is increased. In the conventional control structure in Fig. 4-7(a), the suction volumetric flowrate of the slave compressor does not increase even though the ASV opening increases (region A2). As mentioned above, this problem occurs because the STV of the master compressor is opened to control the discharge pressure. The ASV is open as long as the STV of the master compressor reaches the maximum opening. Finally, the ASV opening of the slave compressor reaches 36%, whereas the ASV of the master compressor remains closed. The suction volumetric flowrate of the slave compressor is maintained at the anti-surge control line (9860 m3/h), whereas the suction volumetric flowrate of the master compressor is much larger (12300 m3/h). The master compressor handles 56% of the total load while the two slave compressors handle 44% of the total load. As indicated in Table 4-10, the net

master-to-slave discharge flow-rate ratio is 2.6. Therefore, the master compressor handles a much larger process load than the slave compressor (region A3). As shown in the compressor performance map in Fig. 4-8, the operating points are very different for the master and slave compressors. Because the STV opening is at its maximum, the discharge-pressure control has a control offset up to 1.19 barg (region A3). This poor load sharing causes discharge-pressure control failure and an efficiency loss. In contrast, the improved control structure exhibits the desired load sharing for the same operating scenario. As the anti-surge controller opens the ASV of the slave compressor, the net discharge flowrate decreases. To increase the discharge flowrate, the master compressor opens the STV quickly (region B2). As a result, the net discharge flowrate at the slave compressor is much lower than that at master compressor. To adjust the net discharge flowrates to be the same, the discharge flowrate control signal increases. As a result, the STV opening of the slave compressor slightly increases from 68.0% to 69.6% according to Eq. (3-4). Although the STV opening of the slave compressor increases very slightly, it increases the suction volumetric flowrate of the slave compressor again. Simultaneously, the STV and the ASV openings of the master compressor are both adjusted to control the discharge pressure. As indicated in Fig. 4-8(b), the operating points are almost same for the master and slave compressors. Under the feed forward control structure, the ASV opening of the slave compressor is determined by OPASV_1 and OPASV_2 signals as indicated in equations (2-

12). The OPASV_1 is a function of the feed forward signal while the OPASV_2 is a function of the ASC signal. Under the desired operating condition, the ASC signal is always zero because the feed forward signal make the ASV open before the anti-surge controller is active (Fig. 4-8(b)). In this case, the ASV opening is synchronized with OPASV_1. However, feed forward signal is not able to handle the unpredictable operating disturbance. To avoid the surge under the disturbance, the anti-surge controller is active and ASC signal determined the ASV opening. In that case, the ASV opening is synchronized with OPASV_2 or ASC signal (Fig. 4-8(a)).

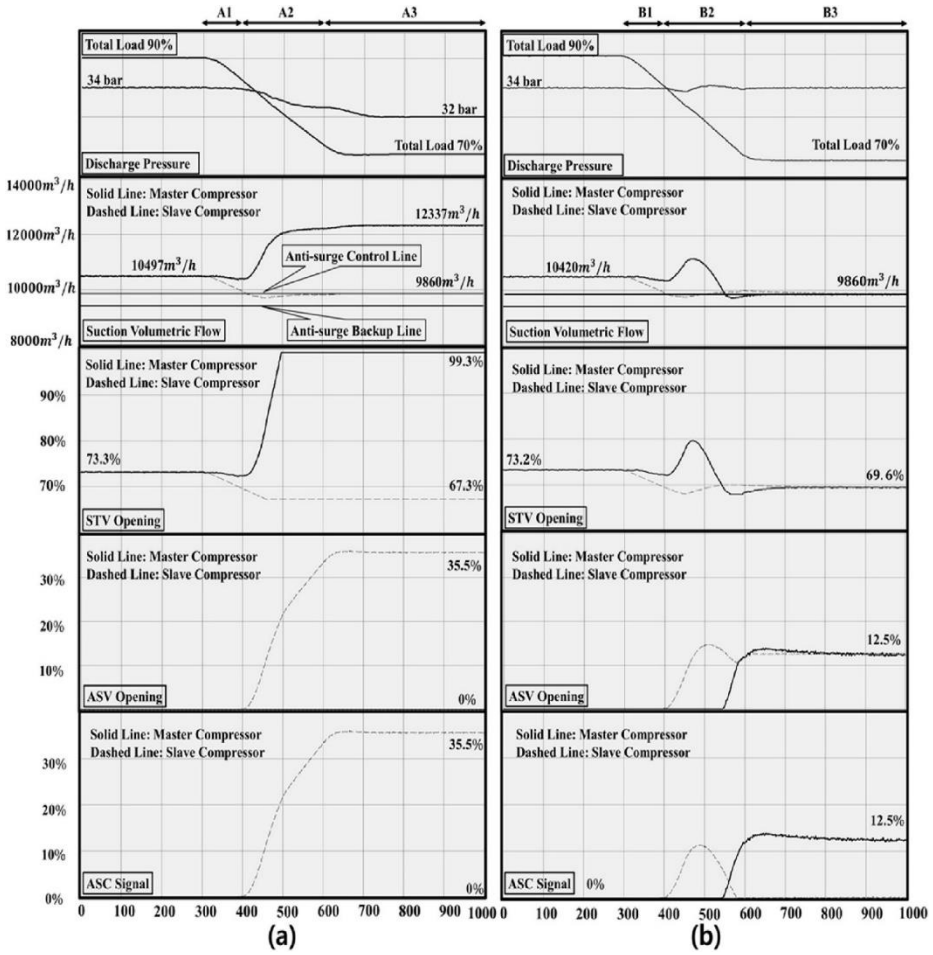

Figure 4-7. Results for the turn-down scenario with (a) a conventional control system and (b) the improved control system.

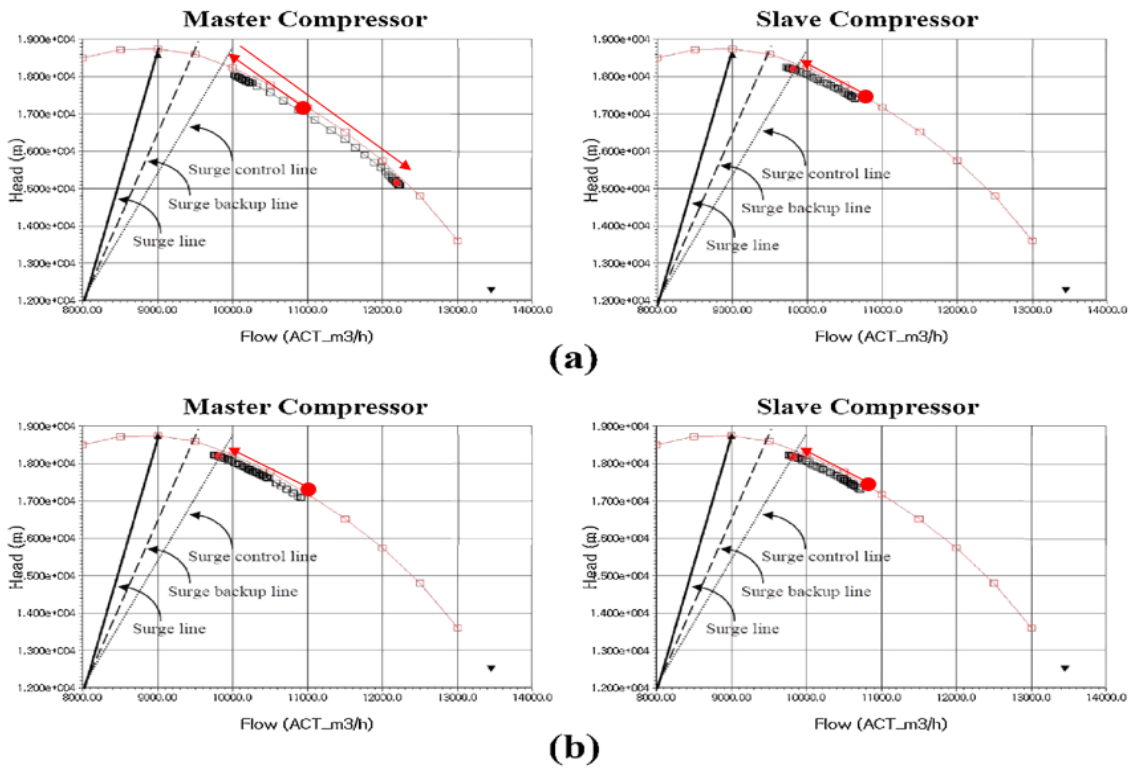

Figure 4-8. Compressor performance map for the (a) conventional control system and (b) improved control system in the turn-down scenario.

Table 4-10. Control performance results of the turn-down scenario.

	Conventional Control System	**Improved Control System**
Total Load	90.0% => 70.0%	90.0% => 70.0%
Discharge Pressure	34.0 barg => 33.3 barg	34.0 barg => 34.0 barg
Master Compressor		
STV Opening (OP_{STV})	71.8 % => 100 %	73.2 % => 69.4 %
ASV Opening (OP_{ASV})	0.00 % => 0.00 %	0.00 % => 12.3 %
Suction Volumetric Flowrate	10250 m^3/hr =>12250 m^3/hr	10500 m^3/hr => 9860 m^3/hr
Operation Region	Normal Operation Mode	Anti-surge Control Region
Slave Compressor		
STV Opening (OP_{STV})	74.0 % => 68.0 %	73.3 % => 69.6 %
OP_{STV_1}	74.0 % => 68.0 %	74.0 % => 68.0 %
OP_{STV_2}	-	36.0 % => 82.0%
ASV Opening	0.00 % => 36.0 %	0.00 % => 12.5 %
Suction Volumetric Flowrate	10600 m^3/hr => 9860 m^3/hr	10500 m^3/hr => 9885 m^3/hr
Operation Region	Anti-surge Control Region	Normal Operation Mode

4.5.2. Anti-surge control performance for the scenario in which there is a suction-side pressure fluctuation

Fig. 4-9 shows the results for the control performance for a scenario in which the suction-side pressure fluctuates in low load operation. As the target load sets 70%, a part of the discharge flow is recycled to the suction side through the ASV to avoid surge. In this condition, the scenario assumes that the suction-side pressure decreases for 30 s and returns to the original state in 30 s with a 10% variation (from 16.0 barg to 14.4 barg). The 10% variation is the maximum value for inspecting the robustness of the control structure. As the suction-side pressure decreases, the master compressor controls the discharge pressure by increasing the STV opening (regions A1 and B1). As a result, the suction volumetric flowrate of the master compressor increases, while the suction volumetric flowrate of the slave compressor decreases. As the suction volumetric flowrate of the slave compressor decreases, the anti-surge controller becomes active.

In the conventional control structure (Fig. 4-9(a)), the ASV opening of the slave compressor does not change immediately, although the anti-surge controller becomes active (region A1). This is because the conventional control structure uses the high signal selector to determine the final ASV opening (OPASV). While the anti-surge controller signal is lower than the feed-forward signal (12.62%), the ASV of the slave compressor maintains a constant opening value. Finally, the volumetric flowrate of the slave compressor gradually

decreases and reaches the backup line (at 225 s). As soon as the volumetric flowrate reaches the backup line, the interlock system of the compressor becomes active and then, ASV of the slave compressor fully opened immediately. Although the quick opening of the ASV successfully protects the compressor against the surge phenomenon, the discharge pressure suddenly decreases from 34.0 barg to 22.0 barg. To adjust discharge pressure, the STV of the master compressor fully opens. As a result, the entire system experiences a large fluctuation and an energy loss.

In contrast, the improved control structure successfully handles the suction-side pressure fluctuation. The ASV opening of the slave compressors immediately increases when the anti-surge controller becomes active (region B1). The nonlinear combination explained via Eq. (4-5) makes the ASV of the slave compressors open immediately. As the ASV opening of the slave compressor increases, the suction volumetric flowrate of the slave compressor increases. After the slave compressor exits the surge control region, the anti-surge control signal gradually decreases without interlock system activation. Simultaneously, the STV and ASV of the master compressor are adjusted to control the discharge pressure. The minimum pressure is 32.5 barg, and the maximum pressure is 36.2 barg for this scenario. The control performance results are compared in Table 4-11.

In the conventional control structure, the ASV opening maintains 12.62% in 200s–220s. It means the conventional control structure was not able to conduct anti-surge control for 20 s. On the other hand, the improved control structure immediately opens the ASV from 12.62% to 18% for 20 s. This rapid response prevents that the suction side flowrate reaches the anti-surge backup line.

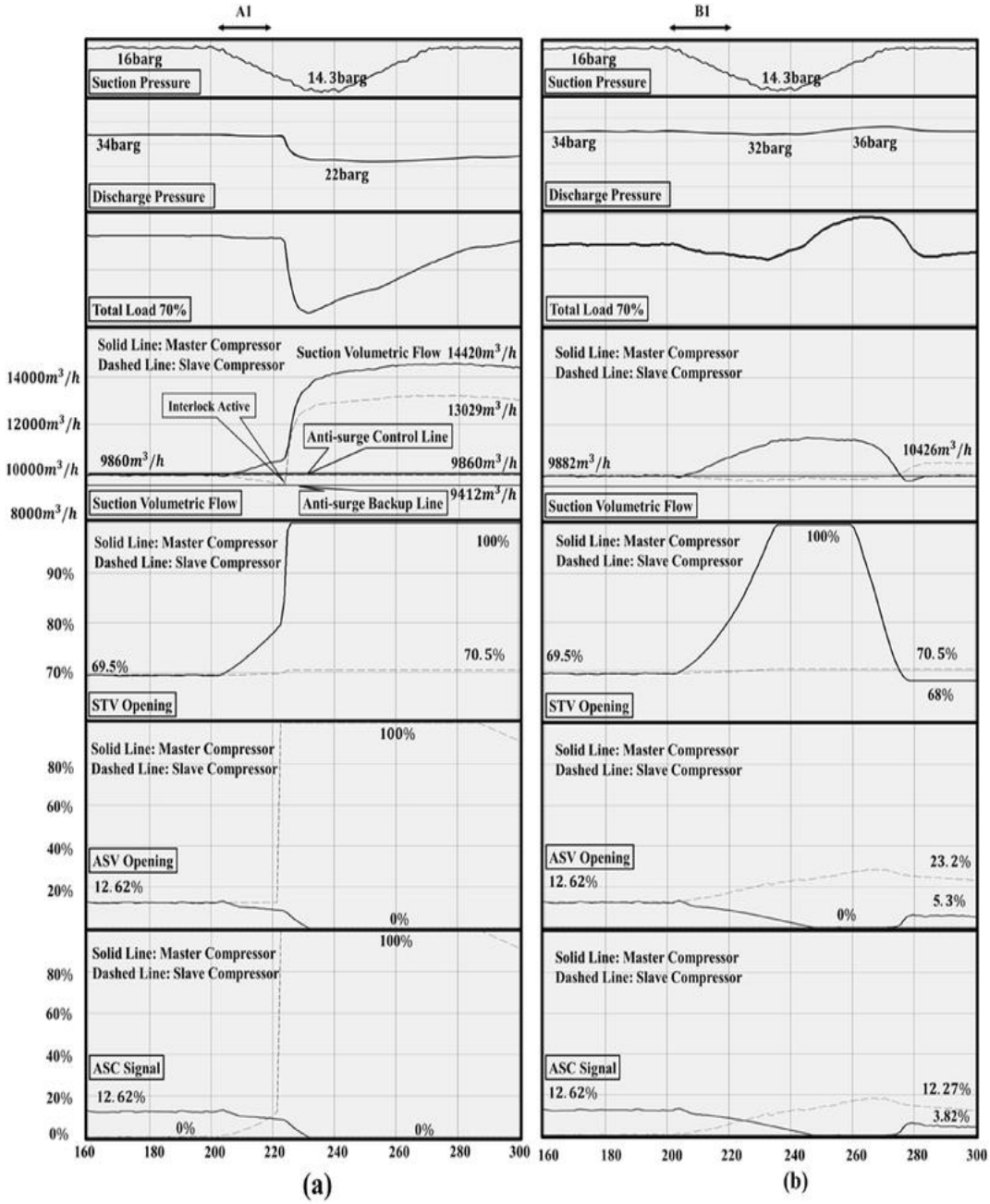

Figure 4-9. Results of the suction-pressure disturbance scenario with the (a) conventional control system and (b) improved control system.

Table 4-11. Control performance results of the scenario in which a suction-side pressure fluctuation occurs.

	Conventional Control System	**Improved Control System**
Suction Pressure	16.0 barg => 14.4 barg	16.0 barg => 14.4 barg
Discharge Pressure	34.0 barg => 22.0 barg	34.0 barg => 32.5 barg
Master Compressor		
STV Opening (OP_{STV})	69.4 % => 100 %	69.4 % => 100 %
ASV Opening (OP_{ASV})	12.3 % => 0.00 %	12.3 % => 0.00 %
Suction Volumetric Flowrate	9860 m^3/hr => 14500 m^3/hr	9860 m^3/hr => 11450 m^3/hr
Operation Region	Normal Operation Mode	Normal Operation Mode
Slave Compressor		
STV Opening (OP_{STV})	69.6 % => 70.5 %	69.6 % => 70.5 %
ASV Opening (OP_{ASV})	0.00 % => 36.0 %	0.00 % => 28.3 %
OP_ASV_1	0.00 % => 12.5 %	0.00 % => 12.5 %
OP_ASV_2	0.00 % => 36.0 %	0.00 % => 18.0 %
Suction Volumetric Flowrate	9885 m^3/hr => 9430 m^3/hr	9885 m^3/hr => 9650 m^3/hr
Operation Region	Quick Opening Region (Interlock System Active)	Surge Control Region

CHAPTER 5. Concluding Remarks

Firstly, in this thesis, the design approach considering the production change of natural gas well is suggested for PRICO® SMR liquefaction process. The optimization result confirmed that the optimum design point changes in the direction of smaller heat exchange area of the main heat exchanger when considering the feed gas load change. The degree of shift is determined by the difference in lower and upper bounds in load determined by the load variation scenario. Increasing the MR flowrate due to the reduction of the heat exchange area leads to an economic loss of increasing the compressor equipment cost and the operating cost at the maximum load operation. However, small heart exchange area has the effect of minimizing the tendency of the MR flowrate to increase with load reduction. The decrease in the fluctuation of the MR flowrate reduces the operating cost under the operation with less than 70% load, meaning that the design approach presented in this study can be economical in a wider operating window. In addition, the increase in compressor equipment cost was minimized in the case of two-trains, and it was found that the economic benefit was also achieved in the overall capital investment. Although it is ultimately dependent on the production shape of the natural gas well, which design approach is economical, the process design approach, which has a wider operating window economically, is of value because it is difficult to predict the

exact production of the well. Although not discussed in detail in this study, changing the optimal design point can also affect the operability of the process. Robust process operation due to load variation is one of the most important issues as well as economical operation. Especially, multi-stage compression system for SMR process is required to secure robust operability due to load variations. It is expected that the decrease of the fluctuation of the MR flowrate caused by the decrease of the heat exchange area may have a positive influence on the overall operability of the process. As the number of trains increases for the same load, the fluctuation of the MR flow decreases because the load variation capacity that each train has to deal with decreases. It is also shown that the new approach proposed in this study can be applied to the multi-train case to more effectively cope with the fluctuation of the MR flow. This analysis provides insight into the economics and operability of multi-train operation.

Secondly, when only limited sensor data and first principle models exist for industrial plants, a modeling methodology to predict the target output from the sensor data more precisely considering the reduction of the efficiency due to the aging of the device and the change of the ambient disturbance is suggested. Many existing studies have trained a simple feed-forward multi- layer perceptron neural networks with steady-state data and have not been able to extract the plant data into a specific feature, leading to an overfitted model. The NARX-NN structure is for a time- series data modeling, where the history of

outputs enters the input during the training. This allows for capturing dynamics with feedback loops and yields reliable predictions for the closed-loop system. Input features were chosen based on the physical properties from the equation of state in Aspen HYSYS simulator and the first-principle models for calculating compressor and expander work. The proposed model was applied to the air-gas compression system, which accounts for a significant portion of energy consumption in the chemical plant, and NARX-NN with feature extraction could reduce the MSE about 43.5% and 20% compared to simple feed-forward multi-perceptron neural networks and NARX-NN without feature extraction respectively. Such a model can handle time-varying stochastic nature such as system efficiency and external disturbances.

Finally, a parallel compressor system experiences inner- and inter-compressor control interference. To decouple the control interference, a feed-forward control structure is introduced and widely applied in industry. This feed-forward control structure usually provides robust control. However, it has two disadvantages in scenarios with unpredictable disturbances. The first drawback pertains to the poor load sharing that arises when the anti-surge controller becomes active in the slave compressor. The second drawback is related to the anti-surge control time delay for low-load operation. To solve these problems, an improved control structure is proposed for the parallel compressor system. The additional flow controller in the structure allows for

the desired load-sharing control for operation in unpredictable surge control regions. For immediate anti-surge control, the improved control structure uses a nonlinear combination of the anti-surge control signals rather than the high signal selector used in the conventional structure. The control performance of the improved control structure is compared with that of the conventional control structure by using a fuel gas supply plant model. Finally, the conventional feed-forward control structure is improved for operation in unpredictable anti-surge control regions.

References

Aspelund, A., Gundersen, T., Myklebust, J., Nowak, M.P., Tomasgard, A., 2010. An optimization-simulation model for a simple LNG process. Comput. Chem. Eng. 34, 1606–1617.

Azlan Hussain, M. (1999). Review of the applications of neural networks in chemical process control — simulation and online implementation. Artificial Intelligence in Engineering, 13, 55-68.

A. Cortinovis, M. Mercangöz, M. Zovadelli, D. Pareschi, A. De Marco, S. Bittanti, 2016. Online performance tracking and load sharing optimization for parallel operation of gas compressors. Comput. Chem. Eng., 88, pp. 145-156.

Botros, K. K., Kibrya, G., & Glover, A. (2000). A Demonstration of Artificial Neural Networks Based Data Mining for Gas Turbine Driven Compressor Stations. V002T003A008.

BP, 2017. BP Energy Outlook Energy 2017. BP Stat. Rev. World Energy 52.

Cao, L., Liu, J., Xu, X., 2016. Robustness analysis of the mixed refrigerant composition employed in the single mixed refrigerant (SMR) liquefied natural gas (LNG) process. Appl. Therm. Eng. 93, 1155–1163.

Castillo, L., Dorao, C.A., 2012. Consensual decision-making model based on game theory for LNG processes. Energy Convers. Manag. 64, 387–396.

Çoruh, S., Geyikçi, F., Kılıç, E., & Çoruh, U. (2014). The use of NARX neural network for modeling of adsorption of zinc ions using activated almond shell as a potential biosorbent. Bioresource Technology, 151, 406-410.

Couper, J.R., 2005. Chemical Process Equipment: Selection and Design, Chemical, Petrochemical & Process. Elsevier.

C. Hansen, 2008. Dynamic Simulation of Compressor Control Systems, Master of Science in Oil and Gas Technology. Aalborg University Esbjerg.

D.P. Xenos, M. Cicciotti, G.M. Kopanos, A.E. Bouaswaig, O. Kahrs, R. Martinez-Botas, N.F. Thornhill, 2015. Optimization of a

network of compressors in parallel: real time optimization (RTO) of compressors in chemical plants – an industrial case study. Appl. Energ.,

Ghorbanian, K., & Gholamrezaei, M. (2009). An artificial neural network approach to compressor performance prediction. Applied Energy, 86, 1210-1221.

Gravdahl, J. T., & Egeland, O. (2012). Compressor surge and rotating stall: modeling and control: Springer Science & Business Media.

Gresh, K. K. (1998). Field analysis of multisection compressors: Maintenance & retrofitting: A special report. Hydrocarbon processing, 77, 55-58.

G. Li, Y. Gu, J. Kong, G. Jiang, L. Xie, Z. Wu, Z. Li, Y. He, P. Gao, 2013. Intelligent control of air compressor production process. Appl. Math., 7, pp. 1051-1058.

Han, I. S., & Han, C. (2003). Modeling of multistage air compression systems in chemical processes. Industrial & Engineering Chemistry Research, 42, 2209-2218.

Han, I. S., Han, C., & Chung, C. B. (2004). Optimization of the Air- and Gas-supply Network of a Chemical Plant. Chemical Engineering Research and Design, 82, 1337-1343.

Haykin, S. (1994). Neural Networks: A Comprehensive Foundation: Prentice Hall PTR.

He, X.-D., Liu, S., Asada, H. H., & Itoh, H. (1998). Multivariable Control of Vapor Compression Systems. HVAC&R Research, 4, 205-230.

IRS, 2015. How To Depreciate Property. Publ. 946 Cat. No. 13081F 120.

Jung, J., Lee, W. J., Park, S., Kim, Y., Lee, C.-J., & Han, C. (2017). Improved control strategy for fixed-speed compressors in parallel system. Journal of Process Control, 53, 57-69.

J.T. Gravdahl, O. Egeland, S.O. Vatland, 2002. Drive torque actuation in active surge control of centrifugal compressors. Automatica, 38, pp. 1881-1893.

Khan, M.S., Karimi, I.A., Wood, D.A., 2017. Retrospective and future perspective of natural gas liquefaction and optimization technologies contributing to efficient LNG supply: A review. J. Nat. Gas Sci. Eng. 45, 165–188.

Khan, M.S., Lee, M., 2013. Design optimization of single mixed refrigerant natural gas liquefaction process using the particle swarm paradigm with nonlinear constraints. Energy 49, 146–155.

Kroschwitz, J. I., & Howe-Grant, M. (1991). Encyclopedia of chemical technology Kirk-Othmer. Wiley & Sons, New York, USA.

Kurz, R., & Brun, K. (2012). Fouling Mechanisms in Axial Compressors. Journal of Engineering for Gas Turbines and Power, 134.

K.A. Manske, D. Reindl, S. Klein, 2000. Load Sharing Strategies in Multiple Compressor Refrigeration Systems.

K.K. Botros, S.T. Ganesan, 2008. Dynamic instabilities in industrial compression systems with centrifugal compressors. Proceedings of the Turbomachinery Symposium.

K.N. Widell, T. Eikevik, 2010. Reducing power consumption in multi-compressor refrigeration systems. Int. J. Refrig., 33, pp. 88-94.

K. Song, C. Jeong, J. Nam, C. Han, 2012. Hybrid compressor model for optimal operation of compressed dry air system in LCD production industry. Ind. Eng. Chem. Res., 51, pp. 4998-5002.

Leducq, D., Guilpart, J., & Trystram, G. (2006). Non-linear predictive control of a vapour compression cycle. International Journal of Refrigeration, 29, 761-772.

Lee, G.C., Smith, R., Zhu, X.X., 2002. Optimal synthesis of mixed-refrigerant systems for low-temperature processes. Ind. Eng. Chem. Res. 41, 5016–5028.

Lee, I., Moon, I., 2016. Total Cost Optimization of a Single Mixed Refrigerant Process Based on Equipment Cost and Life Expectancy. Ind. Eng. Chem. Res. 55, 10336–10343.

Lee, I., Park, J., Moon, I., 2017. Key Issues and Challenges on the Liquefied Natural Gas (LNG) Value Chain: A Review from the Process Systems Engineering Point-of-View. Ind. Eng. Chem. Res. acs.iecr.7b03899.

Lee, S., Long, N.V.D., Lee, M., 2012. Design and Optimization of Natural Gas Liquefaction and Recovery Processes for Offshore Floating Liquefied Natural Gas Plants. Ind. Eng. Chem. Res. 51, 10021–10030.

Lim, W., Choi, K., Moon, I., 2013. Current status and perspectives of Liquefied Natural Gas (LNG) plant design. Ind. Eng. Chem. Res. 52, 3065–3088.

Maggio, G., Cacciola, G., 2012. When will oil, natural gas, and coal peak? Fuel 98, 111–123.

Mehrpooya, M., Ansarinasab, H., 2015. Advanced exergoeconomic evaluation of single mixed refrigerant natural gas liquefaction processes. J. Nat. Gas Sci. Eng. 26, 782–791.

Menezes, J. M. P., & Barreto, G. A. (2008). Long-term time series prediction with the NARX network: An empirical evaluation. Neurocomputing, 71, 3335-3343.

Mingot, A., Cristiani, H., 1997. Peak shaving plant at General Rodriguez (Buenos Aires, Argentina) and its rule to fulfill natural gas demand. SPE 1997 Lat. Am. gas Electr. Congr.

Ministry of Business Innovation and Employment, 2014. Energy in New Zealand 2014 66.

Moein, P., Sarmad, M., Ebrahimi, H., Zare, M., Pakseresht, S., Vakili, S.Z., 2015. APCI- LNG single mixed refrigerant process for natural gas liquefaction cycle: Analysis and optimization. J. Nat. Gas Sci. Eng. 26, 470–479.

Mokarizadeh Haghighi Shirazi, M., Mowla, D., 2010. Energy optimization for liquefaction process of natural gas in peak shaving plant. Energy 35, 2878–2885.

Morin, A., Wahl, P.E., Mølnvik, M., 2011. Using evolutionary search to optimise the energy consumption for natural gas liquefaction. Chem. Eng. Res. Des. 89, 2428–2441.

M.G. Nored, K. Brun, R. Kurz, 2008. Development of a guideline for the design of surge control systems. ASME Turbo Expo Power for Land, Sea, and Air, American Society of Mechanical Engineers, pp. 565-573.

M.P. Boyce, 2003. Centrifugal Compressors: a Basic Guide. PennWell Books

Na, J., Lim, Y., Han, C., 2017. A modified DIRECT algorithm for hidden constraints in an LNG process optimization. Energy 126, 488–500.

Nguyen, X.C., Regt, C. De, Mihaeye, K., Kim, M., Kim, M., Yoo, D., Lee, C., 2017. Comparative Economic and Technical Evaluation of AG FLNG with One vs . 1–19.

Nguyen, T. Van, de Oliveira Júnior, S., 2018. System eva luation of offshore platforms with gas liquefaction processes. Energy 144, 594–606.

Park, J., 2015. Refrigerant Optimization for Integrated Design and Control of Cryogenic Systems under Uncertainty.

Park, K., Won, W., Shin, D., 2016. Effects of varying the ambient temperature on the performance of a single mixed refrigerant liquefaction process. J. Nat. Gas Sci. Eng. 34, 958–968.

Peters, M.S., Timmerhaus, K.D., West, R.E., 2003. Plant Design and Economics for Chemical Engineers, Civil Engineering. McGraw-Hill Education.

Pham, T.N., Khan, M.S., Minh, L.Q., Husmil, Y.A., Bahadori, A., Lee, S., Lee, M., 2016. Optimization of modified single mixed refrigerant process of natural gas liquefaction using multivariate Coggin's algorithm combined with process knowledge. J. Nat. Gas Sci. Eng. 33, 731–741.

Pham, T.N., Long, N.V.D., Lee, S., Lee, M., 2017. Enhancement of single mixed refrigerant natural gas liquefaction process through process knowledge inspired optimization and modification. Appl. Therm. Eng. 110, 1230–1239.

Psichogios, D. C., & Ungar, L. H. (1992). A hybrid neural network-first principles approach to process modeling. AIChE Journal, 38, 1499-1511.

Puig-Arnavat, M., Bruno, J. C., & Coronas, A. (2010). Review and analysis of biomass gasification models. Renewable and Sustainable Energy Reviews, 14, 2841-2851.

P.C. Rasmussen, R. Kurz, 2009. Centrifugal compressor applications-upstream and midstream. 38th Turbo Machinery Symposium, Houston, TX September, pp. 14-17.

Qyyum, M.A., Long, N.V.D., Minh, L.Q., Lee, M., 2018. Design optimization of single mixed refrigerant LNG process using a hybrid modified coordinate descent algorithm. Cryogenics (Guildf). 89, 131–140.

Qyyum, M.A., Qadeer, K., Lee, M., 2017. Comprehensive review of the design optimization of natural gas liquefaction processes: Current status and perspectives. Ind. Eng. Chem. Res. acs.iecr.7b03630.

Remeljej, C.W., Hoadley, A.F.A., 2006. An exergy analysis of small-scale liquefied natural gas (LNG) liquefaction processes. Energy 31, 1669–1683.

Romeo, L. M., Bolea, I., Lara, Y., & Escosa, J. M. (2009). Optimization of intercooling compression in CO2 capture systems. Applied Thermal Engineering, 29, 1744-1751.

Ruiz, L., Cuéllar, M., Calvo-Flores, M., & Jiménez, M. (2016). An Application of Non-Linear Autoregressive Neural Networks to Predict Energy Consumption in Public Buildings. Energies, 9.

R.J. McKee, A. Garcia-Hernandez, 2007. Simulation of centrifugal compressor trips for surge avoidance system design. PSIG Annual Meeting, Pipeline Simulation Interest Group

R. Stanley, W. Bohannan, 1997. Dynamic simulation of centrifugal compressor systems. Proceedings of the Sixth Turbomachinery Symposium, pp. 123-131.

R.S. Shehata, H.A. Abdullah, F.F. Areed, 2009. Variable structure surge control for constant speed centrifugal compressors. Control Eng. Pract., 17, pp. 815-833.

R. Rammler, 1994. Considerations for advanced centrifugal compressor control. ISA Trans., 33, pp. 153-157e.

R. Kurz, R.C. White, 2009. Modeling emergency shutdowns of centrifugal compressors. PSIG Annual Meeting, Pipeline Simulation Interest Group.

S. Wright, C. Ditzel, M. Somani, 1998. Compressor station optimization. PSIG Annual Meeting, Pipeline Simulation Interest Group.

Tsay, C., Baldea, M., 2018. Scenario-Free Optimal Design under Uncertainty of the PRICO Natural Gas Liquefaction Process. Ind. Eng. Chem. Res. acs.iecr.7b03634.

Tsungna, L., Bill, G., Peter, T., & C, L., Giles. (1996). Learning Long-Term Dependencies in NARX Recurrent Neural Networks. IEEE Transactions on Neural Networks and Learning Systems, 7.

T. Bentaleb, A. Cacitti, S. De Franciscis, A. Garulli, 2015. Model predictive control for pressure regulation and surge prevention in centrifugal compressors. Control Conference (ECC), 2015 European, IEEE, pp. 3346-3351.

T. Kvangardsnes, 2009. Anti-surge Control: Control Theoretic Analysis of Existing Anti-surg

T. Kazuhiro, H. Kengo, 2006. Advanced control technique of centrifugal compressor for complex gas compression processes. Proceedings of the Turbomachinery Symposium, pp. 25-32.

T.F. Overvåg, 2013. Centrifugal Compressor Load Sharing with the Use of MPC. 144, pp. 51-63.

T.S. Grong, 2009. Modeling of Compressor Characterisics and Active Surge Control.

Vikse, M., Watson, H.A.J., Gundersen, T., Barton, P.I., 2018. Versatile Simulation Method for Complex Single Mixed Refrigerant Natural Gas Liquefaction Processes. Ind. Eng. Chem. Res. acs.iecr.7b04131.\

v.J.J. Helvoirt, 2007. Centrifugal compressor surge: modeling and identification for control. Technische Universiteit Eindhoven.

Won, W., Kim, J., 2017. Bi-level optimizing operation of natural gas liquefaction process. Comput. Chem. Eng. 96, 87–102.

Won, W., Lee, K.S., 2017. An energy-efficient operation system for a natural gas liquefaction process: Development and application to a 100 ton-per-day plant. Comput. Chem. Eng. 97, 208–219.

WorleyParsons, 2013. CCS learning from the LNG sector - A report for the GCCSI.

Xenos, D. P., Cicciotti, M., Kopanos, G. M., Bouaswaig, A. E. F., Kahrs, O., Martinez-Botas, R., & Thornhill, N. F. (2015).

Optimization of a network of compressors in parallel: Real Time Optimization (RTO) of compressors in chemical plants – An industrial case study. Applied Energy, 144, 51-63.

Xiong, X., Lin, W., Gu, A., 2016. Design and optimization of offshore natural gas liquefaction processes adopting PLNG (pressurized liquefied natural gas) technology. J. Nat. Gas Sci. Eng. 30, 379–387.

Xu, X., Liu, J., Cao, L., 2014. Optimization and analysis of mixed refrigerant composition for the PRICO natural gas liquefaction process. Cryogenics (Guildf). 59, 60–69.

Xu, X., Liu, J., Jiang, C., Cao, L., 2013. The correlation between mixed refrigerant composition and ambient conditions in the PRICO LNG process. Appl. Energy 102, 1127–1136.

Yang, H.J., Hwang, K.S., Lee, C.J., 2018. Stochastic Optimization of a Natural Gas Liquefaction Process Considering Seawater Temperature Variation Based on Particle Swarm Optimization. Ind. Eng. Chem. Res. 57, 2200–2207.

Nomenclature

AD	Annual depreciation
AGP	Annual gross profit
AOCF	Annual operating cash flow
AS	Annual sales
ATPC	Annual total production cost
C3MR	Propane pre-cooled mixed refrigerant
CAPEX	Capital expenditure
DMR	Dual mixed refrigerant
FLNG	Flating LNG
FPSO	Floating production, storage, and offloading
GA	Genetic algorithm
LNG	Liquefied natural gas
MACRS	Modified accelerated cost recovery system
MFCP	Mixed fluid cascade process
MR	Mixed refrigerant
MTPA	Million tons per annum
NGL	Natural gas liquid
NLP	Nonlinear programming
NPV	Net present value
OPEX	Operational expenditure

PMR	Parallel mixed refrigerant
PSE	Process sysems engineering
SC	Startup cost
SMR	Single mixed refrigerant
TAC	Total annualized cost
TACF	Total annual cash flow
$\boldsymbol{h_j}$	Predefined equality constraints
$\boldsymbol{h_p}$	Convergence of process simulator
$\boldsymbol{\Delta T_{min}}$	Minimum temperature difference
$\boldsymbol{W_c}$	Power consumption
$\boldsymbol{g_i}$	Inequality constraints
$\boldsymbol{s_k}$	Hidden constraints
LMTD	Logarithmic average of the temperature difference
p	Penalty function
P	Pressure
T	Temperature
T^{dew}	Dew point temperature
UA	Heat transfer coefficient × heat exchange area
x	Vector of desicion variables
β	Present value factor
γ	Penalty function value
ΔP	Pressure drop

$\boldsymbol{\theta}$ Tax rate

$\boldsymbol{x}$ Decision variables

NARX RNN = Nonlinear Autoregressive eXogenous Recurrent Neural Net model

RTO = Real Time Optimization

TPA = TerePhthalic Acid

Ai = Air interconnection

Gi = Gas interconnection

T_(n,cm_in) = The temperature entering the mth compression stage of the nth compression system, K

P_(n,cm_in) = The pressure entering the mth compression stage of the nth compression system, kgf/cm2

T_(n,cm_out) = The temperature from the mth compression stage of the nth compression system, K

P_(n,cm_out) = The pressure from the mth compression stage of the nth compression system, kgf/cm2

T_(n,ek_in) = The temperature entering the kth expansion stage of the nth compression system, K

P_(n,ek_in) = The pressure entering the kth expansion stage of the nth compression system, kgf/cm2

T_(n,ek_out) = The temperature from the kth expansion stage of the nth compression system, K

P_(n,ek_out) = The pressure from the kth expansion stage of the nth compression system, kgf/cm2

W_(1,motor_real) = The actual amount of power of the first compression system motor, kW

W_(1,motor_model) = The amount of power of the 1st compression system motor of hysys model, kW

W_(1,c1) = The energy of the first compression stage of the first compression system of the hysys model, kW

W_(1,c2) = The energy of the second compression stage of the first compression system of the hysys model, kW

W_(1,c3) = The energy of the third compression stage of the first compression system of the hysys model, kW

W_(1,e1) = The energy of the first expansion stage of the first compression system of the hysys model, Kw

W_(1,e2) = The energy of the second expansion stage of the first compression system of the hysys model, kW

W_(n,c)^ideal = The average ideal power consumption of the compression stage of the nth compression system, kW

W_(n,e)^ideal = The average ideal power output of the expansion stage of the nth compression system, kW

N_c = Number of compression stages

N_e = Number of expansion stages

$\tilde{k}$_air = mean adiabatic exponent of air

$\tilde{k}$_gas = mean adiabatic exponent of gas

$\tilde{M}$_air = mean molecular weight of air, kg/kgmol

$\tilde{M}$_gas = mean molecular weight of gas, kg/kgmol

$\tilde{F}$_c = mean mass flow rate of air, kg/s

$\tilde{F}$_g = mean mass flow rate of gas, kg/s

P_amb = ambient pressure, kgf/cm2

T_amb = ambient temperature, K

H_amb = ambient humidity, %

V_(n,c) = volumetric flow rate of air of the nth compression system, kNm3/hr

V_(n,e) = volumetric flow rate of gas of the nth compression system, kNm3/hr

γ_(n,o2) = volume percent of O2 in off-gas of the nth compression system, %

$\gamma_{(n,co2)}$ = volume percent of CO2 in off-gas of the nth compression system, %

$\gamma_{(n,co)}$ = volume percent of CO in off-gas of the nth compression system, %

$x_{(n,cm,1)}$ = Manipulated variables of the mth compression stage model of the nth compression system

$x_{(n,cm,2)}$ = The external disturbance variables of the mth compression stage model of the nth compression system

$x_{(n,ek,1)}$ = Manipulated variables of the kth expansion stage model of the nth compression system

$x_{(n,ek,2)}$ = The external disturbance variables of the kth expansion stage model of the nth compression system

$h_{(n,cm)}$ = The external disturbance influence function at the mth compression stage of the nth compression system

$h_{(n,ek)}$ = The external disturbance influence function at the kth expansion stage of the nth compression system

$g_{(n,cm)}$ = Thermodynamic-based function at the mth compression stage of the nth compression system

$g_{(n,ek)}$ = Thermodynamic-based function at the kth expansion stage of the the nth compression system

$f_{(n,cm)}$ = The influence function due to the degradation of the device at the mth compression stage of the nth compression system

$f_{(n,ek)}$ = The influence function due to the degradation of the device at the kth expansion stage of the nth compression system

u_t = The input set of the NARX RNN model at time t

y_t = The output set of the NARX RNN model at time t

d_y = time delay of input set, hr

d_u = time delay of output set, hr

$X_{(opt,L)}$ = Lower limit value of the optimization variable of the nth compression system

$X_{(opt,U)}$ = Upper limit value of the optimization variable of the nth compression system

$W_{(n,M,L)}$ = The minimum operable power value of the electric motor of the nth compression system

$W_{(n,M,U)}$ = The maximum operable power value of the electric motor of the nth compression system

$\alpha_{(n,c\_surge)}$ = The first regression parameter of surge limit line of the nth compression system

$\alpha_{(n,c\_stonewall)}$ = The first regression parameter of stonewall limit line of the nth compression system

$\beta_{(n,c\_surge)}$ = The second regression parameter of surge limit line of the nth compression system

$\beta_{(n,c\_stonewall)}$ = The second regression parameter of stonewall limit line of the nth compression system

Abstract in Korean (국문초록)

압축시스템은 화학 공정에서 가장 중요한 부분 중에 하나이다. 압축 시스템은 공정 내에서 중요한 역할을 수행하지만 많은 양의 전력을 소모한다는 특징을 가진다. 일반적으로 압축기 시스템은 일정한 토출 압력을 유지하기 위한 목적을 가지고 설비되며, 압축기는 써지 현상으로부터 보호되어야 할 필요성을 가진다. 써지는 진동을 동반한 역류 현상으로 압축기 내부뿐 만 아니라 주변 부분까지 손상을 야기시킨다. 따라서, 효율적이고 강건한 압축시스템의 운전은 화학 공장의 설계와 관리 측면에서 가장 중요한 이슈를 가진다. 압축기는 공정 운전 단계에서뿐 만 아니라 설계 단계에서부터 적절한 운전 범위에서 운전될 수 있도록 고려되어야 한다.

먼저 저자는 기존의 경제성만을 고려한 설계 접근법에서 벗어나 압축 시스템의 운전성을 높일 수 있는 새로운 공정 설계 방법을 제안한다. 제안한 설계 방법은 로드의 변화에 따라서 다수의 정상 상태 운전 영역을 고려한다는 점에서 기존의 설계 방법과 차이점을 가진다. 각각의 설계 방법이 가지는 경제성은 실제 가스전의 생산량을 기준으로 계산되는 매년의 수익을 반영한 경제성 평가

모델을 기반으로 평가된다. 제안한 설계 방법은 압축기 설치 비용에서 경제적인 손실을 가지지만 더 많은 운전 범위에서 운전 비용의 이점을 가지기 때문에 전반적인 공정의 경제성을 높일 뿐만 아니라 압축기의 유연한 운전을 가능하게 한다. 두 번째로 저자는 산업 규모의 다단 압축기 시스템의 효율적이고 경제적인 운전을 위한 실시간 최적화 기법 기반의 비선형 자기회귀 인공신경망 모델을 제안한다. 비선형 자기회귀 인공신경망 모델은 실제 공정 운전 데이터로부터 시간에 따라 변하는 시스템의 특성을 반영하기에 적합한 모델이다. 또한 화학 공정이 가지는 열역학적인 특성을 하나의 인공신경망 구조의 특성점으로 사용함으로써 모델의 예측 성능을 높이고자 하였다. 그리고 최적의 운전 지점을 실시간으로 결정해 주기 위해 실시간 최적화 기법을 사용하였으며 결정된 최적 지점은 다음 시간에서의 의사 결정을 위해 모델에 반복적으로 갱신된다. 제안한 모델과 최적화 기법은 실제 공장과 99.6%의 정확도를 보이는 가상의 시뮬레이션 모델을 통해 검증된다. 제안한 특성점 추출을 결합한 비선형 자기회귀 인공신경망 모델은 기존의 단순 피드포워드 다중 신경망 모델에 비해 43.5%의 정확도 향상을 보였다. 또한 실시간 최적화 기법을 통하여 총 전력 소모량의 4%를 감소시켰다. 마지막으로 저자는 평형

압축기 시스템의 강건한 운전을 위한 고도화된 제어 시스템을 제안한다. 평형 압축기 시스템의 제어는 일정한 토출압 유지, 써지 현상 방지, 그리고 로드 분배라는 목적을 가진다. 그러나 평형 압축기 시스템의 제어는 서로 다른 제어 루프의 존재로 인한 서로간의 제어 간섭으로 인해 어려움을 가진다. 또한 예측하지 못하는 외란의 존재는 이러한 제어를 보다 어렵게 한다. 대부분의 이러한 문제는 로드의 분배를 동등하게 하지 못하는 문제를 야기시키며 이로 인해 압축기가 재순환 모드로 운전되게 한다. 더욱이 이러한 조건에서는 써지 현상이 발생할 확률이 높아진다. 추가적인 토출 유량 제어기 신호와 비선형 신호 계산 체계를 도입함으로써 이러한 문제들을 해결한다.

주요어: 압축기 시스템; 공정 설계; 공정 모사; 로드 흔들림; 비선형 자기 회귀 인공 신경망 구조; 실시간 최적화; 초구조 최적화; 제어 간섭; 써지 방지 제어; 로드 분배

학 번: 2014-21586